

Improvement of photocatalytic activity of visible-light-responsive
TiO₂ by controlling the valence states of metal ions

(金属イオンの原子価状態の制御による可視光応答型光触媒の高活性化)

by

Naoto Nishiyama

Graduate School of Science and Engineering
Yamaguchi University

September, 2018

Contents

Chapter 1 Introduction	1
Chapter 2 Factors affecting the photocatalytic activity of Pt-TiO₂ under visible light irradiation	
2. 1. Introduction.....	18
2. 2. Experimental.....	19
2. 2. 1. Materials	
2. 2. 2. Preparation of Pt-TiO ₂ powder	
2. 2. 3. Characterization of Pt-TiO ₂ powder	
2. 2. 4. Photocatalytic degradation of 4-CP by using Pt-TiO ₂ powder	
2. 3. Results and discussion.....	26
2. 3. 1. Effect of Pt ion doping	
2. 3. 2. Valence states of the doped Pt ions near the surface or in the bulk of TiO ₂	
2. 3. 3. Quantitative method of Pt(II) existing near the surface of TiO ₂	
2. 3. 4. Effect of Pt(II)/Pt(IV) on the photocatalytic activity	
2. 3. 5. Effect of Pt(II)/Pt(IV) on the dynamics of the photogenerated carriers of Pt-TiO ₂	
2. 3. 6. Photocatalytic activity of Pt-TiO ₂ and TiO ₂ under irradiation from solar simulator	
2. 4. Conclusion.....	58
References.....	59
Chapter 3 Factors affecting the photocatalytic activity of Cr-TiO₂ under visible light irradiation	
3. 1. Introduction.....	61
3. 2. Experimental.....	62
3. 2. 1. Materials	
3. 2. 2. Preparation of Cr-TiO ₂ powder	
3. 2. 3. Characterization of Cr-TiO ₂ powder	
3. 2. 4. Photocatalytic degradation of 4-CP by using Cr-TiO ₂ powder	
3. 3. Results and discussion.....	64
3. 3. 1. Effect of doping amount on the photocatalytic activity of Cr-TiO ₂	
3. 3. 2. Valence states of the doped Cr ions near the surface and bulk of TiO ₂	
3. 3. 3. Relationship between Cr(VI)/Cr(III) ratio and photocatalytic activity on Cr-TiO ₂	
3. 3. 4. Effect of forming the mixed valence states on the lifetime of photogenerated carriers	
3. 3. 5. The structure of 0.8 atom% Cr-TiO ₂ and factors influencing on photocatalytic	

activity	
3. 4. Conclusion.....	91
References.....	92

Chapter 4 Factors affecting the photocatalytic activity of Cr-grafted TiO₂ under visible light irradiation

4. 1. Introduction.....	94
4. 2. Experimental.....	95
4. 2. 1. Materials	
4. 2. 2. Preparation of Cr-grafted TiO ₂ powder	
4. 2. 3. Characterization and evaluation of the photocatalytic activity of Cr-grafted TiO ₂ powder	
4. 3. Results and discussion.....	96
4. 3. 1. Comparison of Cr-grafted TiO ₂ and Cr-TiO ₂	
4. 3. 2. Effect of number density of Cr ion of Cr-grafted TiO ₂ on the 4-CP conversion	
4. 3. 3. Effect of the sintering for Cr-grafted TiO ₂ on the 4-CP conversion	
4. 4. Conclusion.....	109
References.....	110

Chapter 5 Conclusion.....111

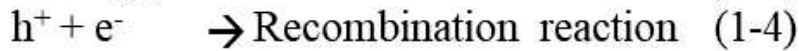
Acknowledgements.....113

Publication list.....115

Chapter 1 Introduction

Environmental contamination is a critical issue in modern society. Various inorganic semiconductor photocatalysts have been studied for decontamination of air pollution and improvement of water quality environment. Among them, titanium dioxide (TiO_2) is very effective for environmental remediation because it possesses advantages such as low cost, non-toxicity, high chemical stability, and strong oxidizing power.¹⁻⁶⁾ In addition to being used for environmental purification, it is also widely applied to dye sensitized solar cells⁷⁻¹⁰⁾, antibacterial agents¹¹⁻¹⁴⁾, optical treatment of cancer¹⁵⁾, and so on. TiO_2 consists of the valence band (VB) filled with electrons, the conduction band (CB) composed of an empty orbital without electrons, and a band gap separating them. Photogenerated holes (h^+) with the oxidative power are formed by exciting electrons from the VB to the CB of TiO_2 under irradiation of light whose energy is greater than the bandgap energy (Equation 1-1). The standard electrode potential (E^0) of h^+ is 3.0 V vs. NHE, indicating the stronger oxidation power than chlorine ($E^0 = 1.36$ V) used for water purification, hydrogen peroxide ($E^0 = 1.77$ V), and OH radical ($E^0 = 2.80$ V). Therefore, electron donors adsorbed on the TiO_2 surface ($\text{D}_{\text{ads.}}$) such as H_2O and organic substrates are oxidized (Equation 1-2). The OH radicals generated by the oxidation of H_2O can degrade organic compounds. On the other hand, the photoexcited electrons (e^-) reduce the electron acceptor ($\text{A}_{\text{ads.}}$) such as oxygen adsorbed on the TiO_2 surface (Equation 1-3). Equation 1-4 shows the recombination of photogenerated

electron-hole pairs, which is deactivation of the photocatalytic reaction. These reaction mechanisms are shown in Scheme 1-1 (a).



The band gap energy of TiO_2 is 3.2 eV and thus these reactions occur only under UV light irradiation ($\lambda \leq 387$ nm).¹⁶⁻¹⁸⁾ As shown in Figure 1-1, the solar radiation spectra contain UV light less than 3-5%.¹⁷⁻²⁰⁾ Moreover, for energy saving, the conventional fluorescent lamp is replaced with LED light which does not emit any UV light. Therefore, development of visible light driven TiO_2 photocatalyst has been desired from the viewpoint of effective utilization of solar energy and for achieving indoor environmental purification.

Doping of a foreign element in TiO_2 narrows the band gap to absorb the visible light. Many research groups have reported that the doping of nonmetallic ions such as nitrogen²¹⁻²⁸⁾, sulfur²⁹⁻³²⁾, carbon³³⁻³⁹⁾, phosphorous⁴⁰⁻⁴²⁾ and boron^{43, 44)} which are substituted with the oxygen site of TiO_2 exhibits the photocatalytic activity under visible light irradiation. In these cases, the dopants exist as anion and an isolated level derived from the p orbital of the anion is formed above the VB. As a result, the visible light is absorbed but the mobility and the oxidizing power of h^+ become low.^{45, 46)}

As another approach, visible light responsive TiO₂ doped with a transition metal ion⁴⁷⁻⁵⁰ such as iron⁵¹⁻⁵⁹, nickel^{20, 60, 61}, vanadium⁶²⁻⁶⁷, chromium (Cr)⁶⁸⁻⁷⁶ and platinum (Pt)⁷⁶⁻⁷⁸ has been reported. These metal ion dopants form the impurity level in the band gap (Scheme 1-1(b)). Solid-phase reaction is used to dope the metal ions but the sintering at the temperature higher than 1000°C is necessary to substitute Ti for the dopants, which significantly decreases the specific surface area of TiO₂.^{79, 80} An ion implantation method is also used for doping of metal ions but there is a problem of low versatility and high cost because it requires a large-scale apparatus.⁶⁹

Sol – gel synthesis which utilizes chemical reaction in solution is easy and cost effective. A typical procedure is as follows: metal alkoxides such as titanium tetraisopropoxide dissolved into alcohols are added to aqueous acidic solution. Then, metal oxide nanoparticles are formed by hydrolysis and condensation. After drying, the obtained xerogels are sintered at higher temperature than ca. 400°C to decompose the organic byproducts. By adding a metal ion to the initial acidic solution, metal ions are doped into the Ti site during chemical reaction process to form Ti - O network. In this method, the common equipment such as beaker, magnetic stirrer or oven is needed.^{20, 46-48, 58, 59, 65, 67, 71, 73-78} Therefore, the sol – gel synthesis is simple and environmentally friendly, without any special equipment. In our laboratory, we have synthesized porous TiO₂ by using only water as solvents and conducting dialysis.⁸¹⁻⁸⁴ Our typical procedures are as follows: hydrolysis of

titanium alkoxide is conducted in an acidic aqueous solution ($\text{pH} \approx 1$) and the obtained precipitates are peptized for 6 days to obtain a highly dispersed sol. After conducting dialysis, the sol is dried and sintered. During dialysis, protons adsorbed on the surface of TiO_2 nanoparticles are gradually removed and then the particles tend to undergo aggregation with the formation of pores. As a result, porous TiO_2 with the large BET specific surface area is obtained (Scheme 1-2).

As another approach to synthesize TiO_2 with high specific surface area by the sol – gel method, several research groups have reported that surfactants or polymers are added as template and then they are removed to form pores.⁸⁵⁻⁸⁹⁾ However, in order to remove these template compounds, strong acid treatment or sintering at high temperature are required. Our method is more beneficial since the template compound is not necessary.

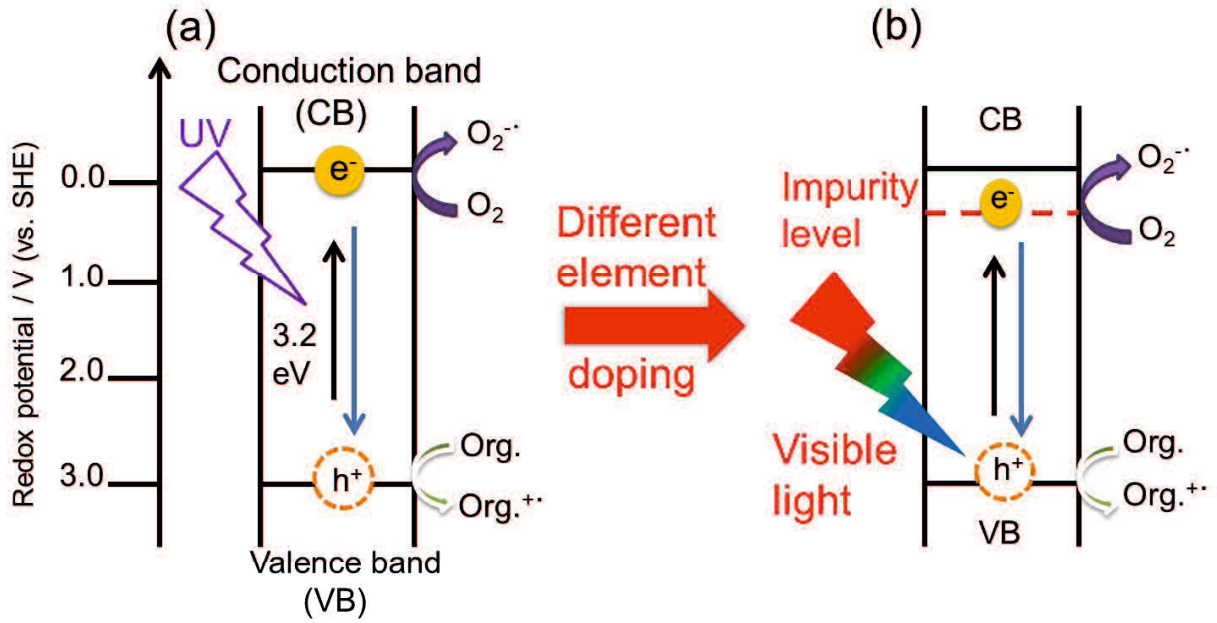
We have synthesized visible light responsive TiO_2 (M- TiO_2) by our method with the addition of different 7 metal ions (Pt(IV), Cr(III), Fe(III), Ru(IV), Ru(III), Cu(II) and Co(II)). On the prepared M- TiO_2 , the degradation experiments of 4-chlorophenol (4-CP) were carried out under visible light irradiation.⁹⁰⁻⁹²⁾ Chlorophenols such as 4-CP are widely used as wood preservatives, fungicides, herbicides, dye intermediates, cosmetic raw materials, drugs and so on.⁹³⁻⁹⁵⁾ However, chlorophenols are carcinogenic and persistent environmental contaminants.⁹⁶⁻⁹⁸⁾ General treatment to degrade organochlorine compounds includes biological treatment^{94, 99)} and chlorine treatment^{95, 100)}. However, the former takes a long time

to degrade them and the latter produces harmful chlorinated byproducts. Therefore, the development of the method to degrade chlorophenols efficiently to harmless compounds is required. We have reported that Pt and Cr ion doped TiO₂ (Pt-TiO₂, Cr-TiO₂) can degrade 4-CP among the 7 metal ions mentioned above.⁹¹⁾ Comparison of our Pt-TiO₂ with Pt-TiO₂ synthesized by the conventional sol – gel method reported in the literature revealed that the photocatalytic activity was improved about 2.5 times.⁹⁰⁾ Thus, we have demonstrated that our method is superior to the literature method for the degradation and detoxification of 4-CP under visible light irradiation. In addition, we also found that the photocatalytic activity drastically changed by the metal ion used.

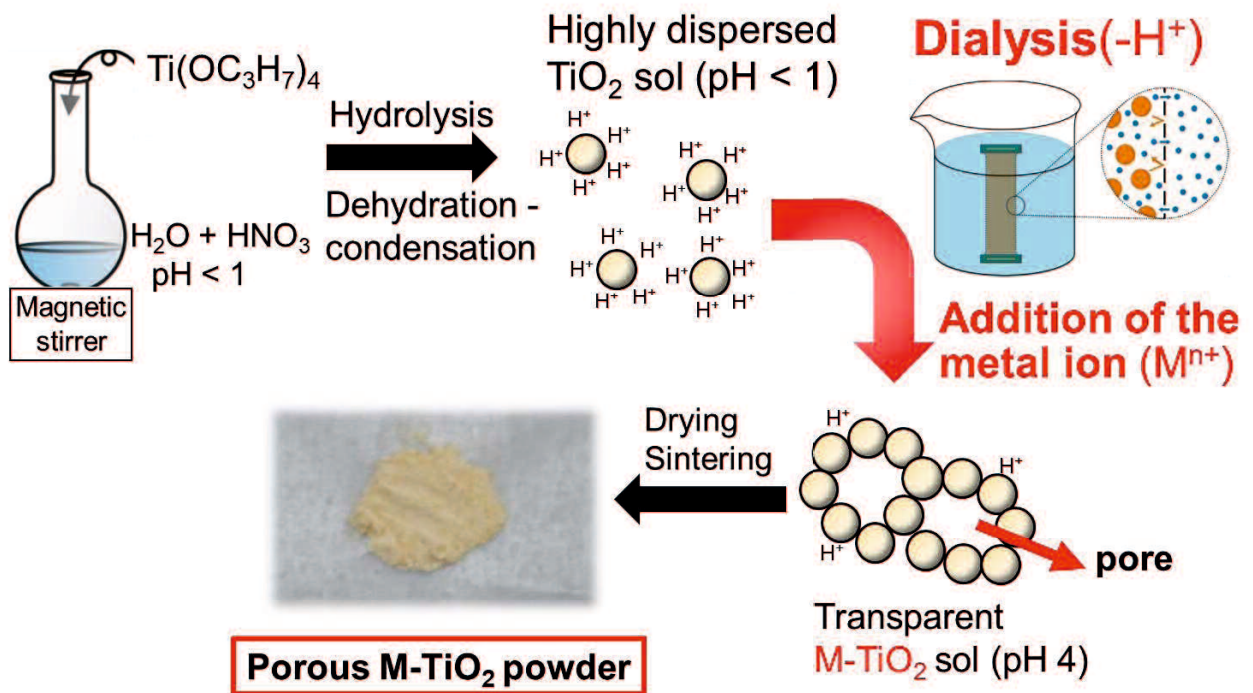
Table 1-1 lists some optimal synthetic conditions of M-TiO₂ reported so far for degradation of contaminants. The optimum synthesis conditions are different depending on the metal ion. Even if the same metal ions are used, the optimum conditions are different depending on the synthetic method. In addition, various physical properties such as BET specific surface area¹⁰³⁾, crystal type⁷⁶⁾, degree of crystallinity⁷¹⁾, the number of oxygen defects¹⁰⁴⁾, are reported to be responsible for the photocatalytic performance. These properties are changed depending on the synthesis conditions. Moreover, it is well-known that the metal ion dopants act as a recombination center of photogenerated holes and electrons, thereby lowering photocatalytic activity.^{101, 102)} Although there are an enormous number of studies on visible light responsive metal ion doping in TiO₂ over 30 years, the most important factor

affecting the photocatalytic activity is not fully understood. The elucidation of the factor leads to the development of highly active M-TiO₂ photocatalyst and research will be greatly advanced toward practical application of visible light responsive TiO₂, which has not yet been realized.

The purpose of this thesis is to elucidate the most important factor influencing the photocatalytic activity of metal ion doped TiO₂ under visible light irradiation. I focused on the valence states and the location of the doped metal ions. In Chapter 2, I have investigated the influence of the specific surface area, the valence state and the existence position of Pt ion on the photocatalytic activity and found that the coexistence of Pt(II) and Pt(IV) are important to improve the photocatalytic activity. In Chapter 3, I have focused on Cr ions which have some stable valence states like Pt ions and found that coexistence of Cr(III) and Cr(VI) enhances the photocatalytic activity of Cr-TiO₂. In Chapter 4, I have studied on the photocatalytic activity and the physical properties of Cr-grafted TiO₂. Grafting of metal ions onto TiO₂ has been recently developed as a novel method to synthesize visible light responsive photocatalyst. I have compared Cr-TiO₂ with Cr-grafted TiO₂ and found that the photocatalytic activity of Cr-grafted TiO₂ is much lower than that of Cr-TiO₂ but can be improved significantly by coexisting Cr(III) and Cr(VI).



Scheme 1-1 Photoassisted redox reaction on (a) TiO_2 under UV light irradiation and (b) M-TiO_2 under visible light irradiation.



Scheme 1-2 Synthetic route of porous visible light responsive M-TiO_2 photocatalysts.

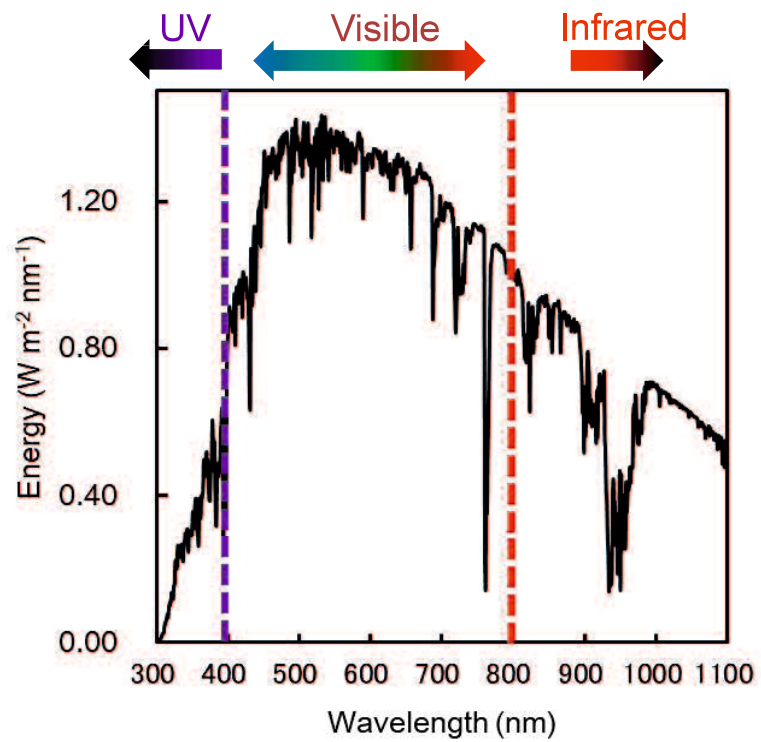


Figure 1-1 Solar radiation spectra at A. M. 1.5. This spectra data was cited from National Renewable Energy Laboratory (NREL).

<https://www.nrel.gov/grid/solar-resource/spectra.html> (2018. 08. 22)

Table 1-1 Synthesis of the visible light responsive TiO₂.

Metal ion	Method (solvent) TiO ₂ precursor	Optimal synthetic condition (doping amount, sintering temperature)	Evaluation of photocatalytic performance	Ref No.
Pt	Sol – gel (ethanol + H ₂ O) TTIP	0.5 atom%, 400°C	Dichloroacetate, 4-CP ($\lambda > 420$ nm)	77
	Sol – gel (ethanol + H ₂ O) TTIP	0.3 atom%, 400°C	MB, Phenol, Tri-iodide ($\lambda > 320, 420$ nm)	76
	Sol – gel (ethanol + H ₂ O) TBT	0.4 atom%, 400°C	NO (Gas phase) ($\lambda = 365$ nm, $\lambda > 420$ nm)	78
Cr	Sol – gel (ethanol + H ₂ O) TTIP	0.3 atom%, 400°C	MB, Phenol, Tri-iodide ($\lambda > 320, 420$ nm)	76
	Sol – gel (water) Titanylsulfate	0.25 mol%, 800°C	MB ($\lambda = 410 - 800$ nm)	71
	Sol – gel (water) TTIP	5 atom%, 500°C	MB ($\lambda > 420$ nm, or UV (500 W Xe lamp))	75
	Sol – gel (water) TTIP	3 mol%, 400°C	MB ($\lambda > 410$ nm)	73
V	Sol – gel and hydrothermal (isopropanol) TTIP	0.15 mass% (visible) Lower than TiO ₂ under UV irradiation HT at 200°C	XRG dye ($\lambda = 365$ nm (UV), $\lambda > 380$ nm (visible))	74
	Solid phase reaction P-25	1 mol%, 500°C	Propylene (Gas phase) ($\lambda > 420$ nm)	66
	Sol – gel (water) TiCl ₄	0.06 atom%, 550°C	Congo red (Solar light, 11 a.m. - 2 p.m. during May – June in Bangalore, India)	65

	Sol – gel (ethanol) TBT	0.3 atom%, 500°C	MB (50 W LED, major emission at 460 nm)	67
Fe	Plasma oxidative pyrolysis TBT	Less than 1 atom% (visible) Lower than TiO ₂ under UV irradiation (At any doping amount)	MO ($\lambda = 365, 316$ nm (UV) or 405, 436 nm (visible))	54
	Sol – gel (t-butyl alcohol), TiCl ₄	0.1 mol%, 300°C	MB ($\lambda > 420$ nm)	59
	Sol – gel (ethanol + H ₂ O), TTIP	0.5 mol%, 400°C	MO ($\lambda > 400$ nm)	58
In	Sol – gel (ethanol), TBT	7 mol%, 450°C	4-CP ($\lambda > 400$ nm)	47
W	Sol – gel (ethanol + H ₂ O), TBT	5 mol%, 550°C	MB (visible light)	48
Mn	Sol – gel (ethanol + H ₂ O), TBT	0.5 mol%, 550°C	MB (visible light)	48
Ce	Sol – gel (ethanol + H ₂ O), TBT	0.03 atom%, 500°C	Rhodamine B ($\lambda > 420$ nm)	50
Ni	Sol – gel (ethanol + H ₂ O), TTIP	1 wt%, 500°C	p-arsanilic acid (Blue light LED, 450 nm)	20
Co	Hydrothermal TOS	0.3 % HT at 150°C	Phenol ($\lambda = 400 – 700$ nm)	49

Abbreviation: TTIP: titanium tetraisopropoxide, TBT: titanium tetrabutoxide, TOS: titanium oxysulfate, HT:

hydrothermal treatment, MB: methylene blue, MO: methyl orange. Unless otherwise stated, photocatalytic

performance experiments were carried out in an aqueous system.

References

- 1) D.F. Ollis, H. Al-Ekabi, *Photocatalytic Purification and Treatment of Water and Air*, Elsevier, Amsterdam 1993.
- 2) M. R. Hoffmann, S. T. Martin, W. Choi, D. W. Bahnemann, *Chem. Rev.*, 1995, **95**, 69-96.
- 3) A. Fujishima, T. N. Rao, D. A. Tryk, *J. Photochem. Photobiol. C: Rev.*, 2000, **1**, 1-21.
- 4) U. I. Gaya, A. H. Abdullah, *J. Photochem. Photobiol. C: Rev.*, 2008, **9**, 1-12.
- 5) B. Ohtani, *J. Photochem. Photobiol. C: Rev.*, 2010, **11**, 157-178.
- 6) Y. Ohko, K. Hashimoto, A. Fujishima, *J. Phys. Chem. A*, 1997, **101**, 8057-8062.
- 7) C.-W. Lee, H.-P. Lu, C.-M. Lan, Y.-L. Huang, Y.-R. Liang, W.-N. Yen, Y.-C. Liu, Y.-S. Lin, E. W.-G. Diao, C.-Y. Yeh, *Chem. Eur. J.*, 2009, **15**, 1403-1412.
- 8) R. Ma, P. Guo, H. Cui, X. Zhang, M. K. Nazeeruddin, M. Grätzel, *J. Phys. Chem. A*, 2009, **113**, 10119-10124.
- 9) H. Imahori, T. Umeyama, S. Ito, *Acc. Chem. Res.*, 2009, **42**, 1809-1818.
- 10) A. Mishra, M. K. R. Fischer, P. Bauerle, *Angew. Chem. Int. Ed.*, 2009, **48**, 2474-2499.
- 11) Y. Ohko, Y. Utsumi, C. Niwa, T. Tatsuma, K. Kobayakawa, Y. Satoh, Y. Kubota, A. Fujishima, *J. Biomed. Mater. Res: Appl. Biomater.*, 2001, **58**, 97-101.
- 12) Y. Yao, Y. Ohko, Y. Sekiguchi, A. Fujishima, Y. Kubota, *J. Biomed. Mater. Res. B*, 2007, **85B**, 453-460.
- 13) Y. Yao, T. Ochiai, H. Ishiguro, R. Nakano, Y. Kubota, *Appl. Catal. B: Environ.*, 2011, **106**, 592-599.
- 14) Y. Hou, X. Li, Q. Zhao, G. Chen, C. L. Raston, *Environ. Sci. Technol.*, 2012, **46**, 4042-4050.
- 15) S. Yamaguchi, H. Kobayashi, T. Narita, K. Kanehira, S. Sonezaki, N. Kudo, Y. Kubota, S. Terasaka, K. Houkin, *Ultrason. Sonochem.*, 2011, **18**, 1197-1204.
- 16) S. Kitano, N. Murakami, T. Ohno, Y. Mitani, Y. Nosaka, H. Asakura, K. Teramura, T.

- Tanaka, H. Tada, K. Hashimoto, H. Kominami, *J. Phys. Chem. C*, 2013, **117**, 11008-11016.
- 17) T. Ohno, N. Murakami, T. Tsubota, H. Nishimura, *Appl. Catal. A:Gen*, 2008, **349**, 70-75.
- 18) C. Zhang, T. Uchikoshi, J. Li, T. Watanabe, T. Ishigaki, *J. Alloy. Compd.*, 2014, **606**, 37-43.
- 19) N. Murakami, T. Chiyoya, T. Tsubota, T. Ohno, *Appl. Catal. A:Gen*, 2008, **348**, 148-152.
- 20) M. Patricia, B. Vega, M. Hinojosa-Reyes, A. Hernández-Ramírez, J. L. G. Mar, V. Rodríguez-González, L. Hinojosa-Reyes, *J. Sol - Gel. Sci. Techn.*, 2018, **85**, 723-731.
- 21) A. Fujishima, X. Zhang, D. A. Tryk, *Surf. Sci. Rep.*, 2008, **63**, 515-582.
- 22) X. Zhang, K. Udagawa, Z. Liu, S. Nishimoto, C. Xu, Y. Liu, H. Sakai, M. Abe, T. Murakami, A. Fujishima, *J. Photochem. Photobiol. A: Chem.*, 2009, **202**, 39-47.
- 23) R. Asahi, T. Morikawa, T. Ohwaki, K. Aoki, Y. Taga, *Science*, 2001, **293**, 269-271.
- 24) J. Wang, D. N. Tafen, J. P. Lewis, Z. Hong, A. Manivannan, M. Zhi, M. Li, N. Wu, *J. Am. Chem. Soc.*, 2009, **131**, 12290-12297.
- 25) H. Irie, Y. Watanabe, K. Hashimoto, *J. Phys. Chem. B.*, 2003, **107**, 5483-5486.
- 26) S. Sakthivel, H. Kisch, *ChemPhysChem.*, 2003, **4**, 487-490.
- 27) C. Burda, Y. Lou, X. Chen, A. C. S. Samia, J. Stout, J. L. Gole, *Nano Lett.*, 2003, **3**, 1049-1051.
- 28) J. L. Gole, J. D. Stout, C. Burda, Y. Lou, X. Chen, *J. Phys. Chem. B*, 2004, **108**, 1230-1240.
- 29) T. Umebayashi, T. Yamaki, S. Tanaka, K. Asai, *Chem. Lett.*, 2003, **32**, 330-331.
- 30) W. Ho, J. C. Ya, S. Lee, *J. Solid State Chem.*, 2006, **179**, 1171-1176.
- 31) K. Nishijima, N. Murakami, T. Ohno, *Appl. Catal. B-Environ.*, 2008, **84**, 584-590.
- 32) Y. Wang, Y. L. Meng, H. M. Ding, Y. K. Shan, X. Zhao, X. Z. Tang, *J. Phys. Chem. C*, 2008, **112**, 6620-6626.

- 33) W. Ren, Z. Ai, L. Zhang, X. Fan, Z. Zou, *Appl. Catal. B: Environ.*, 2007, **69**, 138-144.
- 34) S. Sakthivel, H. Kisch, *Angew. Chem. Int. Ed.*, 2003, **42**, 4908-4911.
- 35) Y. Park, W. Kim, H. Park, T. Tachikawa, T. Majima, W. Choi, *Appl. Catal. B: Environ.*, 2009, **91**, 355-361.
- 36) S. U. M. Khan, M. Al-Shahry, W. B. Ingler Jr., *Science*, 2002, **297**, 2243-2245.
- 37) Y. Choi, T. Umebayashi, M. Yoshikawa, *J. Mater. Sci.*, 2004, **39**, 1837-1839.
- 38) H. Irie, Y. Watanabe, K. Hashimoto, *Chem. Lett.*, 2003, **32**, 772-773.
- 39) T. Tachikawa, S. Tojo, K. Kawai, M. Endo, M. Fujitsuka, T. Ohno, K. Nishijima, Z. Miyamoto, T. Majima, *J. Phys. Chem. B.*, 2004, **108**, 19299-19306.
- 40) L. Lin, W. Lin, Y. Zhu, B. Zhao, Y. Xie, *Chem. Lett.*, 2005, **34**, 284-285.
- 41) Q. Shi, D. Yang, Z. Jiang, J. Li, *J. Mol. Catal. B-Enzym.*, 2006, **43**, 44-48.
- 42) H.-F. Yu, *J. Phys. Chem. Solids*, 2007, **68**, 600-607.
- 43) W. Zhao, W. Ma, C. Chen, J. Zhao, Z. Shuai, *J. Am. Chem. Soc.*, 2004, **126**, 4782-4783.
- 44) S. In, A. Orlov, R. Berg, F. Garcia, S. P. Jimenez, M. S. Tikhov, D. S. Wright, R. M. Lambert, *J. Am. Chem. Soc.*, 2007, **129**, 13790-13791.
- 45) H. Yu, H. Irie, Y. Simodaira, Y. Hosogi, Y. Kuroda, M. Miyauchi, K. Hashimoto, *J. Phys. Chem. C.*, 2010, **114**, 16481-16487.
- 46) M. Liu, X. Qiu, M. Miyauchi, K. Hashimoto, *J. Am. Chem. Soc.*, 2013, **135**, 10064-10072.
- 47) E. Wang, W. Yang, Y. Cao, *J. Phys. Chem. C*, 2009, **113**, 20912-20917.
- 48) S. Liu, E. Guo, L. Yin, *J. Mater. Chem. C*, 2012, **22**, 5031-5041.
- 49) P. Jiang, W. Xiang, J. Kuang, W. Liu, W. Cao, *Solid State Sci.*, 2015, **46**, 27-32.
- 50) Z. Liu, L. Xing, H. Ma, L. Cheng, J. Liu, J. Yang, Q. Zhang *Environ. Prog. Sustain.*, 2017, **36**, 494-504.
- 51) X. W. Zhang, L. C. Lei, *Mater. Lett.*, 2008, **62**, 895-897.

- 52) S. Nahar, K. Hasegawa, S. Kagaya, *Chemosphere*, 2006, **65**, 1976-1982.
- 53) J. F. Zhu, F. Chen, J. L. Zhang, H. J. Chen, M. Anpo, *J. Photochem. Photobiol. A: Chem.*, 2006, **180**, 196-204.
- 54) X. H. Wang, J.-G. Li, H. Kamiyama, Y. Moriyoshi, T. Ishigaki, *J. Phys. Chem. B*, 2006, **110**, 6804-6809.
- 55) Y. Yelda, K. Murat, C. Zekiye, *Appl. Catal. B: Environ.*, 2010, **99**, 469-477.
- 56) S. Tieng, A. Kanaer, K. Chhor, *Appl. Catal. A: General*, 2011, **399**, 191-197.
- 57) P. Pongwan, B. Inceesungvorn, K. Wetchakun, S. Phanichphant, N. Wetchakun, *Engineering Journal*, 2012, **16**, 143-151.
- 58) V. Moradi, M. B. G. Jun, A. Blackburn, R. A. Herring, *Appl. Surf. Sci.*, 2018, **427**, 791-799.
- 59) J. Zhu, J. Ren, Y. Huo, Z. Bian, H. Li, *J. Phys. Chem. C*, 2007, **111**, 18965-18969.
- 60) R. Nishiro, H. Kato, A. Kudo, *Phys. Chem. Chem. Phys.*, 2005, **7**, 2241-2245.
- 61) D. H. Kim, K. S. Lee, Y. S. Kim, Y. C. Chung, S. J. Kim, *J. Am. Ceram. Soc.*, 2006, **89**, 515-518.
- 62) K. Iketani, R. D. Sun, M. Toki, K. Hirota, O. Yamaguchi, *Mater. Sci. Eng. B*, 2004, **108**, 187-193.
- 63) S. Klosek, D. Raftery, *J. Phys. Chem. B*, 2001, **105**, 2815-2819.
- 64) J. C. S. Wu, C. H. Chen, *J. Photochem. Photobiol. A: Chem.*, 2004, **163**, 509-515.
- 65) L. G. Devi, B. N. Murthy, S. G. Kumar, *Mater. Sci. Eng. B*, 2010, **166**, 1-6.
- 66) F. Ren, H. Li, Y. Wang, J. Yang, *Appl. Catal. B: Environ.*, 2015, **176-177**, 160-172.
- 67) J-H. Yu, S-H. Nam, J. W. Lee, D. In. Kim, J-H. Boo *Appl. Surf. Sci.*, 2018, **In press** Doi. 10.1016/j.apsusc.2018.04.125.
- 68) E. Borgarello, J. Kiwi, M. Gratzel, E. Pelizzetti, M. Visca, *J. Am. Chem. Soc.*, 1982, **104**, 2996-3002.

- 69) M. Anpo, Y. Ichihashi, M. Takeuchi, H. Yamashita, *Stud. Surf. Sci. Catal.*, 1999, **121**, 305-310.
- 70) C. C. Pan, J. C. S. Wu, *Mater. Chem. Phys.*, 2006, **100**, 102-107.
- 71) K. B. Jaimy, S. Ghosh, S. Sankar, K. G. K. Warriar, *Mater. Res. Bull.*, 2011, **46**, 914-921.
- 72) X. Fan, X. Chen, S. Zhu, Z. Li, T. Yu, J. Ye, Z. Zou, *J. Mol. Catal. A: Chem.*, 2008, **284**, 155-160.
- 73) H. M. Yadav, T. V. Kolekar, A. S. Barge, N. D. Thorat, S. D. Delekar, B. M. Kim, B. J. Kim, J. S. Kim, *J. Mater. Sci.*, 2016, **27**, 526-534.
- 74) J. Zhu, Z. Deng, F. Chen, J. Zhang, H. Chen, M. Anpo, J. Huand, L Zhang. *Appl. Catal. B: Environ.*, 2006, **62**, 329-335.
- 75) M. Hamadani, A. S. Sarabi, A. M. Mehra, V. Jabbari, *Mat. Sci. Semicon. Proc.*, 2014, **62**, 161-166.
- 76) J. Choi, H. Park, M. R. Hoffmann, *J. Phys. Chem. C*, 2010, **114**, 783-792.
- 77) S. Kim, S-J. Hwang, W. Choi, *J. Phys. Chem. B*, 2005, **109**, 24260-24267.
- 78) Y. Hu, X. Song, S. Jiang, C. Wei, *Chem. Eng. J.*, 2015, **274**, 102-112.
- 79) H. Kato, A. Kudo, *J. Phys. Chem. B*, 2002, **106**, 5029-5034.
- 80) T. Ohno, F. Tanigawa, K. Fujihara, S. Izumi, M. Matsumura, *J. Photochem. Photobiol. A Chem.*, 1999, **127**, 107-110.
- 81) S. Yamazaki, K. Ichikawa, A. Saeki, T. Tanimura, K. Adachi, *J. Phys. Chem. A*, 2010, **114**, 5092-5098.
- 82) S. Yamazaki, T. Tanimura, A. Yoshida, K. Hori, *J. Phys. Chem. A*, 2004, **108**, 5183-5188.
- 83) T. Tanimura, A. Yoshida, S. Yamazaki, *Appl. Catal. B: Environ.*, 2005, **61**, 346-351.
- 84) S. Yamazaki, H. Tsukamoto, K. Araki, T. Tanimura, I. Tejedor-Tejedor, M. A. Anderson, *Appl. Catal. B: Environ.*, 2001, **33**, 109-117.

- 85) S. Enyan, E. Guo, L. Yin, *J. Mater. Chem.*, 2012, **22**, 5031-5041.
- 86) G. Calleja, D. P. Serrano, R. Sanz, P. Pizarro, A. Garcia, *Ind. Eng. Chem. Res.*, 2004, **43**, 2485-2492.
- 87) R. Liu, Y. Ren, Y. Shi, F. Zhang, L. Zhang, B. Tu, D. Zhao, *Chem. Mater.*, 2008, **20**, 1140-1146.
- 88) Yue, X. Xu, J. T. S. Irvine, P. S. Attidekou, C. Liu, H. He, D. Zhao, W. Zhou, *Chem. Mater.*, **2009**, 21, 2540-2546.
- 89) X. Liu, J. Yang, L. Wang, X. Yang, L. Lu, X. Wang, *Mater. Sci. Eng. A: Struct.*, **2000**, 289, 241-245.
- 90) S. Yamazaki, Y. Fujiwara, S. Yabuno, K. Adachi, K. Honda, *Appl. Catal. B: Environ.*, 2012, **121-122**, 148-153.
- 91) N. Nishiyama, Y. Fujiwara, K. Adachi, S. Yamazaki, *Appl. Catal. B: Environ.*, 2015, **176-177**, 347-353.
- 92) N. Nishiyama, K. Kozasa, S. Yamazaki, *Appl. Catal. A: Gen.*, 2016, **527**, 109-115.
- 93) K. Oujehani, P. Boule, *J. Photochem. Photobiol. A: Chem*, 1992, **68**, 363-373.
- 94) J. Theurich, M. Linder, D. W. Bahnemann, *Langmuir*, 1996, **12**, 6368-6376.
- 95) M. Moonsiri, P. Rangsunvigit, S. Chavadej, E. Gulari, *Chem. Eng. J.*, 2004, **97**, 241-248.
- 96) J.-C. D'Oliveira, G. Al-Sayyed, P. Pichat, *Environ. Sci. Technol.*, 1990, **24**, 990-996.
- 97) S. A. Boyd, D. R. Shelton, *Appl. Environ. Microb.*, 1984, **47**, 272-277.
- 98) H. Al-Ekabi, N. Serpone, E. Pelizzetti, C. Minero, M. Fox, R. B. Draper, *Langmuir*, 1989, **5**, 250-255.
- 99) C. D. Little, A. V. Palumbo, S. E. Herbes, M. E. Lidstrom, R. L. Tyndall, P. J. Gilmer, *Appl. Environ. Microb.*, 1988, **54**, 951-956.
- 100) J. C. Yu, W. Ho, J. Yu, H. Yip, P. K. Wong, J. Zhao, *Environ. Sci. Technol.*, 2005, **39**, 1175-1179.

- 101) A. D. Paola, G. Marci, L. Palmisano, M. Schiavello, K. Uosaki, S. Ikeda, B. Ohtani, *J. Phys. Chem. B*, 2002, **106**, 637-645.
- 102) K. Nagaveni, M. S. Hegde, G. Madras, *J. Phys. Chem. B*, 2004, **106**, 20204-20212.
- 103) H. Feng, M. Zhang, E. L. Yu, *Appl. Catal. A: Gen.*, 2012, **413-414**, 238-244.
- 104) L. Zhang, S. Wang, C. Lu, *Anal. Chem.*, 2015, **87**, 7313-7320.

Chapter 2 Factors affecting the photocatalytic activity of Pt-TiO₂ under visible light irradiation

2. 1. Introduction

Many researchers have reported the synthesis of visible light responsive TiO₂ doped with metal ions.¹⁻¹⁰⁾ A variety of the optimal conditions of M-TiO₂ is ascribed to the difference in the metal ion dopants, the preparation conditions, and chemical reactions used to estimate the photocatalytic activity. Besides, many factors that affect the photocatalytic activity of M-TiO₂ under visible light irradiation have been reported. For example, they are changes in trapping and dynamics of photogenerated carriers due to existence of different oxidation states of doped Pt ions¹⁾, the number of oxygen vacancies²⁾, crystallinity of anatase phase³⁾ and BET specific surface area⁴⁾, etc. However, the most important factor affecting the photocatalytic activity of M-TiO₂ is not fully understood.

Previously, we have prepared porous M-TiO₂ doped with 7 different metal ions by the sol-gel method using only water as solvent and conducting dialysis to purify the obtained TiO₂ sol before drying and reported that Pt-TiO₂ sintered at 200°C showed the highest photocatalytic activity for the degradation of 4-CP.¹¹⁾ 4-CP was oxidatively degraded to hydroquinone and benzoquinone by photogenerated holes and finally degraded to CO₂ (ca. 90.7% of 4-CP was mineralized at the visible light irradiation for 390 min).¹²⁾ However, the most important factors affecting the photocatalytic activity is still unknown. Elucidation of the factor will give a

guideline for the development of more highly active photocatalyst.

In this Chapter, various Pt-TiO₂ photocatalysts with different BET specific surface area or with various ratios of Pt(II)/Pt(IV) were synthesized to clarify the factor affecting the photocatalytic activity.

2. 2. Experimental

2. 2. 1. Materials.

All reagents were purchased from Wako Pure Chemicals Industries Ltd (Osaka, Japan) and used without further purification unless otherwise noted. Ethylenediaminetetraacetic acid (EDTA) was purchased from Kanto Chemical Co., Inc. (Tokyo, Japan). 4-Chlorophenol (4-CP) was purchased from Fluka. P25 (commercially available TiO₂, NIPPON AEROSIL, Tokyo, Japan, AEROXIDE P25, BET specific surface area: 50 m² g⁻¹, average crystalline size: 21 nm, crystal phase: anatase : rutile = 8 : 2) was used for the comparison with the synthesized Pt-TiO₂. Ultrapure water was obtained using a Milli-Q water purification system (Millipore, USA) and used for all experiments. Dialysis tubes were purchased from Spectrum Laboratories (CA, USA) and used after washing. Six of dialysis tubes (molecular weight cut-off: 3500) cut into 23 cm were placed in 1 L of aqueous solution containing 1.0 x 10⁻³ mol dm⁻³ EDTA and 2% NaHCO₃. This solution was stirred for 30 minutes while heating at about 80°C on a hot stirrer

(AS ONE Corporation, Osaka, Japan, CHIPS-170AN), then allowed to cool to room temperature and washed thoroughly with water. The same procedure as above was repeated by using 1 L of water.

2. 2. 2. Preparation of Pt-TiO₂ powder.

Titanium tetraisopropoxide (Ti(OC₃H₇)₄, 95%, 0.955 g cm⁻³, hereafter denoted as TTIP, 0.75 – 20.0 ml) was added dropwise to 180 ml of aqueous solutions containing 1.3 ml of HNO₃. Unless otherwise noted, the TTIP amount of 15 ml is the standard condition. The obtained mixture was peptized at room temperature for 6 days to form a highly dispersed colloidal solution. This TiO₂ sol was then dialyzed in a molecularly porous dialysis tube for 2 days until pH 3 was obtained. An aqueous solution of H₂PtCl₆ · 6H₂O (content of Pt was 0.2 – 1.0 atom% against Ti + Pt) was added to the TiO₂ sol followed by the dialysis for another 1 day. The obtained sol was dried in an oven (ESPEC Corp., Osaka, Japan, ST-120) at 40°C for 3 days and the resulting xerogel was ground into fine powders by using agate mortar and pestle. The powders were sintered by ramping at 3°C min⁻¹ and keeping at 200°C for 2 h (AS ONE corp., Osaka, Japan, MMF-1). Concentration of Pt ion which came out of the TiO₂ sol into water during the dialysis was determined by inductively coupled plasma spectroscopy (Varian, USA, ICP-AES Liberty Series II and Agilent technologies, CA, USA, 5110 ICP-OES) and was used for the calculation of the Pt ion content in Pt-TiO₂. Pure TiO₂ without Pt ions and Pt-TiO₂ prepared without conducting dialysis (Pt-TiO₂(ND)) were also synthesized.

For comparison, Pt-TiO₂(ref) powders were prepared by modifying the literature method.¹⁾ An ethanol solution (25 ml) containing TTIP (1.25 – 20 ml) was added dropwise to 250 ml of H₂PtCl₆ · 6H₂O aqueous solutions containing 0.6 ml of HNO₃ (pH 1.5), in which the amount of H₂PtCl₆ · 6H₂O was varied to keep the Pt content to be 0.5 atom%. The obtained mixture was stirred at room temperature for 5 days and then evaporated at 50°C using a rotary evaporator. The obtained powder was ground into fine powders by using agate mortar and pestle and then sintered at 200°C for 2 h after being heated at the raising rate of 3°C min⁻¹.

2. 2. 3. Characterization of Pt-TiO₂ powder.

X-ray diffraction (XRD, Rigaku, Tokyo, Japan, miniflex 600) analysis was performed with Cu K α radiation (40 kV, 15 mA) at 2 θ angles from 10° to 90° with a scan speed of 10° min⁻¹. The crystallite sizes of the Pt-TiO₂ samples were estimated using the Scherrer formula:

$$D(\text{\AA}) = \frac{K\lambda}{\beta \cos\theta}$$

where D is the approximate crystallite size, λ is the wavelength of the X-ray radiation (Cu: 1.54056 Å), K is the Scherrer constant (0.9), and β is the peak width at half-maximum height. The values of β and θ of anatase and rutile were taken from anatase (101) and rutile (110) diffraction peaks, respectively.^{13, 14)} The BET specific surface area was measured with nitrogen as the adsorptive gas at -195.8°C by automatic surface area analyzer (Micromeritics, USA, Trister II 3020).^{15, 16)} Diffuse reflectance UV-vis absorption spectra of the powder samples

were obtained by using a spectrophotometer (JASCO Corporation, Tokyo, Japan, V-670). The band gap energy of the Pt-TiO₂ sample was estimated from Tauc plot using the following formula:

$$(h\nu\alpha)^{\frac{1}{n}} = A(h\nu - E_g)$$

where h is Planck constant, ν is frequency, α is absorption coefficient, A is proportionality constant, and E_g is the band gap energy. Since TiO₂ is an indirect allowed transition, $n = 2$. The obtained diffuse reflection spectra are Kubelka - Munk converted and the vertical axis is proportional to the absorption coefficient to obtain the following formula:

$$(h\nu(FR_{\infty}))^{\frac{1}{2}} = A(h\nu - E_g)$$

Where FR_{∞} is the K-M function. The valence state of Pt ion near the TiO₂ surface was analyzed by X-ray photoelectron spectroscopy (XPS, Thermo SCIENTIFIC, USA, K-Alpha).

The Pt-TiO₂ powder was placed in a Clear Disk (JASCO, CD-05) and pressed into pellet of 5 mm in diameter using a hand press. The binding energies were calibrated with reference to the C 1s peak (284.8 eV) originating from the surface impurity carbons. The valence state of Pt ion in the TiO₂ bulk was analyzed by X-ray absorption near edge spectroscopy (XANES). The XANES spectra for Pt L_{III} edge were recorded on a beamline 11 at Kyusyu Synchrotron Light Research Center. As reference samples, PtCl₂ and PtO₂ powders were used. Each powder was mixed with boron nitride in an agate mortar for 10 min and then molded into a pellet of 7 mm in diameter by using the hand press. The XANES spectra of this pellet placed in a polyethylene

bag were measured in transmission mode. The synthesized Pt-TiO₂ powder sample was placed in the polyethylene bag and the XANES spectra were measured in fluorescence mode by using a Lytle detector. The femtosecond diffuse reflectance spectra were measured by the pump and probe method by using a regeneratively amplified titanium sapphire laser (Spectra-Physics, Spitfire Pro F, 1 kHz) pumped by a Nd:YLF laser (Spectra-Physics, Empower 15). The seed pulse was generated by a titanium sapphire laser (Spectra-Physics, Mai Tai VFSJW, fwhm 80 fs). The second harmonic generation of the fundamental light was used as the excitation pulse (400 nm, 3 - 4 μJ pulse⁻¹). The white light continuum pulse, which was generated by focusing the residual of the fundamental light on a sapphire crystal, was divided into two parts and used as the probe and the reference lights, of which the latter was used to compensate the laser fluctuation. Pt-TiO₂ was added to ethanol and dispersed by ultrasonication. Then this dispersion solution was spread onto glass cover slip. Both probe and reference lights were directed to the Pt-TiO₂ powder coated on the glass cover slip and the reflected lights were detected by a linear InGaAs array detector with the polychromator (Solar, MS3504).

2. 2. 4. Photocatalytic degradation of 4-CP by using Pt-TiO₂ powder.

The synthesized Pt-TiO₂ (0.2 g) was suspended to 100 ml of 1.0×10^{-4} mol dm⁻³ 4-CP solution in a transparent Pyrex bottle which was immersed in water bath at 30°C. Under air purging (GEX Co., Ltd., Osaka, Japan, LUNG GX100), the suspension was kept in the dark for 30 min to reach the adsorption-desorption equilibrium and then irradiated by 150 W halogen

lamp (ASANUMA & Co., Ltd. Tokyo, Japan, CABIN CS-15) for 150 min. The light intensity through a long pass filter (Edmund, USA, cut-on wavelength: 400 nm) was measured by solar power meter (SATO SHOUJI INC., Japan, SPM-SD) at the center of the Pyrex bottle to be 26 mW cm⁻². For comparison, photocatalytic experiments were performed by using four 4 W black-lights (TOSHIBA CORPORATION, Tokyo, Japan, FL4BLB) as UV light source or solar simulator (ASAHI SPECTRA, Tokyo, Japan, HAL-320). The UV light and solar simulator light intensity was measured to be 3.5 mW cm⁻² by a radiometer (Iuchi, Osaka, Japan, UVR-400, S-365) and 0.1 – 1.0 sun by light intensity meter (ASAHI SPECTRA, Tokyo, Japan, CS-20), respectively. An aliquot sample (7 ml) was withdrawn from the suspension at appropriate times and centrifuged at 2000 rpm for 15 min (AS ONE Corporation, HSIANGTAI CN-1040). The supernatant liquid was filtrated through a 0.20 µm filter (Pall Corporation, NY, USA, E134) and then 4-CP concentration was analyzed by a high performance liquid chromatograph (HPLC, Shimadzu Corporation, Kyoto Japan) equipped with a UV detector (SPD-10AVP, detection wavelength: 280 nm) and a C18 column (Shim-pack, VP-ODS 4.6 mm × 25 cm, column oven CTO-10ASVP, at 40°C). The eluent was a mixture of water with methanol (1 : 1 by volume, flow rate: 1.0 ml min⁻¹ : LC-10ADVP). The conversion of 4-CP associated with light irradiation was calculated by the following formula.

$$\left(\text{Conversion of 4 - CP (\%)}\right) = \frac{(C_0 - C_t)}{C_0} \times 100$$

Where C_0 and C_t represented the initial concentration of 4-CP (mol dm^{-3}) and the concentration of 4-CP (mol dm^{-3}) at the light irradiation time respectively. The photodegradation experiment of 4-CP by using the synthesized photocatalysts were shown in Figure 2-1. Figure 2-2 shows the spectra of the irradiation light measured with a UV-Vis spectrophotometer using a fiber probe.

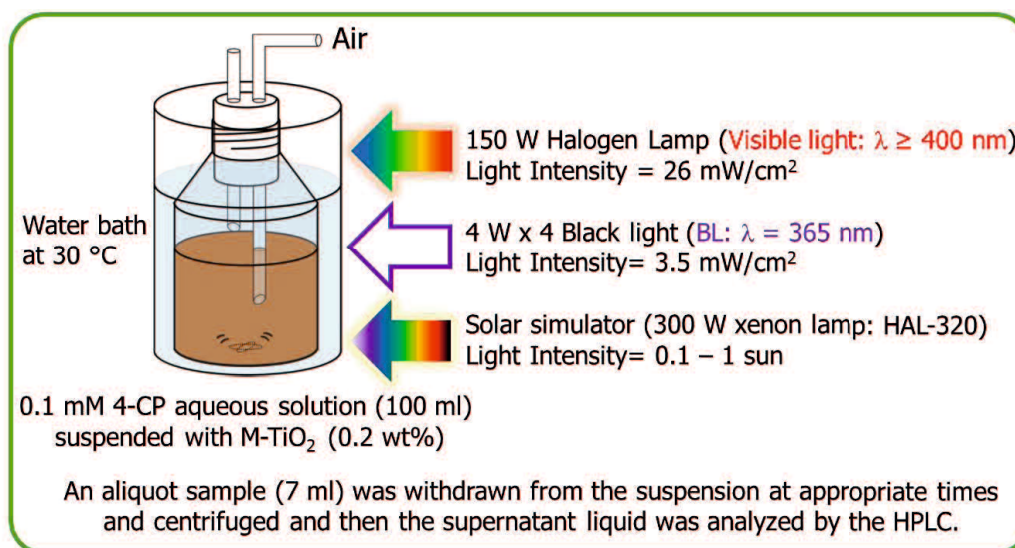


Figure 2-1 Schematic representation of the experimental apparatus.

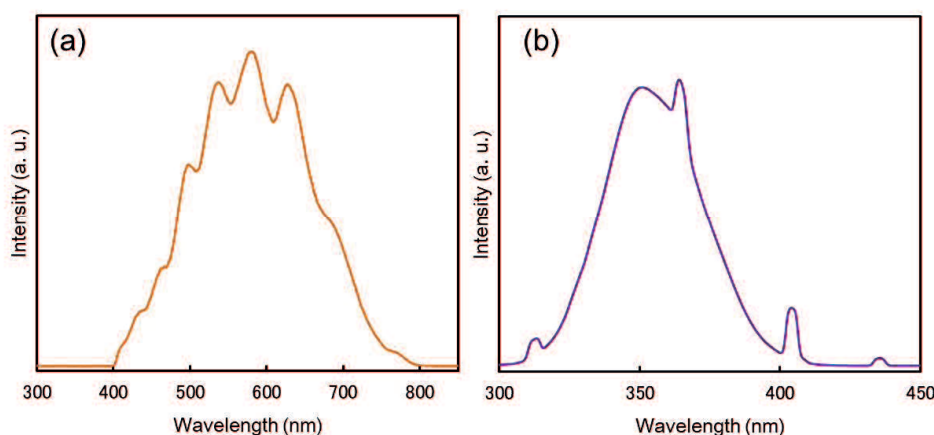


Figure 2-2 Spectra of the light emitted from (a) 150 W halogen lamp and (b) 4 W-black light.

2. 3. Results and Discussion

2. 3. 1. Effect of Pt ion doping.

Figure 2-3 shows the time course of 4-CP conversion on 0.5 atom% Pt-TiO₂, Pt-TiO₂(ND) and TiO₂ under UV or visible light irradiation. Complete degradation of 4-CP, i.e. 100% conversion, was obtained on Pt-TiO₂ under UV irradiation for 60 min or under visible light irradiation for 120 min. It is worthy to note that the photocatalytic activity of Pt-TiO₂ is much higher than TiO₂ under UV irradiation, suggesting that the doped Pt ions hardly act as recombination center of the photogenerated holes and electrons. Figure 2-3 also indicates that the 4-CP conversion is almost the same on Pt-TiO₂ and Pt-TiO₂(ND) under visible light irradiation whereas that on Pt-TiO₂ is higher than that of Pt-TiO₂(ND) under UV irradiation. As shown in Figure 2-4, both Pt-TiO₂ and Pt-TiO₂(ND) were anatase and the crystallite size was estimated to be 4.5 or 4.3 nm, respectively, which was evaluated by Scherrer equation. As shown in Table 2-1, the BET specific surface area of Pt-TiO₂ is 250 m² g⁻¹ which is higher than Pt-TiO₂(ND) by a factor of 1.5. It is generally believed that higher photocatalytic activity is obtained for the catalysts with higher specific surface area since the photocatalytic reaction proceeds on the surface. Thus, higher activity of Pt-TiO₂ than Pt-TiO₂(ND) under UV irradiation as shown in Figure 2-3 is explainable. However, Figure 2-3 also indicates that the photocatalytic activity of Pt-TiO₂ is not affected by the BET specific surface area under visible light irradiation. The reason will be discussed later.

Figure 2-5 shows the effect of Pt doping amount in the range of 0.2 – 1.0 atom% on the 4-CP conversion after visible light irradiation for 90 min, indicating that the photocatalytic activity increases with an increase in the doping amount. Even for 1.0 atom% Pt-TiO₂, no diffraction peak attributable to Pt metal or PtO₂ was detected by XRD measurements (Figure 2-6).¹⁷⁾ Thus, the doped Pt ions are present homogenously inside or between the TiO₂ lattice. With an increase in the doping amount, the band gap energy of Pt-TiO₂ decreases from 2.98 to 2.82 eV (Table 2-1), indicating that higher photocatalytic activity observed at higher doping amount is attributable to an increase in the visible light absorption ability.

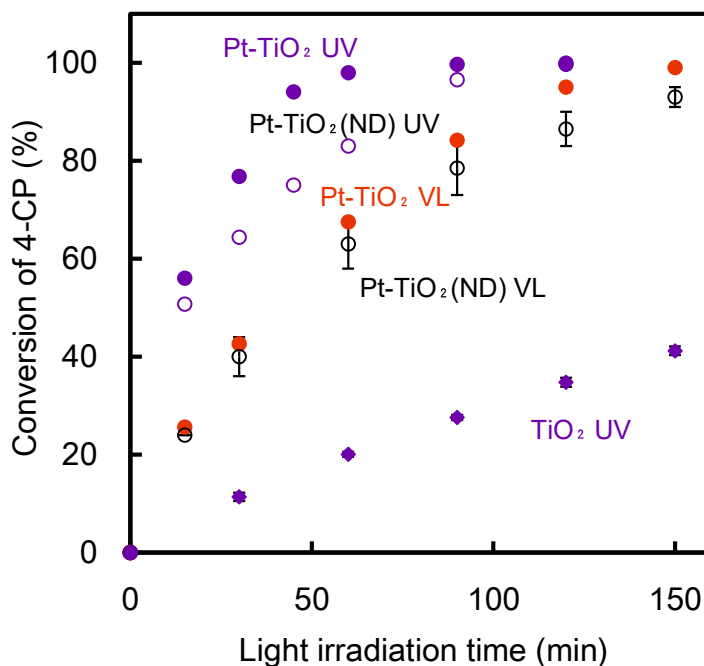


Figure 2-3 Time course of the 4-CP conversion on Pt-TiO₂, Pt-TiO₂(ND) and TiO₂ under visible light (VL) or UV irradiation.

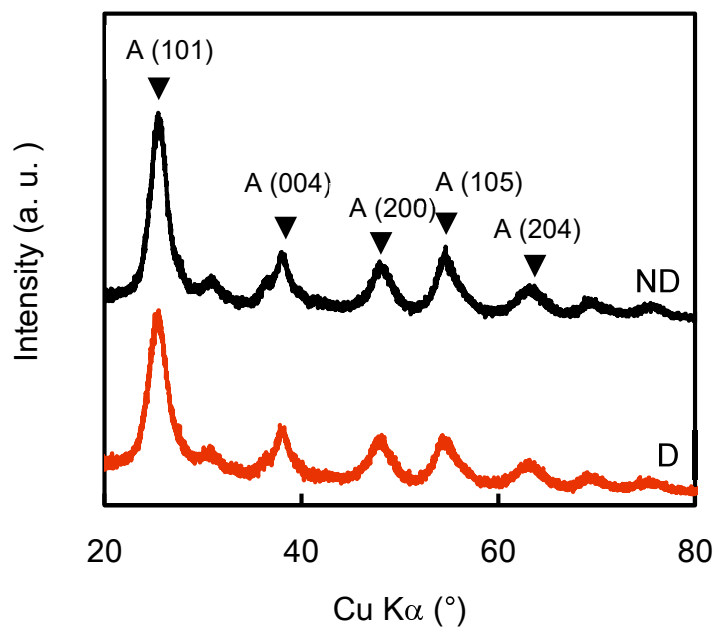


Figure 2-4 XRD patterns of 0.5 atom% Pt-TiO₂(black line) and Pt-TiO₂(ND) (red line).

Symbol A indicates anatase phase.

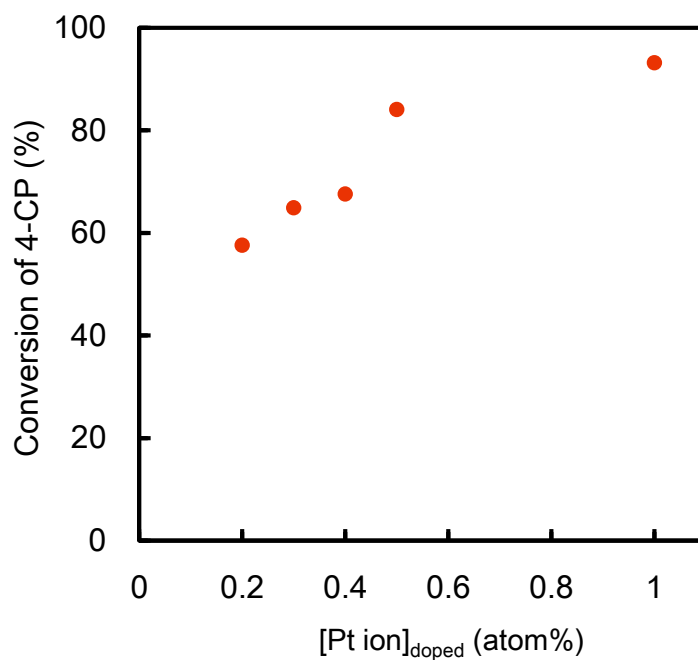


Figure 2-5 Effect of doping amount of Pt ion on the 4-CP conversion after visible light irradiation for 90 min.

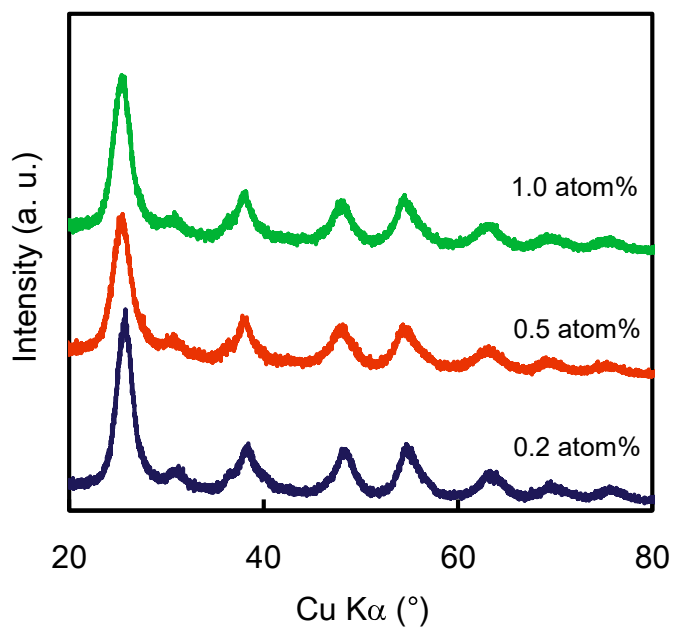


Figure 2-6 XRD patterns of 0.2, 0.5 and 1.0 atom% Pt-TiO₂.

Table 2-1 BET specific surface area, crystallite size and band gap energy of Pt-TiO₂.

doping amount (atom%)	BET specific surface area (m ² g ⁻¹)	crystallite size (nm) ^a	band gap (eV)
0.2	249	4.5	2.98
0.5	250	4.5	2.89
	Without dialysis	4.3	2.86
1.0	270	4.0	2.82

a) Crystallite size was estimated from the XRD peak of anatase (101).

2. 3. 2. Valence states of the doped Pt ions near the surface or in the bulk of TiO₂.

Figure 2-7 shows XPS spectra of 0.5 atom% Pt-TiO₂ and its deconvoluted bands indicate the presence of Pt(II) and Pt(IV) states on the surface. The Pt L_{III} edge XANES spectra of 0.2 – 1.0 atom% Pt-TiO₂ and 0.5 atom% Pt-TiO₂(ND) are presented in Figure 2-8 with reference spectra of PtCl₂ and PtO₂. The sharp absorption band at the Pt L_{III} edge, which is called white line, corresponds to the electron transition from 2p_{3/2} to 5d_{5/2} transition.¹⁸⁾ In general, when the oxidation state of Pt is lower, the density of unoccupied d states is lower, resulting in the decrease in the white line intensity.¹⁹⁾ The Pt ion exists as Pt(IV) in the bulk since the XANES spectra of all Pt-TiO₂ samples resembled the spectrum of PtO₂. Choi *et al.* have reported that a metal ion having an ionic radius similar as Ti(IV) (0.745 Å) is doped by being substituted in the Ti(IV) site while a larger metal ion is most likely located in interstitial positions of the TiO₂ lattice.⁵⁾ The ionic radius of Pt(II) or Pt(IV) is 0.94 Å or 0.765 Å, respectively,²⁰⁾ and thus Pt(II) is significantly larger than Ti(IV). This is coincident with our findings that Pt(II) was detected only by XPS which mainly reflect the chemical environment on the surface and no Pt(II) was detected by XANES which can provide information on the bulk. Kim *et al.* have reported that Pt(II) and Pt(IV) in Pt-TiO₂ synthesized in ethanol-water mixed solvent by the sol-gel method act as trap sites of the photogenerated holes and electrons, respectively, resulting in the suppression of their recombination.¹⁾ As described above, since the photocatalytic activity of Pt-TiO₂ was not affected by the BET specific surface area despite

the surface reaction, we attempted to quantify Pt(II) on the surface of Pt-TiO₂.

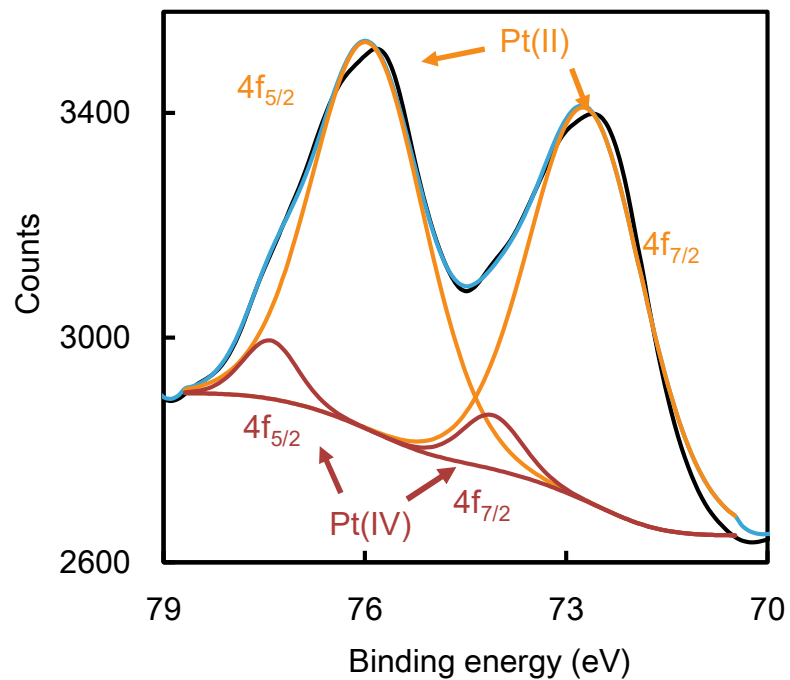


Figure 2-7 XPS spectra of 0.5 atom% Pt-TiO₂.

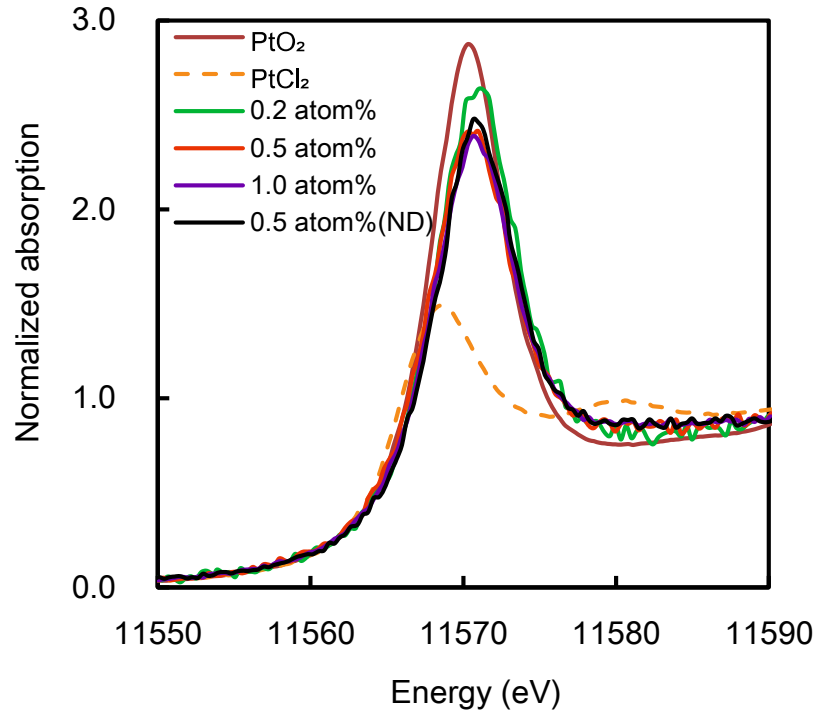


Figure 2-8 XANES spectra of PtO₂, PtCl₂ and Pt-TiO₂ (0.2 - 1.0 atom%) and 0.5 atom% Pt-TiO₂(ND).

2. 3. 3 Quantitative method of Pt(II) existing near the surface of TiO₂.

0.01 g of PtCl₂ (Purity: 98%, 3.68×10^{-5} mol) was mixed with 0.09 g of TiO₂ sintered at 200°C using an agate mortar and pestle for 10 minutes. 0.01 g of the obtained powder was further mixed with 0.09 g of TiO₂ (Pt(II): 3.68×10^{-6} mol) to prepare sample (a). Next, 0.075 g of sample (a) was mixed with 0.025 g of TiO₂ for sample (b). Similarly, 0.05 g of (a) was mixed with 0.05 g of TiO₂ and 0.025 g of (a) was mixed with 0.075 g of TiO₂ to prepare samples (c) and (d), respectively. Sample (e) was TiO₂ powder. Only 0.07 g of each samples ((a) – (e))

was placed in a Clear Disk and formed into pellet of 5 mm in diameter by using a hand press. These pellets were placed in an XPS chamber for 1 day under vacuum before the measurements. Figure 2-9 (a) – (e) shows XPS spectra of the mixture of PtCl₂ and TiO₂. Table 2-2 lists the moles of Pt(II) in samples (a) – (e) used for making a calibration curve where the moles of Pt(II) was multiplied by a factor of 0.7 since only 0.07 g of each samples (total: 0.1 g) was employed for the XPS measurements. Figure 2-9 shows that Pt(0) was detected in sample (a) – (c) although no Pt(0) was observed in Pt-TiO₂ prepared by the sol-gel method. This finding indicates that reduction of Pt(II) to Pt(0) occurs mechanochemically by mixing with TiO₂ powder. Therefore, the following procedures were used to obtain a calibration curve for quantitative Pt(II) near the surface of TiO₂. First, a linear relationship between moles of PtCl₂ used for these samples and the peak area of Pt(II) in the XPS spectra was obtained with a slope of $3.28 \times 10^9 \text{ mol}^{-1}$ (slope A in Figure 2-10).

$$\frac{\text{Peak area of Pt(II)}}{\text{Pt(all) (mol)}} = \text{slope A}$$

Next, a linear relationship between moles of PtCl₂ used for these samples and the sum of the peak areas of Pt(0), Pt(II) and Pt(IV) was obtained with a slope of $5.02 \times 10^9 \text{ mol}^{-1}$ (slope B in Figure 2-11).

$$\frac{\text{Sum of the peak areas of Pt(0), Pt(II) and Pt(IV)}}{\text{Pt(all) (mol)}} = \text{slope B}$$

Thus, the ratio of slope A to slope B was evaluated to be 0.653.

$$\frac{\text{slope A}}{\text{slope B}} = \frac{\text{Peak area of Pt(II)}}{\text{Sum of the peak areas of Pt(0), Pt(II) and Pt(IV)}} = 0.653$$

This value was multiplied by moles of Pt(II) in Table 2-2 for correction and these values were used to make calibration curve for quantitative Pt(II) near the surface of TiO₂. Figure 2-12 shows a linear relationship between moles of Pt(II) (4.21 x 10⁻⁷ - 1.68 x 10⁻⁶ mol) and the peak area due to Pt(II) after the deconvolution of the XPS spectra. Using this linearity, the moles of Pt(II) in 0.2 – 1.0 atom% Pt-TiO₂ were estimated from the XPS spectra. As listed in Table 2-3, the moles of Pt(II) increased from 0.68 x 10⁻⁷ mol in 0.2 atom% Pt-TiO₂ to 10.65 x 10⁻⁷ mol in 1.0 atom% Pt-TiO₂. These values indicate that the Pt(II) ion near the surface is only 3.88 - 12.1% of the total Pt amounts in 0.2 - 1.0 atom% Pt-TiO₂. As an example, the calculation method of 0.2 atom% Pt-TiO₂ is as follows. For the photocatalytic degradation experiments of 4-CP, 0.2 g of Pt-TiO₂ (ca. 2.50 x 10⁻³ mol) was used. In 0.2 atom% Pt-TiO₂, 5.01 x 10⁻⁶ mol of Pt was contained. 0.68 x 10⁻⁷ mol of Pt(II) was detected for 0.07 g of 0.2 atom% Pt-TiO₂ from the XPS measurements. Thus, the percentage of the Pt(II) near the surface

was calculated by the following equation:

$$\frac{0.68 \times 10^{-7} \times \frac{0.2}{0.07}}{5.01 \times 10^{-6}} \times 100 = 3.8779 \approx 3.88 \%$$

Table 2-3 also lists the ratios of peak area of Pt(II) to that of Pt(IV) (Pt(II)/Pt(IV)) which were calculated by deconvoluted bands in the XPS spectra, suggesting that the Pt(II)/Pt(IV) ratios increase with an increase in the doping amounts and are almost the same for 0.5 atom% Pt-TiO₂ and Pt-TiO₂(ND) whose photocatalytic activities are almost the same as shown in Figure 2-3. Higher photocatalytic activity was obtained on Pt-TiO₂ with higher doping amount as mentioned above. Therefore, it is expected that the photocatalytic activity as well as the Pt(II)/Pt(IV) ratios increase by increasing the doping amount more than 1.0 atom%. However, an increase in the Pt doping amounts is costly and thus we tried to find a way to increase the Pt(II)/Pt(IV) ratio of 0.5 atom% Pt-TiO₂ by changing the synthetic conditions.

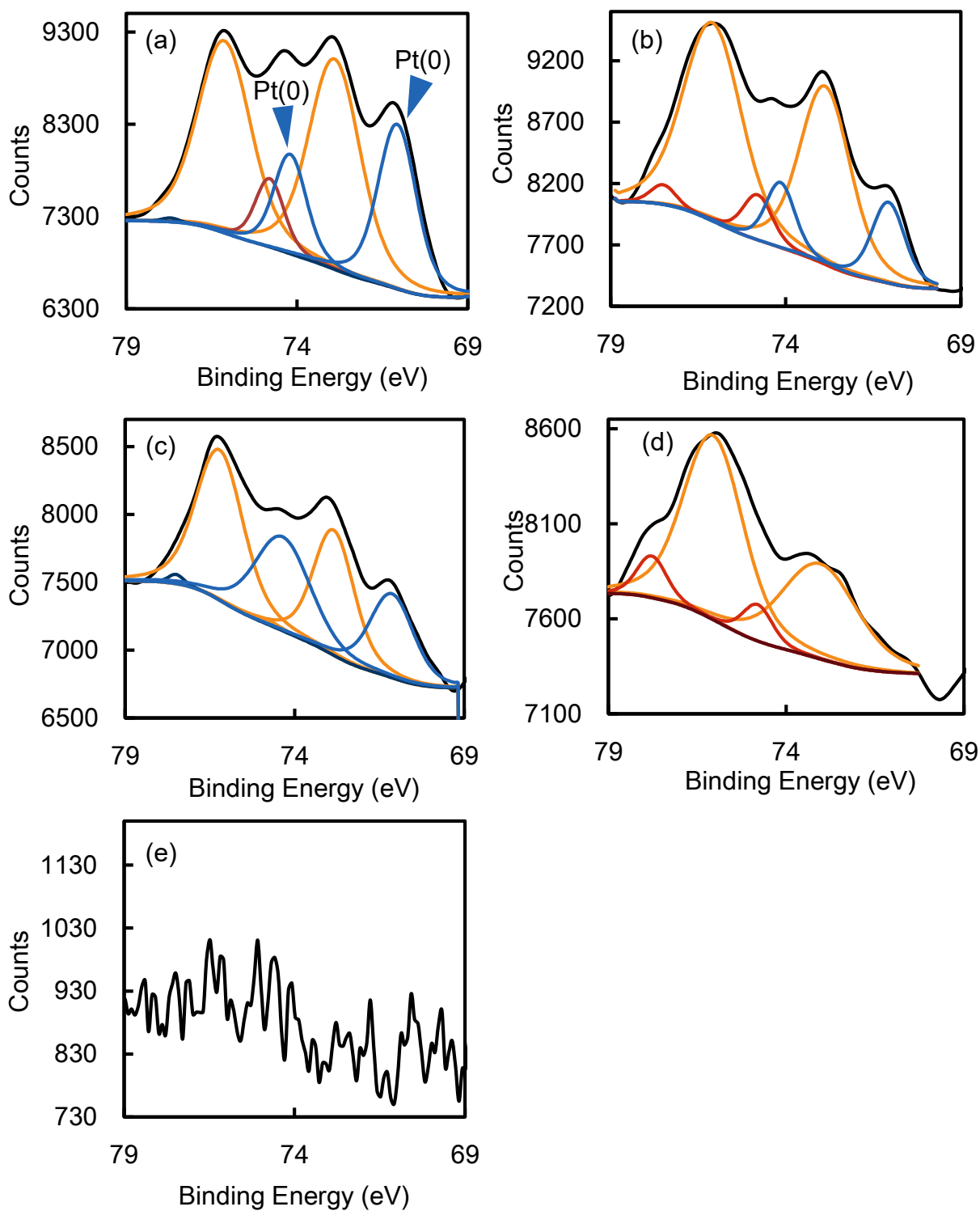


Figure 2-9 XPS spectra of samples (a) – (e) used for making a calibration curve.

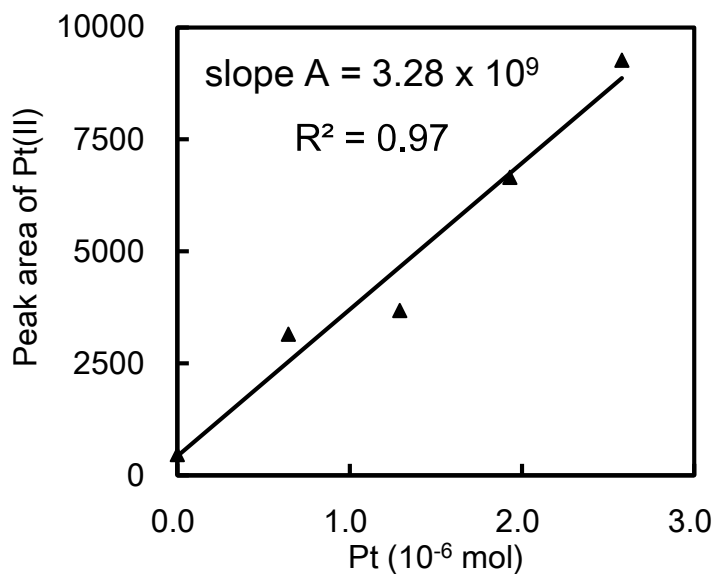


Figure 2-10 Relationship between moles of Pt(II) used for preparation of samples (a) – (e) and the peak area of Pt(II) in XPS spectra.

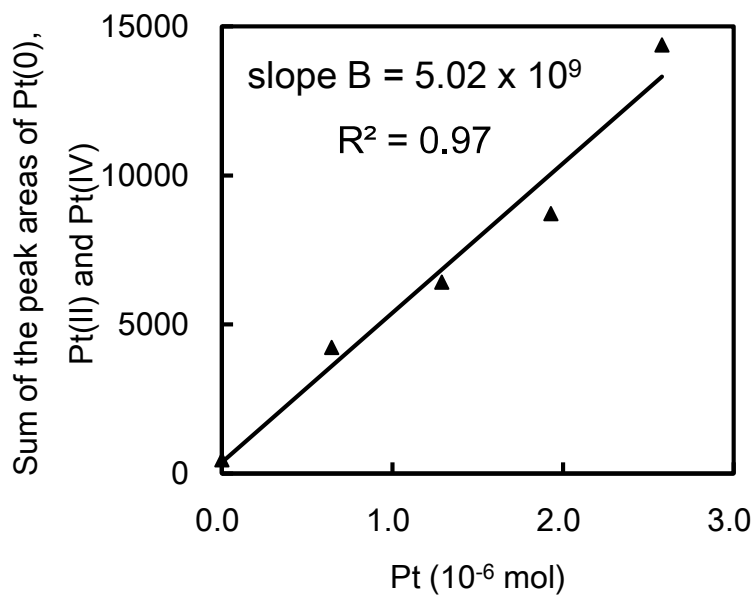


Figure 2-11 Relationship between moles of Pt(II) used for preparation of samples (a) – (e) and the sum of the peak areas of Pt(0), Pt(II) and Pt(IV) in the XPS spectra.

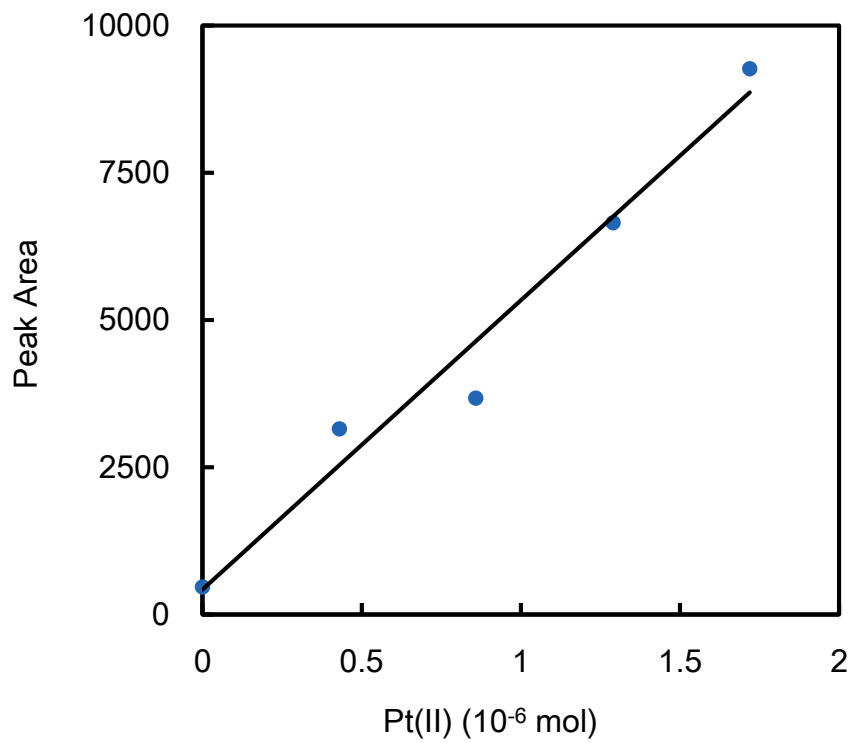


Figure 2-12 Dependence of the peak area of Pt(II) obtained by peak deconvolution of XPS spectra on the moles of Pt(II) mixed with TiO₂.

Table 2-2 Moles of Pt(II) and their corrected values for making a calibration curve.

sample	moles of Pt(II) (10^{-6} mol)	moles of Pt(II) corrected (10^{-6} mol)
(a)	2.58	1.68
(b)	1.93	1.26
(c)	1.29	0.84
(d)	0.64	0.42
(e)	0	0

Table 2-3 Amounts and the peak area of Pt(II) and the Pt(II)/Pt(IV) ratio of Pt-TiO₂ and Pt-TiO₂(ND).

doping amount (atom%)	[Pt(II)] (10^{-7} mol)	peak area of Pt(II) (10^2)	$\frac{\text{peak area of Pt(II)}}{\text{peak area of Pt(IV)}}$
0.2	0.68	7.65	2.0
0.5	5.13	29.96	14.0
	Without dialysis	4.49	26.75
1.0	10.65	57.69	31.5

2. 3. 4. Effect of Pt(II)/Pt(IV) on the photocatalytic activity.

We have found that the Pt(II)/Pt(IV) ratio in 0.5 atom% Pt-TiO₂ can be controlled by changing the volume of TTIP used for TiO₂ synthesis (Table 2-4). Figure 2-13 shows that Pt(II) estimated from the XPS spectra of 0.5 atom% Pt-TiO₂ increases from 1.08×10^{-7} to 1.46×10^{-6} mol by adding 0.75 – 20 ml of TTIP to 180 ml of aqueous HNO₃ solution in the sol-gel method. Concerning the formation of Pt(II), it is likely that some of H₂PtCl₆ are reduced by C₃H₇OH which is produced via hydrolysis of TTIP. An increase in the TTIP volume used in the synthesis gives high concentration of C₃H₇OH, leading to acceleration of the reduction of Pt(IV) to Pt(II). The Pt(II)/Pt(IV) ratio was estimated from the peak area of the deconvoluted bands in XPS spectra and its dependence on the moles of TTIP was plotted in Figure 2-13, indicating a similar dependence to the amounts of Pt(II) determined quantitatively.

The photocatalytic degradation of 4-CP was performed on 0.5 atom% Pt-TiO₂ with various Pt(II)/Pt(IV) ratios. Figure 2-14 indicates that the 4-CP conversion increases linearly with an increase in the Pt(II)/Pt(IV) ratio regardless of the visible light irradiation time of 30, 60 and 90 min. This finding suggests that the Pt(II)/Pt(IV) ratio is the important factor affecting the photocatalytic activity of Pt-TiO₂.

In order to examine the validity of this finding, Pt-TiO₂(ref) was synthesized by conducting hydrolysis of TTIP in HNO₃ aqueous solution containing ethanol. In our method using only water as the solvent, white precipitates (Ti(OH)₄) are formed and stirring vigorously

for a few days is necessary to disperse them into homogenous sol. For saving time, many research groups have synthesized metal ion doped TiO₂ in an aqueous solution containing ethanol and metal ion precursors.^{1, 5)} Previously, we compared the photocatalytic activity of Pt-TiO₂ with Pt-TiO₂(ref) that was prepared by the standard method reported by Kim *et al.*¹⁾ and reported that the photocatalytic activity of our Pt-TiO₂ was much higher than Pt-TiO₂(ref) under both UV and visible light irradiation.¹²⁾ However, in this study, we have found that the Pt(II)/Pt(IV) ratio in 0.5 atom% Pt-TiO₂ and Pt-TiO₂(ref) were 14.0 and 10.3, respectively. The Pt-TiO₂(ref) powders with the Pt(II)/Pt(IV) ratio of 4.2, 9.7, 10.3 and 13.8 was prepared by changing the TTIP concentration. As shown in Figure 2-14 with open circles, the 4-CP conversion on Pt-TiO₂(ref) increases linearly with an increase in the Pt(II)/Pt(IV) ratio and nearly equals to that on Pt-TiO₂ when being compared at the same Pt(II)/Pt(IV) ratio. Figure 2-15 indicates that the 4-CP conversion on Pt-TiO₂ increases linearly with an increase in the Pt(II)/Pt(IV) ratio under UV irradiation for 15 or 30 min. Therefore, regardless of the synthetic method and the light source, similar linearly was obtained between the 4-CP conversion and the Pt(II)/Pt(IV) ratio, indicating that the Pt(II)/Pt(IV) ratio is a key factor affecting the photocatalytic activity of Pt-TiO₂.

On the basis of the above results, a schematic representation of the reaction mechanism of Pt-TiO₂ is shown in Scheme 2-1. The XPS and XANES measurements revealed that Pt(II) and Pt(IV) existed near the TiO₂ surface and only Pt(IV) existed in the TiO₂ bulk. It

is likely that the photogenerated electrons are trapped at Pt(IV) in the bulk and the photogenerated holes can escape from the recombination with the photogenerated electrons and reach the Pt(II) site on the surface, where 4-CP is oxidized. Since Pt(IV) is present from the surface to the bulk, the trapped electrons migrate by hopping towards to the surface and react with oxygen. Spatial separation of photogenerated carriers through the co-existence of Pt(II) and Pt(IV) and the presence of more Pt(II) near the surface might be the reason why the Pt(II)/Pt(IV) ratio affect the photocatalytic activity under visible light irradiation. At higher Pt(II)/Pt(IV) ratio on the surface, the distribution of Pt(II) is more biased and more photogenerated holes can exist near the surface for the degradation of 4-CP.

The photocatalytic activity under visible light irradiation was not dependent on the BET specific surface area whereas, under UV irradiation, Pt-TiO₂ (specific surface area: 250 m² g⁻¹) exhibited higher activity than Pt-TiO₂(ND) (167 m² g⁻¹). Such a difference might be due to the number of photogenerated holes and electrons. Under visible light irradiation whose energy is less than the band gap, electrons are excited from the VB of TiO₂ to the energy levels below the CB, which are formed by the doped Pt ion. The flat band potentials of Pt-TiO₂(ref) were shifted positively by 50 mV, indicating that the CB edge position in Pt-TiO₂ is slightly lowered.¹⁾ Therefore, the charge separation of absorbed photons to electrons and holes occurs near the doped Pt ion. On the other hand, under UV irradiation, electrons are excited to the CB on all the illuminated surface of TiO₂. That is, more holes and electrons are generated on the

Pt-TiO₂ surface under UV irradiation, suggesting that the surface reaction with the adsorbed 4-CP is rate-determining step. The presence of more 4-CP adsorbed on Pt-TiO₂ with larger specific surface area can enhance the degradation rate of 4-CP. On the other hand, under visible light irradiation, migration of photogenerated holes and electrons to the Pt-TiO₂ surface is rate-determining step and thus the amounts of 4-CP adsorbed on the Pt-TiO₂ surface do not affect the degradation rate.

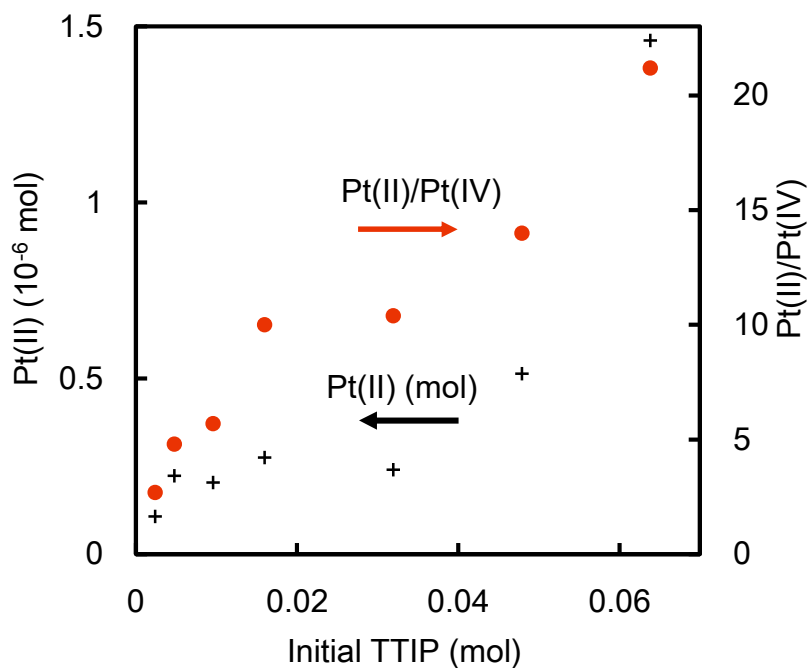


Figure 2-13 Dependence of the moles of Pt(II) or the Pt(II)/Pt(IV) ratio in 0.5 atom% Pt-TiO₂ on the moles of TTIP used for the sol-gel synthesis.

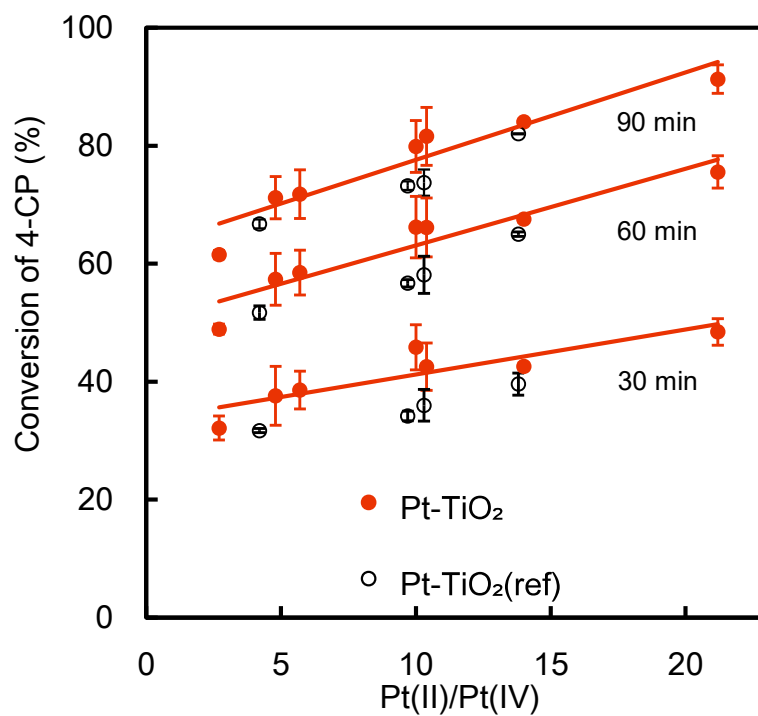


Figure 2-14 Effect of the Pt(II)/Pt(IV) ratio of Pt-TiO₂ (red solid circle) and Pt-TiO₂(ref) (black open circle) on the 4-CP conversion at the visible light irradiation for 30, 60 and 90 min.

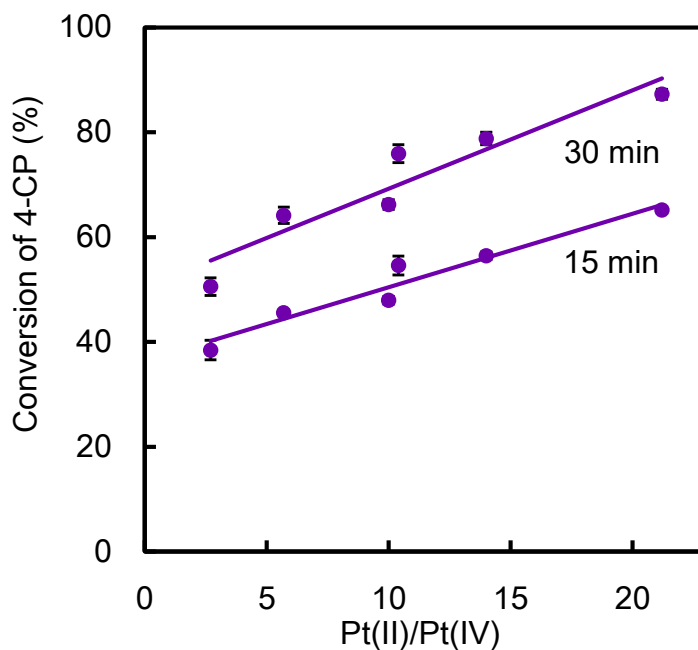
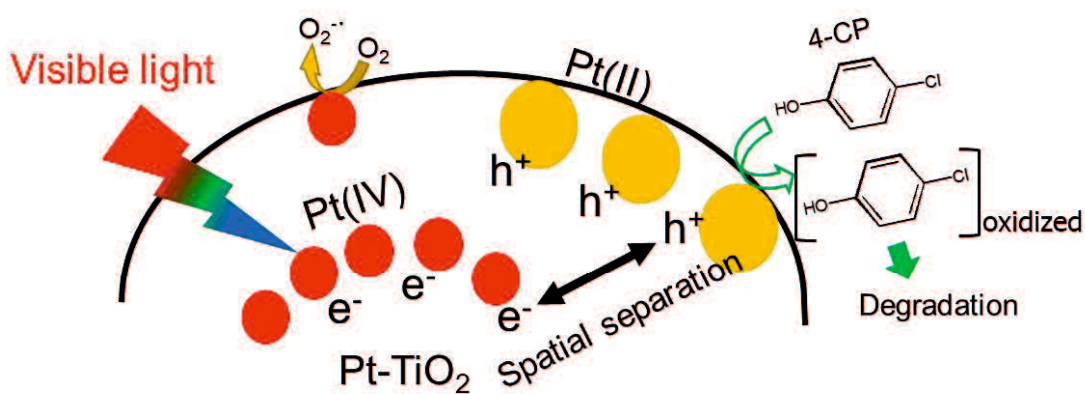


Figure 2-15 Effect of the Pt(II)/Pt(IV) ratio of Pt-TiO₂ on the 4-CP conversion at the UV irradiation for 15 and 30 min.



Scheme 2-1 Proposed mechanism of separation of photogenerated carriers by Pt(II) and Pt(IV) which act as hole and electron traps, respectively.

Table 2-4 Moles of TTIP, crystallite size, band gap energy and Pt(II)/Pt(IV) ratio.

TTIP (10 ⁻² mol)	BET specific surface area (m ² g ⁻¹)	crystallite size (nm) ^a	band gap (eV)	$\frac{\text{peak area of Pt(II)}}{\text{peak area of Pt(IV)}}$
0.239	282	3.9	2.94	2.7
0.479	277	4.1	2.89	4.8
0.958	259	3.9	2.90	5.7
1.596	276	4.0	2.86	10.0
3.192	263	4.1	2.88	10.4
4.788	250	4.5	2.89	14.0
6.385	256	4.6	2.93	21.2

a) Crystallite size was evaluated from the XRD peak of anatase (101).

2. 3. 5. Effect of Pt(II)/Pt(IV) on the dynamics of the photogenerated carriers of Pt-TiO₂.

In order to investigate the lifetime and dynamics of photogenerated carriers, time-resolved diffuse reflectance (TDR) spectra measurements were carried out. Figure 2-16 shows TDR spectra of 0.5 atom% Pt-TiO₂ sintered at 200°C (Pt(II)/Pt(IV) = 14.0), indicating a broad absorption around 820 - 1050 nm. Similar spectra were obtained with Pt-TiO₂ regardless of the Pt(II)/Pt(IV) values. Many researchers have reported that absorption around 800 - 1000 nm is assigned to the absorption of trapped electrons.²¹⁻²⁴⁾ Electrons in Pt-TiO₂ are excited from VB of TiO₂ to the acceptor level due to Pt(IV) under visible light. Pt(IV) acts as an electron acceptor.^{1, 25)} That is, the absorption shown in Figure 2-16 is attributed to electrons trapped in Pt(IV). Figure 2-17 shows the time profile of normalized transient absorbance at ca. 1000 nm

of 0.5 atom% Pt-TiO₂ with Pt(II)/Pt(IV) ratio of 2.7 – 21.2. These time profiles were fitted by two-exponential functions and their lifetimes are summarized in Table 2-5 where τ_1 is assigned to trapped electrons on the Pt(IV) and τ_2 is responsible for the diffusion (hopping) of trapped electrons to another Pt(IV) sites. Then, the trapped electrons disappears by charge recombination with the photogenerated holes at VB of TiO₂ or holes trapped by Pt(II). Figure 2-18 (a) and (b) show the relationship between τ_1 , τ_2 and 4-CP conversion at the visible light irradiation for 90 min. Figure 2-19 (a) and (b) show the relationship of the ratio of Pt(II)/Pt(IV) and τ_1 or τ_2 . As shown in Figure 2-18 and 2-19, a linear relationship between lifetime of the photogenerated electrons and the 4-CP conversion or the Pt(II)/Pt(IV) ratio is obtained.

Besides, it has reported that the absorption of trapped holes of TiO₂ appears around 400 - 700 nm.^{21, 26, 27)} Therefore, in order to investigate the lifetime and dynamics of photogenerated holes, the TDR spectra were measured in the visible light region. Figure 2-20 shows the TDR spectra in the visible light region of 0.5 atom% Pt-TiO₂ sintered at 200°C with the Pt(II)/Pt(IV) ratio of 14.0, indicating two absorption peaks around 580 and 630 nm. They are assumed to be absorption of holes trapped by Pt(II). Regardless of the Pt(II)/Pt(IV) ratios, two absorption peaks were always obtained. Since the absorption at 630 nm might be affected by the spectra of the photogenerated electrons, the absorption at ca. 580 nm was time-resolved. Figure 2-21 shows the time profile of normalized transient absorbance at ca. 580 nm of 0.5 atom% Pt-TiO₂ with the Pt(II)/Pt(IV) ratio of 2.7 – 21.2. These time profiles were fitted by

two-exponential functions and their lifetimes are summarized in Table 2-6. Where τ_3 is assigned to trapped holes on Pt(II) and τ_4 is responsible for the diffusion (hopping) of trapped holes to another Pt(II) sites. The trapped holes disappear by charge recombination with trapped electrons at Pt(IV). Figure 2-22 (a) and (b) show the relationship between the 4-CP conversion and τ_3 , τ_4 at the visible light irradiation for 90 min. Figure 2-23 (a) and (b) show the relationship of the ratio of Pt(II)/Pt(IV) and τ_3 or τ_4 . As shown in Figure 2-22 and 2-23, a linear relationship between lifetime of the photogenerated holes and the 4-CP conversion or the Pt(II)/Pt(IV) ratio is obtained. As shown in Figures 2-18, 2-19, 2-22, and 2-23, it is revealed that the lifetime of the photogenerated carriers become longer in Pt-TiO₂ with the higher Pt(II)/Pt(IV) ratios. These findings indicate that the spatial separation of trap sites for the photogenerated carriers is very important for the photocatalytic activity under visible light irradiation. These obtained data have qualitatively demonstrated for the first time that the lifetime of the photogenerated carriers are prolonged with Pt-TiO₂ containing the Pt(II) and Pt(IV) shown in Scheme 2-1.

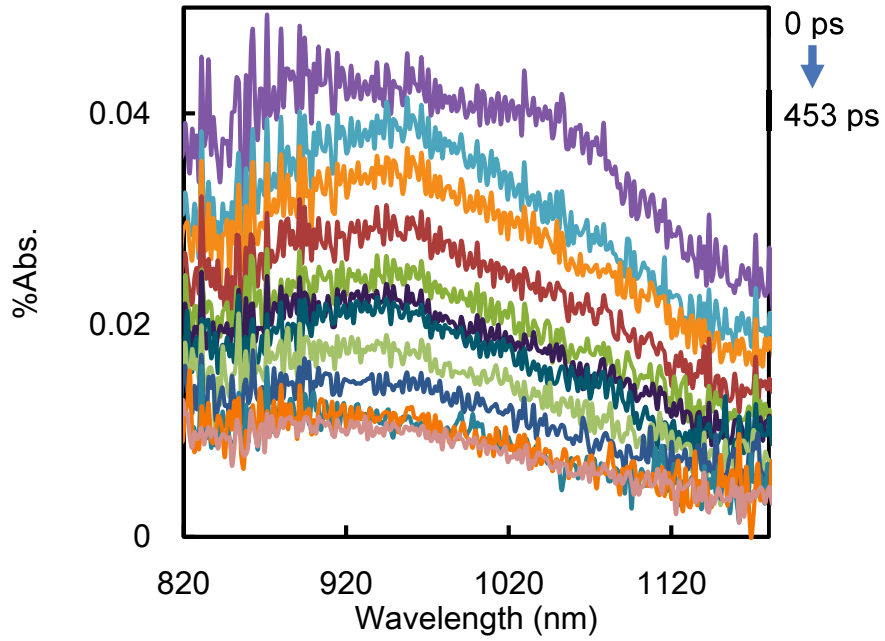


Figure 2-16 TDR spectra of 0.5 atom% Pt-TiO₂ (Pt(II)/Pt(IV) = 14.0) sintered at 200°C.

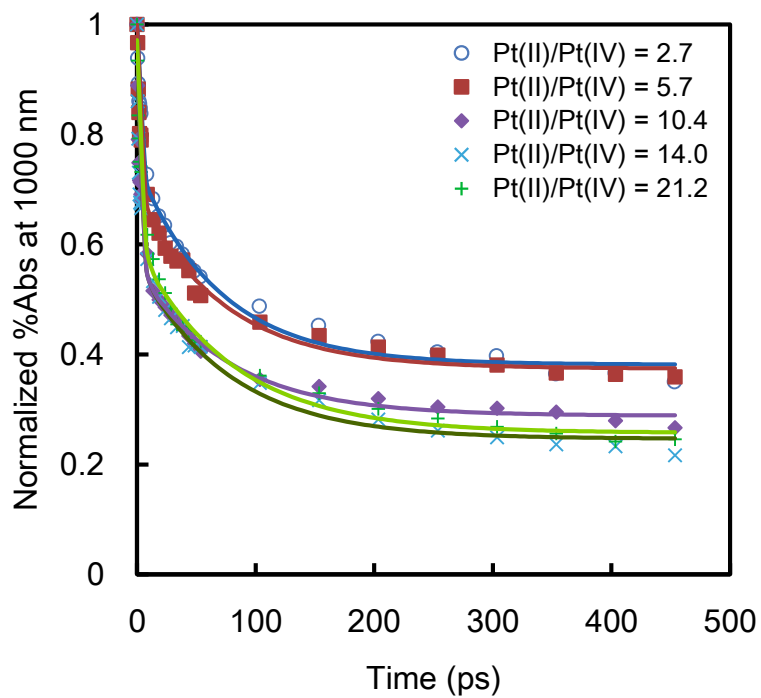


Figure 2-17 Time profiles of normalized transient absorption at ca. 1000 nm of Pt-TiO₂ with various Pt(II)/Pt(IV) ratios.

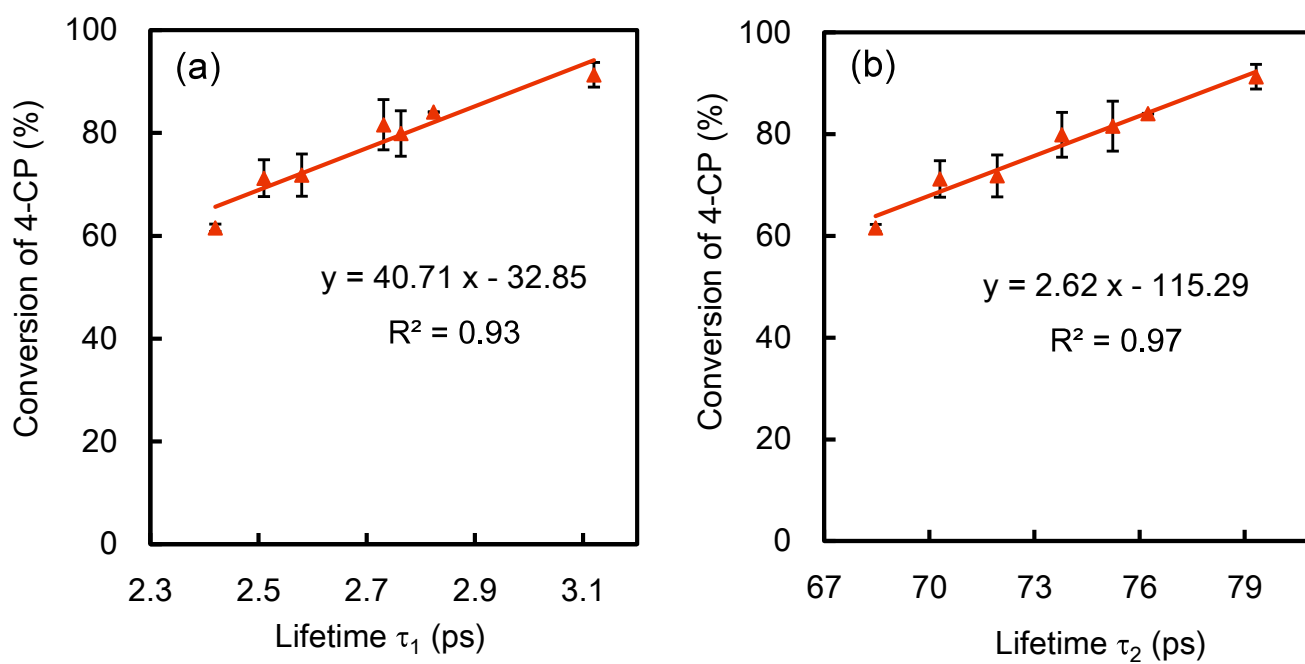


Figure 2-18 Relationship between the 4-CP conversion and the lifetime of the photogenerated electrons (a) τ_1 or (b) τ_2 . The 4-CP conversion was obtained at visible light irradiation for 90 min.

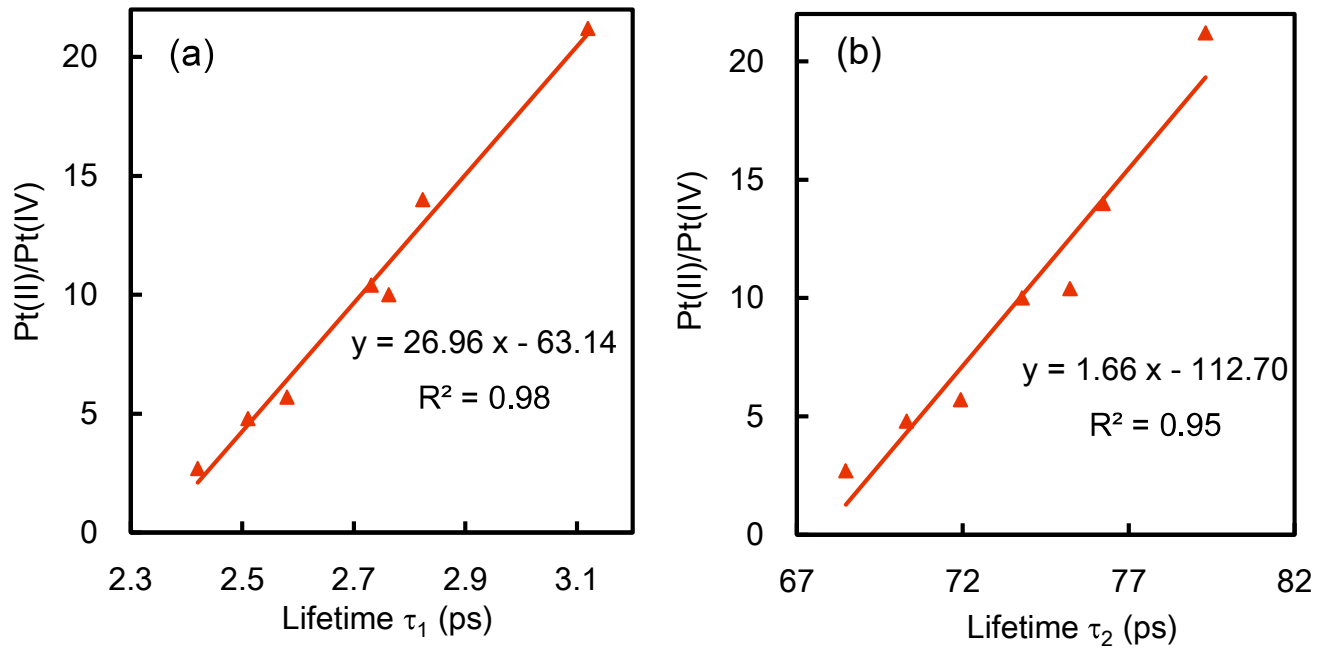


Figure 2-19 Relationship between the Pt(II)/Pt(IV) ratio and the lifetime of the photogenerated electrons (a) τ_1 or (b) τ_2 .

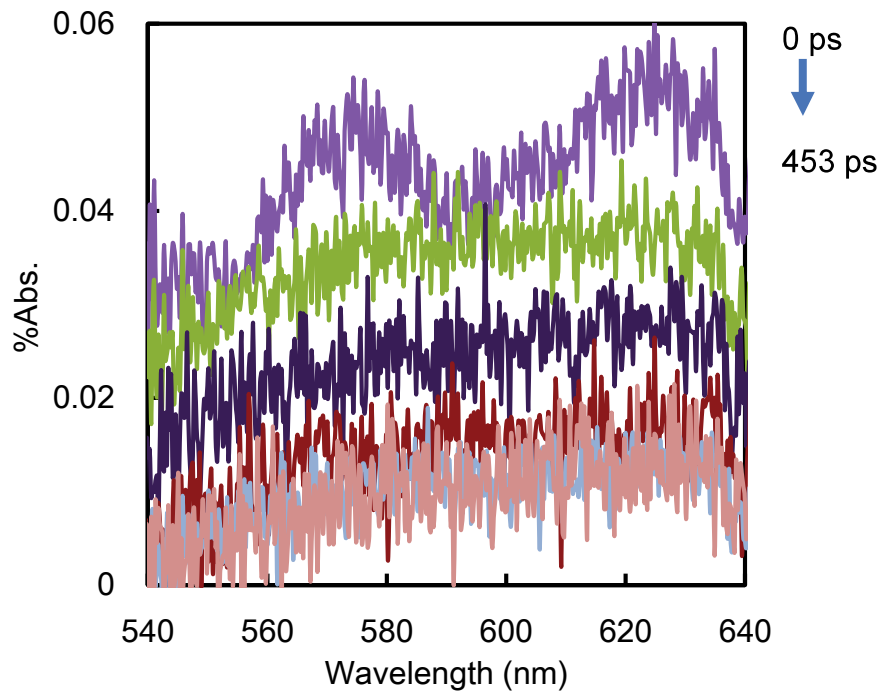


Figure 2-20 TDR spectra of 0.5 atom% Pt-TiO₂ (Pt(II)/Pt(IV) = 14.0) sintered at 200°C.

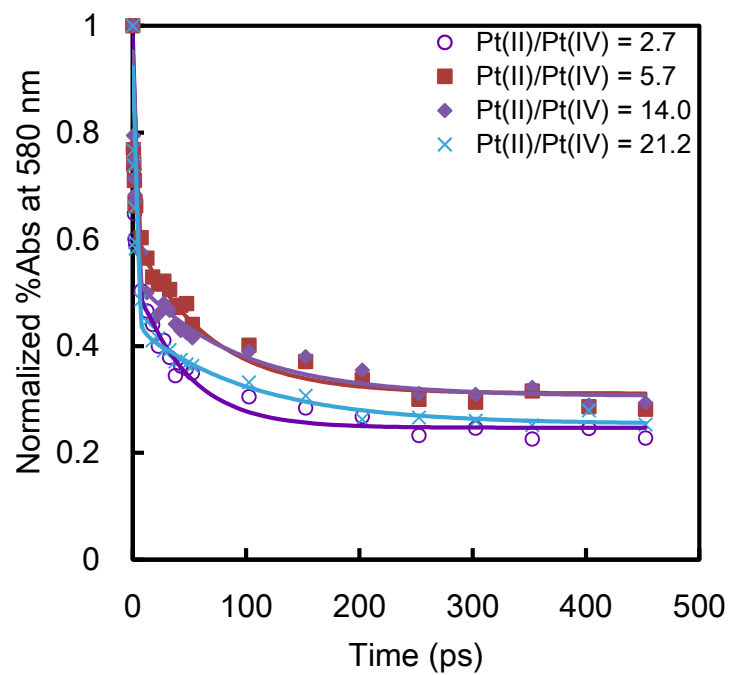


Figure 2-21 Time profiles of normalized transient absorption at 580 nm for Pt-TiO₂ with various Pt(II)/Pt(IV) ratios.

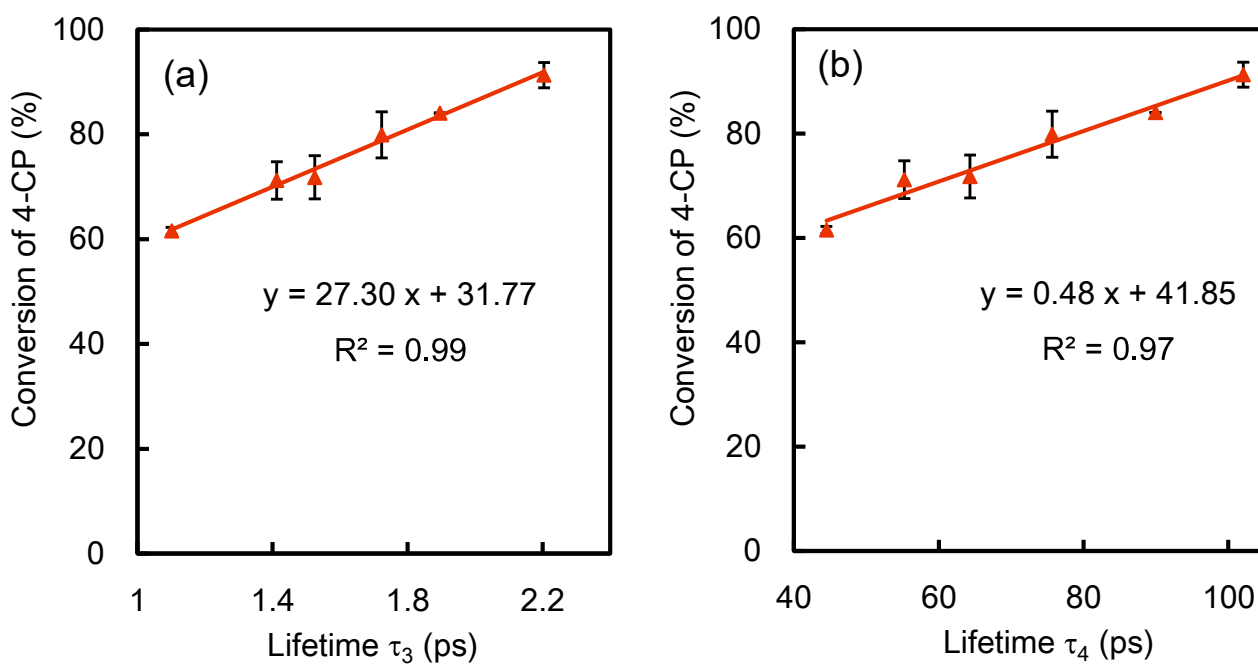


Figure 2-22 Relationship between the 4-CP conversion and the lifetime of photogenerated holes

(a) τ_3 or (b) τ_4 . The 4-CP conversion was obtained at visible light irradiation for 90 min.

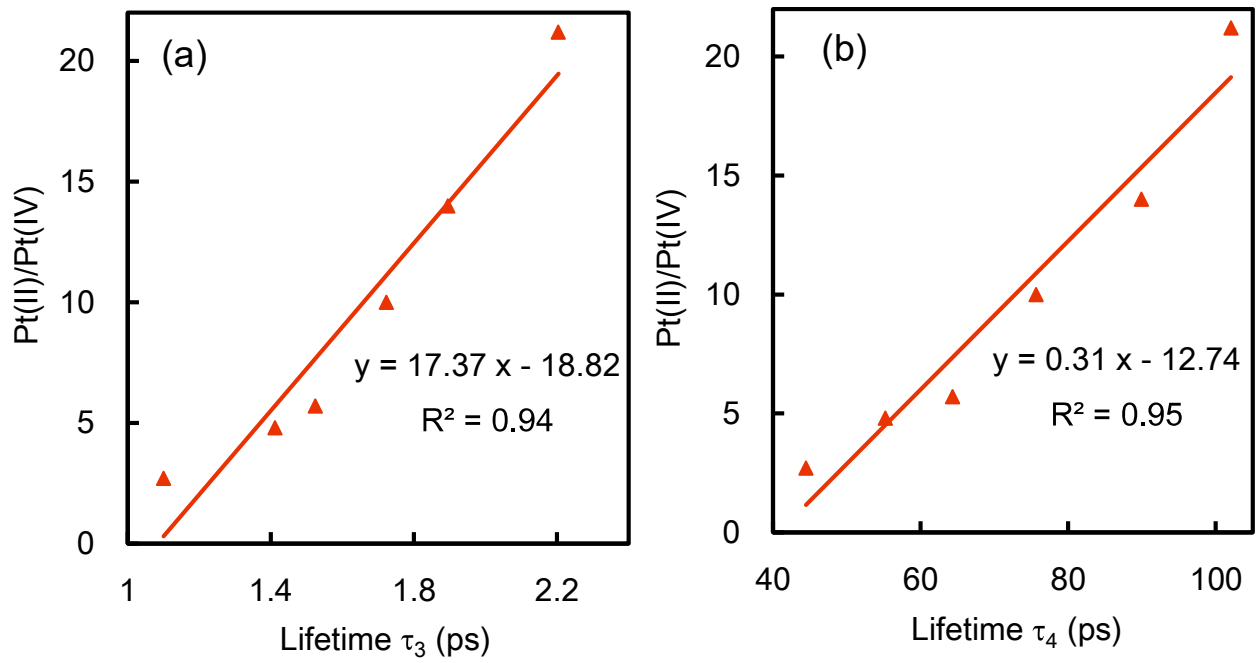


Figure 2-23 Relationship between the Pt(II)/Pt(IV) ratio and the lifetime of the photogenerated holes (a) τ_3 or (b) τ_4 .

Table 2-5 Lifetime of the photogenerated electrons of 0.5 atom% Pt-TiO₂ with various Pt(II)/Pt(IV) ratios. (Excitation wavelength: 400 nm)

Pt(II)/Pt(IV)	τ_1 (ps)	τ_2 (ps)
2.7	2.4 (41.0%)	68.5 (59.0%)
4.8	2.5 (48.1%)	70.3 (51.9%)
5.7	2.6 (48.4%)	71.9 (51.6%)
10.0	2.8 (53.2%)	73.8 (46.8%)
10.4	2.7 (59.7%)	75.2 (40.3%)
14.0	2.8 (52.9%)	76.2 (47.1%)
21.2	3.1 (52.1%)	79.3 (47.9%)

Table 2-6 Lifetime of the photogenerated holes of 0.5 atom% Pt-TiO₂ with various Pt(II)/Pt(IV) ratios. (Excitation wavelength: 400 nm)

Pt(II)/Pt(IV)	τ_3 (ps)	τ_4 (ps)
2.7	1.1 (60.3%)	44.5 (39.7%)
4.8	1.4 (64.5%)	55.2 (35.5%)
5.7	1.5 (51.6%)	64.3 (48.4%)
10.0	1.7 (43.9%)	75.7 (56.1%)
14.0	1.9 (65.6%)	90.0 (34.4%)
21.2	2.2 (71.6%)	102.1 (28.4%)

2. 3. 6. Photocatalytic activity of Pt-TiO₂ and TiO₂ under irradiation from solar simulator.

Figure 2-24 shows the time course of 4-CP conversion on 0.5 atom% Pt-TiO₂, TiO₂ and P25 under irradiation from solar simulator. One Sun corresponds to the light intensity of sunlight of A. M. 1.5 and equals about 100 mW cm⁻². Japan is located at 35° north latitude and the inclination of the earth's axis is 23.4°. Thus, the sun altitude at winter solstice and summer solstice are 31.6° and 78.4°, respectively. That is, each light intensity becomes 100 mW cm⁻² × sin 31.6° or 100 mW cm⁻² × sin 78.4 °, which is calculated to be 52.4 mW cm⁻² or 98.0 mW cm⁻², respectively. It corresponds to about 0.5 or 1.0 Sun, respectively. Under 1 Sun irradiation, 100% 4-CP was degraded on Pt-TiO₂ for 20 min. As the reaction proceeded, some new peaks were observed in the HPLC measurement, which were probably attributable to hydroquinone and benzoquinone. These peaks of the by-products disappeared completely after the irradiation for 50 min. As shown in Figure 2-24, even under 0.1 Sun irradiation, ca. 100% 4-CP is degraded for 90 min. Comparison of Pt-TiO₂ with P25 which is a commercially available TiO₂ has revealed that Pt-TiO₂ is more active photocatalyst than P25 under 1 Sun irradiation. Therefore, Pt-TiO₂ synthesized in this study is superior photocatalyst to P25 for the environmental remediation under solar light.

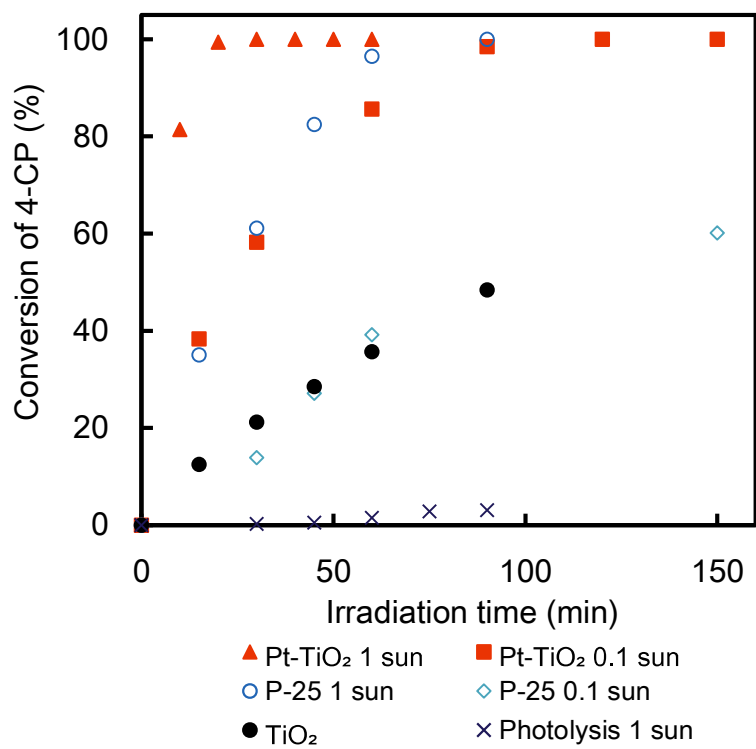


Figure 2-24 Time course of the 4-CP conversion on Pt-TiO₂, TiO₂ and P25 under solar simulator light irradiation.

2. 4. Conclusion

Visible light driven Pt-TiO₂ photocatalysts with the BET specific surface area larger than 240 m² g⁻¹ were prepared by conducting dialysis in the sol-gel method. In Pt-TiO₂, Pt(II) and Pt(IV) existed near the TiO₂ surface and only Pt(IV) existed in the TiO₂ bulk. The amount of Pt(II) as well as the Pt(II)/Pt(IV) ratio in 0.5 atom% Pt-TiO₂ increased by changing the TTIP concentration in aqueous HNO₃ solution during the sol - gel synthesis. We can conclude that the Pt(II)/Pt(IV) ratio is the important factor determining the photocatalytic activity of Pt-TiO₂ under visible light irradiation. We demonstrated for the first time that the photocatalytic activity increased linearly with the ratio of Pt(II)/Pt(IV) in Pt-TiO₂ by developing the analytical method for estimating the Pt(II)/Pt(IV) ratio as well as the synthetic method to prepare Pt-TiO₂ having various Pt(II)/Pt(IV) ratios. This finding was also demonstrated for Pt-TiO₂ prepared by the conventional sol-gel method, suggesting that many inconsistent results which have been reported so far for optimal synthetic conditions of Pt-TiO₂ might be systematically understood by examining the Pt(II)/Pt(IV) ratio of Pt-TiO₂ used for their experiments. In addition, the femtosecond TDR spectra measurements revealed that the lifetime of the photogenerated carriers increased linearly with the Pt(II)/Pt(IV) ratio in Pt-TiO₂. Moreover, linear relationships were obtained between the photocatalytic activities and the lifetime of the photogenerated carriers. Our Pt-TiO₂ showed much higher photocatalytic activity than P25 (commercially available TiO₂) under solar simulator light irradiation. That is, our results indicate that

controlling the mixed valence states of metal dopants in TiO₂ is a new strategy to develop highly active photocatalysts under solar light.

References

- 1) S. Kim, S-J. Hwang, W. Choi, *J. Phys. Chem. B*, 2005, **109**, 24260-24267.
- 2) L. Zhang, S. Wang, C. Lu, *Anal. Chem.*, 2015, **87**, 7313-7320.
- 3) K. B. Jaimy, S. Ghosh, S. Sankar, K. G. K. Warriar, *Mater. Res. Bull.*, 2011, **46**, 914-921.
- 4) H. Feng, M. Zhang, E. L. Yu, *Appl. Catal. A: Gen.*, 2012, **413-414**, 238-244.
- 5) J. Choi, H. Park, M. R. Hoffmann, *J. Phys. Chem. C*, 2010, **114**, 783-792.
- 6) Y. Hu, X. Song, S. Jiang, C. Wei, *Chem. Eng. J.*, 2015, **274**, 102-112.
- 7) J. C. S. Wu, C. H. Chen, *J. Photochem. Photobiol. A: Chem.*, 2004, **163**, 509-515.
- 8) L. G. Devi, B. N. Murthy, S. G. Kumar, *Mater. Sci. Eng. B*, 2010, **166**, 1-6.
- 9) F. Ren, H. Li, Y. Wang, J. Yang, *Appl. Catal. B: Environ.*, 2015, **176-177**, 160-172.
- 10) X. Fan, X. Chen, S. Zhu, Z. Li, T. Yu, J. Ye, Z. Zou, *J. Mol. Catal. A-Chem.*, 2008, **284**, 155-160.
- 11) N. Nishiyama, Y. Fujiwara, K. Adachi, S. Yamazaki, *Appl. Catal. B: Environ.*, 2015, **176-177**, 347-353.
- 12) S. Yamazaki, Y. Fujiwara, S. Yabuno, K. Adachi, K. Honda, *Appl. Catal. B: Environ.*, 2012, **121-122**, 148-153.
- 13) P. Scherrer, *Göttinger Nachrichten Gesell.*, 1918, **2**, 98-100.
- 14) A. L. Patterson, *Phys. Rev.*, 1939, **56**, 978-982.
- 15) S. Brunauer, P. H. Emmett, E. Teller, *J. Am. Chem. Soc.*, 1938, **60**, 309-319.

- 16) K. S. W. Sing, D. H. Everett, R. A. W. Haul, L. Moscou, R. A. Pierotti, J. Roquerol, T. Siemieniewska, *Pure Appl. Chem.*, 1985, **57**, 603-619.
- 17) X. Liu, N. Chen, B. Han, X. Xiao, G. Chen, I. Djerdj, Y. Wang, *Nanoscale*, 2015, **7**, 14872-14880.
- 18) S. W. Price, K. Ignatyev, K. Geraki, M. Basham, J. Filik, N. T. Vo, P. T. Witte, A. M. Beale, J. F. W. Mosselmanns, *Phys. Chem. Chem. Phys.*, 2015, **17**, 521-529.
- 19) Y. W. Tsai, Y. L. Tseng, L. S. Sarma, D. G. Liu, J. F. Lee, B. J. Hwang, *J. Phys. Chem. B*, 2004, **108**, 8148-8152.
- 20) R. D. Shannon, *Acta Crystallogr., Sect. A: Cryst. Phys., Theor. Gen. Crystallogr.*, 1976, **32**, 751-767.
- 21) T. Yoshihara, R. Katoh, A. Furube, Y. Tamaki, M. Murai, K. Hara, S. Murata, H. Arakawa, M. Tachiya, *J. Phys. Chem. B*, 2004, **108**, 3817-3823.
- 22) Z. F. Bian, T. Tachikawa, P. Zhang, M. Fujitsuka, T. Majima, *J. Am. Chem. Soc.*, 2014, **136**, 458-465.
- 23) K. Yamanaka, T. Ohwaki, T. Morikawa, *J. Phys. Chem. C*, 2013, **117**, 16448-16456.
- 24) M. Zhu, S. Kim, L. Mao, M. Fujitsuka, J. Zhang, X. Wang, T. Majima, *J. Am. Chem. Soc.*, 2017, **139**, 13234-13242.
- 25) W. Kim, T. Tachikawa, H. Kim, N. Lakshminarasimhan, P. Murugan, H. Park, T. Majima, W. Choi, *Appl. Catal. B: Environ*, 2014, **147**, 642-650.
- 26) T. Tachikawa, M. Fujitsuka, T. Majima, *J. Phys. Chem. C*, 2007, **111**, 5259-5275.
- 27) T. Tachikawa, P. Zhang, Z. Bian, T. Majima, *J. Mater. Chem. A*, 2014, **2**, 3381-3388.

Chapter 3 Factors affecting the photocatalytic activity of Cr-TiO₂ under visible light irradiation

3. 1 Introduction

In Chapter 2, we have revealed that the mixed valence states of Pt ion in Pt-TiO₂ (Pt(II)/Pt(IV) ratio) can be controlled, and there is a linear relationship between the Pt(II)/Pt(IV) and 4-CP conversion. However, since Pt is a noble metal, it has a large problem of high cost.

As mentioned in Chapter 1, Cr-TiO₂ as well as Pt-TiO₂ can degrade 4-CP among 7 metal ions used for the synthesis of M-TiO₂. Cr ion has multiple stable valence states^{1, 2)} like Pt ion. There are many reports on the photocatalytic activity of Cr-TiO₂ under visible light irradiation.³⁻¹¹⁾ However, few studies have revealed the valence states and location of Cr ions in TiO₂ and expressed the mixed valence states.

We have previously reported that Cr ion mainly exists as Cr(III) in 1.3 and 6.6 atom% Cr-TiO₂ sintered at 200°C.¹³⁾ In this Chapter, we tried to enhance the photocatalytic activity of Cr-TiO₂ by using the mixed valence states similarly to Pt-TiO₂.

3. 2. Experimental

3. 2. 1. Materials.

As mentioned in Chapter 2, all reagents were purchased from Wako Pure Chemicals Industries Ltd (Osaka, Japan) and used without further purification unless otherwise noted. Potassium chromate (K_2CrO_4) and chromium(III) oxide (Cr_2O_3) were purchased from Kanto Chemical Co., Inc. (Tokyo, Japan) and Nacalai Tesque (Kyoto, Japan), respectively. Chromium(III) nitrate nonahydrate ($Cr(NO_3)_3 \cdot 9H_2O$) was purchased from Alfa Aesar (USA). Ultrapure water was obtained using a Milli-Q water purification system (Millipore, USA) and used for all experiments.

3. 2. 2. Preparation of Cr-TiO₂ powder.

Preparation method of Cr-TiO₂ was the same as described in Chapter 2 except for the use of $CrCl_3 \cdot 6H_2O$ (content of Cr was 0.2 - 6.6 atom% against Ti + Cr) instead of $H_2PtCl_6 \cdot 6H_2O$. The obtained powders were sintered by ramping at $3^\circ C \text{ min}^{-1}$ and keeping at 100 - 600°C for 2 h.

For comparison, Cr-TiO₂ powders were prepared by modifying the literature method.¹¹⁾ An ethanol TTIP solution (5 ml) was added dropwise to the mixture solution of 50 ml of ethanol and $Cr(NO_3)_3 \cdot 9H_2O$ aqueous solutions containing 0.51 ml of HNO₃ (pH 1.5), in which the amount of $Cr(NO_3)_3 \cdot 9H_2O$ was added to the Cr content to be 0.8 atom%. The obtained mixture was stirred at room temperature for 24 hours and then evaporated at 45°C

using a rotary evaporator. The obtained powder was ground into fine powders by using agate mortar and pestle and then sintered at 400°C for 1 h after being heated at the raising rate of 100°C min⁻¹.

3. 2. 3. Characterization of Cr-TiO₂ powder.

XRD, BET, diffuse reflectance UV-vis absorption spectra, XPS and femtosecond TDR spectra were carried out in the same way as described in Chapter 2. The XANES spectra for Cr K-edge were recorded on a beamline 11 at Kyusyu Synchrotron Light Research Center. As reference samples, Cr₂O₃ and K₂CrO₄ powders were used. Each powder was mixed with boron nitride in an agate mortar for 10 min and then molded into a pellet of 7 mm in diameter by using the hand press. The XANES spectra of this pellet placed in a polyethylene bag were measured in transmission mode. The synthesized Cr-TiO₂ powder sample was placed in the polyethylene bag and the XANES spectrum was measured in fluorescence yield by using a Lytle detector and a 19-element germanium solid state detector. First-principle calculations of Cr-TiO₂ with oxygen vacancy were conducted by the plane-wave pseudopotential method with the CASTEP code.^{13, 14} Vanderbilt ultrasoft pseudopotentials and the generalized gradient approximation (GGA-PBE)¹⁵ as an exchange-correlation functional were used. Details of the simulation method have been mentioned in the literature.^{1, 2}

3. 2. 4. Photocatalytic degradation of 4-CP by using Cr-TiO₂ powder.

Photocatalytic performance of Cr-TiO₂ was examined in the same way as described in Chapter 2 except that only the halogen lamp ($\lambda > 400$ nm: 26 mW cm⁻²) was used.

3. 3. Results and discussion

3. 3. 1. Effect of doping amount on the photocatalytic activity of Cr-TiO₂.

Figure 3-1 shows the time course of the 4-CP conversion on 0.8 atom% Cr-TiO₂, 0.5 atom% Pt-TiO₂ and 0.8 atom% Cr-TiO₂ synthesized by a reference method (Cr-TiO₂(ref))¹¹ under visible light irradiation. The photocatalytic activity of Cr-TiO₂ synthesized by our method is about 2.5 times that of the Cr-TiO₂ synthesized by the reference method. It is noted that the photocatalytic activity of our Cr-TiO₂ is comparable to that of 0.5 atom% Pt-TiO₂, leading to the savings of cost (ca. 1/100). Figure 3-2 shows the 4-CP conversions on Cr-TiO₂ samples doped with various amounts of Cr (0.2 to 6.6 atom%) and sintered at various temperatures from 200 to 600°C. The 4-CP conversions achieved with 0.68 – 1.3 atom% Cr-TiO₂ sintered at 200°C were greater than 86.0%. Figure 3-2 also shows that on 0.8 atom% Cr-TiO₂, the 4-CP conversion decreased with increasing sintering temperature. In contrast, for Cr-TiO₂ doped at more than 1.7 atom%, sintering at 300 – 500°C increased 4-CP conversion and the optimal sintering temperature was 400°C. However, the 4-CP conversion

on 1.7 atom% Cr-TiO₂ sintered at 300°C was comparable to that for 1.7 atom% Cr-TiO₂ sintered at 400°C. For all doping amounts, sintering at 600°C gave the lowest conversion (less than 18.0%). These results show that the highest photocatalytic activity in 4-CP degradation was obtained with 0.68 – 1.3 atom% Cr-TiO₂ sintered at 200°C. The two different dependences of 4-CP conversion on the sintering temperature suggest that the factors affecting the photocatalytic activity are different for doping amounts less than 1.3 atom% and greater than 1.7 atom%.

Figure 3-3 shows the XRD patterns for 0.8, 1.7, 2.9, and 6.6 atom% Cr-TiO₂ sintered at 200 – 600°C. Diffraction peaks attributable to the anatase phase are observed at 200 and 300°C, small rutile peaks are detected at 400°C, and the rutile is the major phase at 600°C. Even for 6.6 atom% Cr-TiO₂, there are no peaks except those for anatase and rutile phase. As the Cr ion doping amount was increased, a slight diffraction peak of the (101) plane of the anatase was detected in the sintered at 600°C. It is reported that the anatase - rutile phase transition is suppressed when the doping amount of Cr ions less than 10%.^{16, 17)} In addition, Choi *et al.* reported that metal ions having an ionic radius similar to the ionic radius of Ti(IV) are substituted in Ti(IV) sites within TiO₂.¹¹⁾ The ionic radius of Ti(IV) is 0.745 Å and Cr(III) is 0.755 Å.¹⁸⁾ That is, it is suggested that the change in the anatase - rutile phase transition behavior due to Cr(III) ions are substituted (doped) with Ti(IV) ions in TiO₂ lattice.

The N₂ adsorption - desorption isotherms (Figure 3-4) for Cr-TiO₂ sintered at 200°C

showed that the hysteresis loop became smaller as the doping amount increased and then disappeared at 6.6 atom% Cr-TiO₂. However, for samples sintered at $\geq 300^\circ\text{C}$, the hysteresis loop was clearly observed for 6.6 atom% Cr-TiO₂. The presence of a hysteresis loop is characteristic of mesoporous TiO₂ prepared by a sol-gel method. It is therefore deduced that Cr(III) ions were adsorbed on the TiO₂ surface, including the pore walls, during the sol - gel process. At a low doping amount, i.e., 0.8 atom% Cr-TiO₂, the hysteresis loop was observed because of the presence of mesopore. Excess Cr(III) filled the mesopores of 6.6 atom% Cr-TiO₂ sintered at 200°C, resulting in no hysteresis. However, at higher temperatures, Cr(III) diffused into the TiO₂ bulk and opened the mesopores, and a hysteresis loop was generated. These findings suggest that Cr(III) doping occurred by thermal diffusion from the surface into the TiO₂ bulk lattice during sintering. The BET specific surface area and the crystalline size of Cr-TiO₂ synthesized with various doping amounts at sintering temperatures are listed in Table 3-1. Aggregation and particle growth occurred with increasing sintering temperature, resulting in an increase in the crystallite size and a decrease in the specific surface area.¹⁹⁾ These behaviors were observed regardless of the doping amounts in Cr-TiO₂.

Figure 3-5 shows the diffuse reflection spectra of TiO₂, and 0.8, 1.7, and 6.6 atom% Cr-TiO₂ sintered at 200°C; visible light absorption was highest with 6.6 atom% Cr-TiO₂. The absorption peak observed at around 450 and 600 - 800 nm are attributable to charge transfer from Cr(III) to Ti(IV) and the d - d transition of Cr(III), respectively.⁹⁾ Although the visible

light absorption was high, 4-CP conversion on 6.6 atom% Cr-TiO₂ was very low. It has often reported that there is an optimal dopant concentration for metal ions in a TiO₂ matrix and that excess dopant decrease the photocatalytic activity by promoting the recombination of the photogenerated electrons and holes.^{6, 9, 10)} The BET specific surface area, the crystallite size and the crystal phases of Cr-TiO₂ had similar dependence on the sintering temperature, regardless of the doping amount, and therefore cannot explain two different dependences of 4-CP conversion on the sintering temperature mentioned above. Therefore, XPS measurement was carried out to investigate the effect of sintering temperature on the valence state of Cr ions in Cr-TiO₂ near the surface.

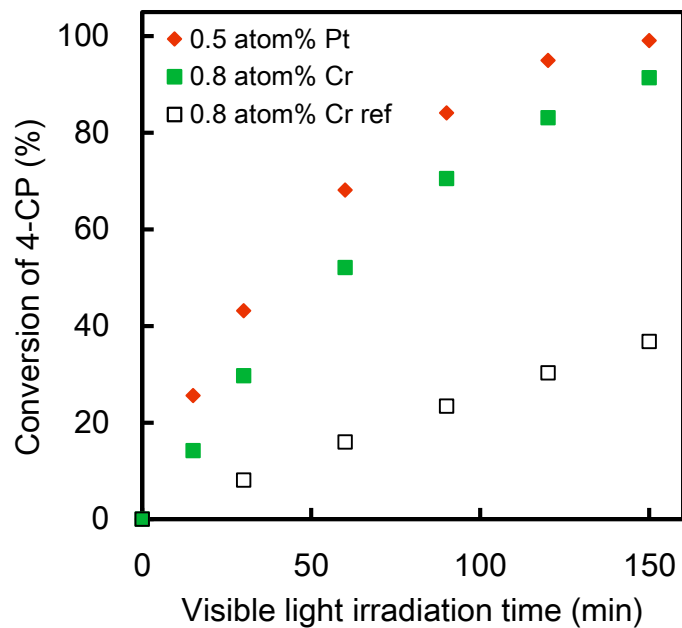


Figure 3-1 Time courses of the 4-CP conversion on 0.5 atom% Pt-TiO₂, 0.8 atom% Cr-TiO₂, and 0.8 atom% Cr-TiO₂(ref) under visible light irradiation.

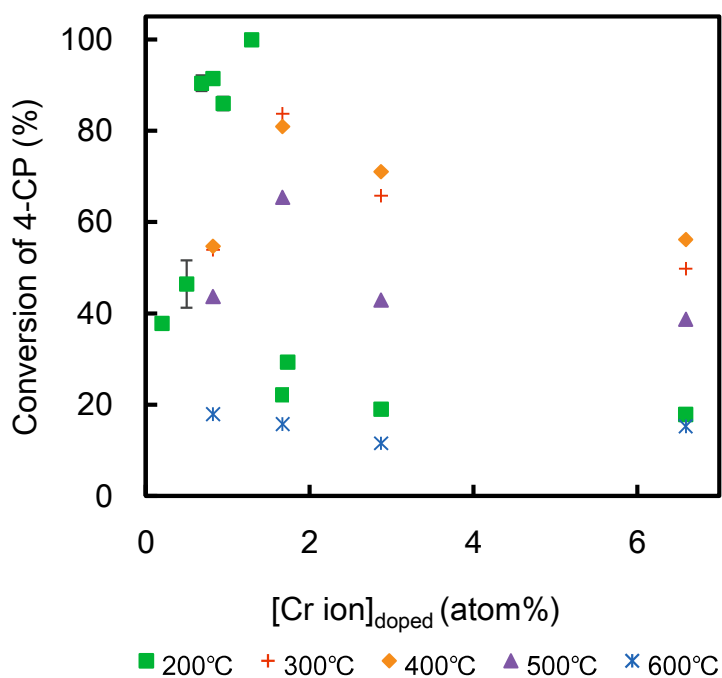
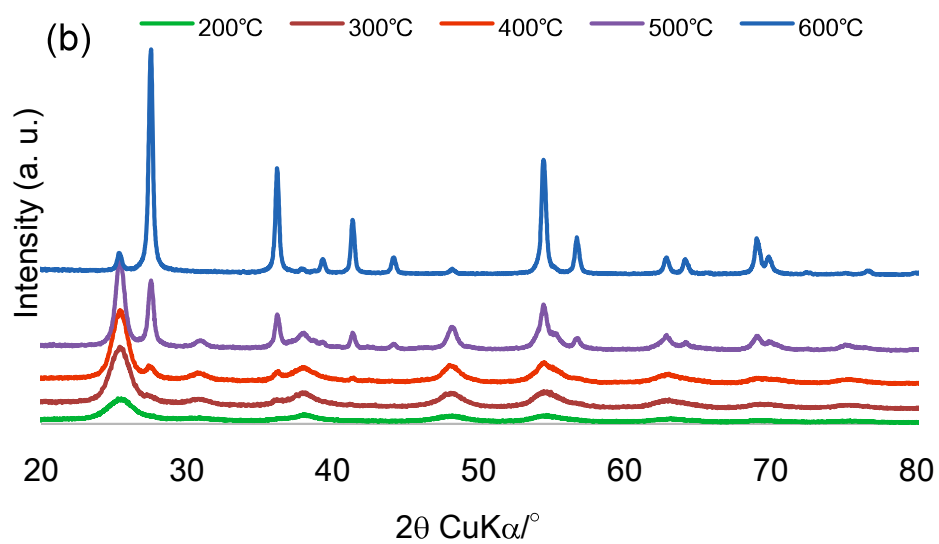
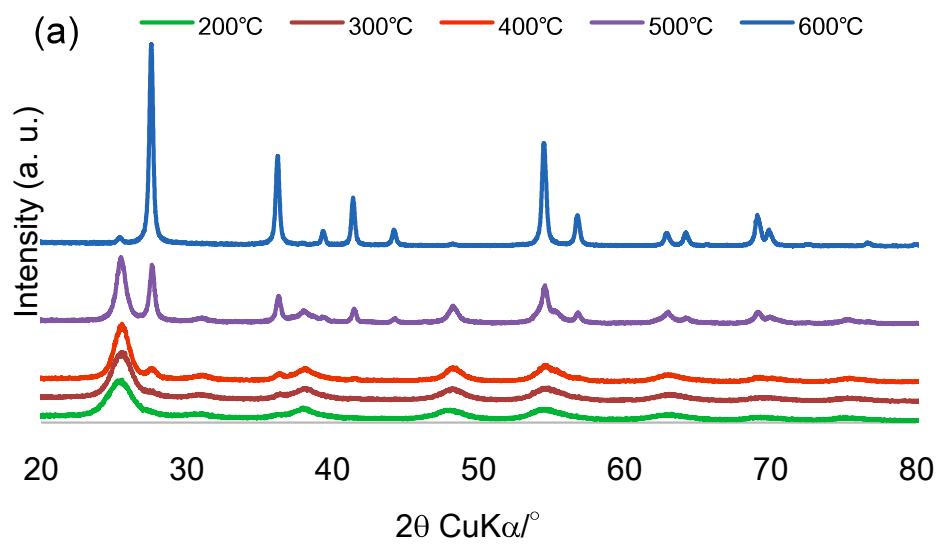


Figure 3-2 Effects of amount of doped Cr ions and sintering temperature on 4-CP conversion after visible light irradiation for 150 min.



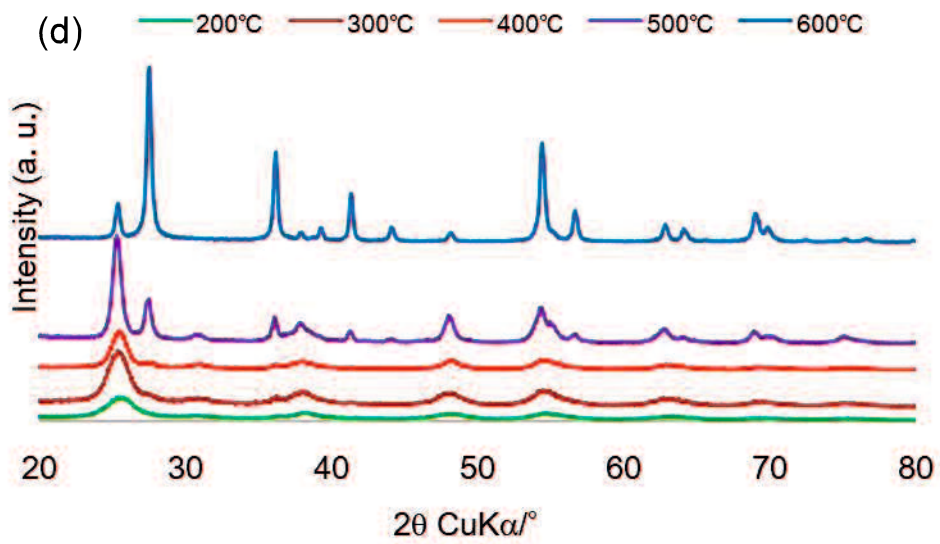
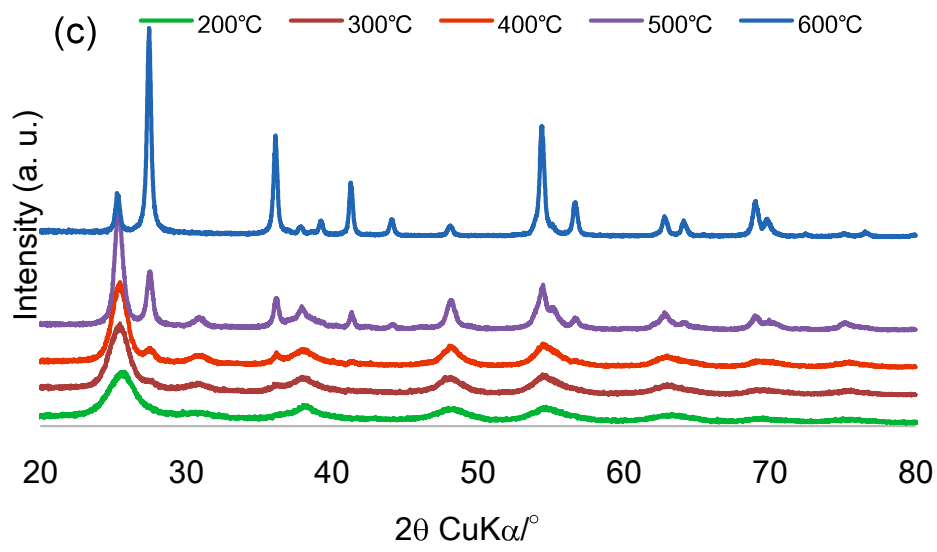


Figure 3-3 XRD patterns of (a) 0.8, (b) 1.7, (c) 2.9 and (d) 6.6 atom% Cr-TiO₂ sintered at 200 - 600°C.

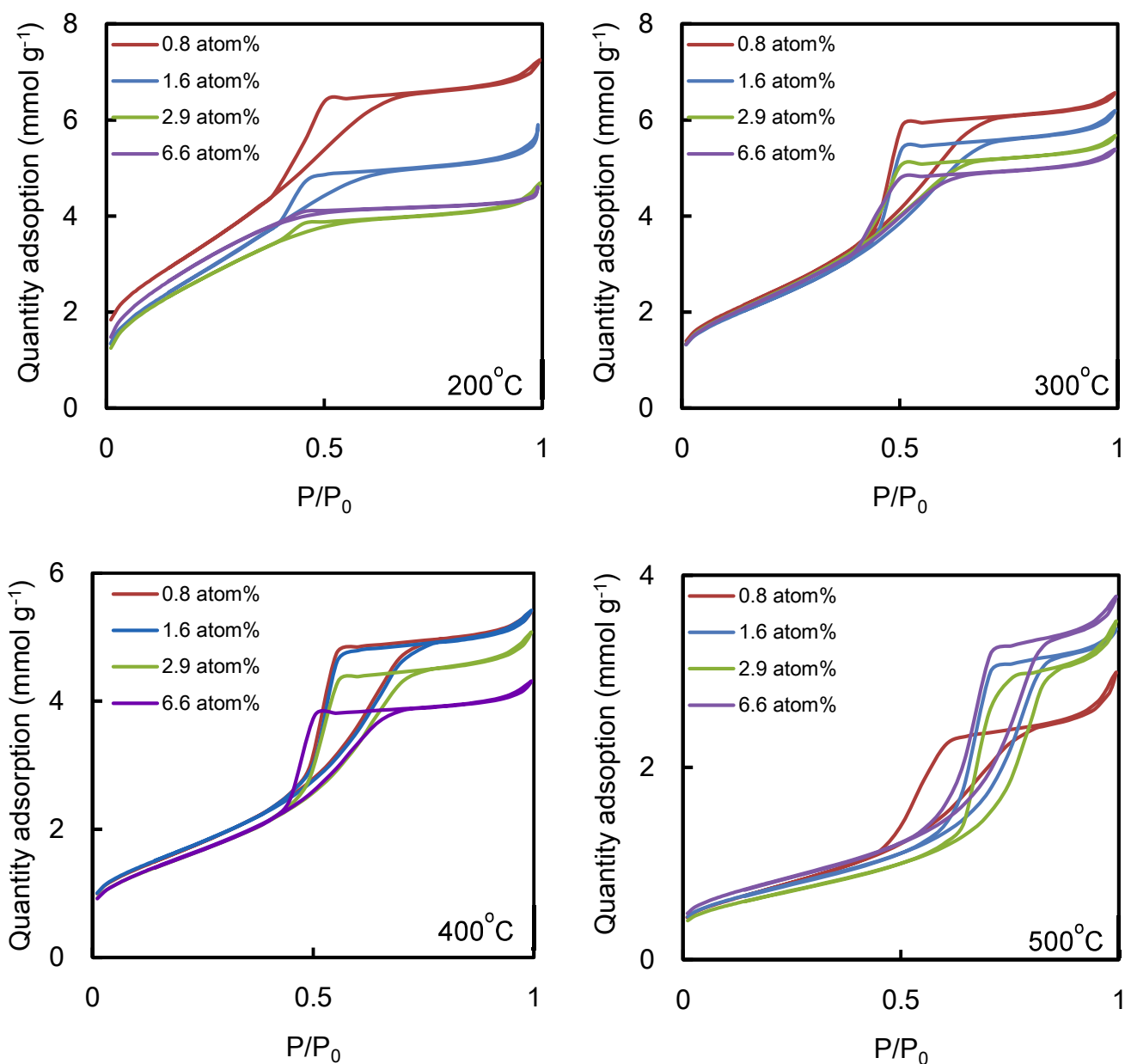


Figure 3-4 N_2 adsorption - desorption isotherms of 0.8 – 6.6 atom% Cr- TiO_2 sintered at 200 – 500°C.

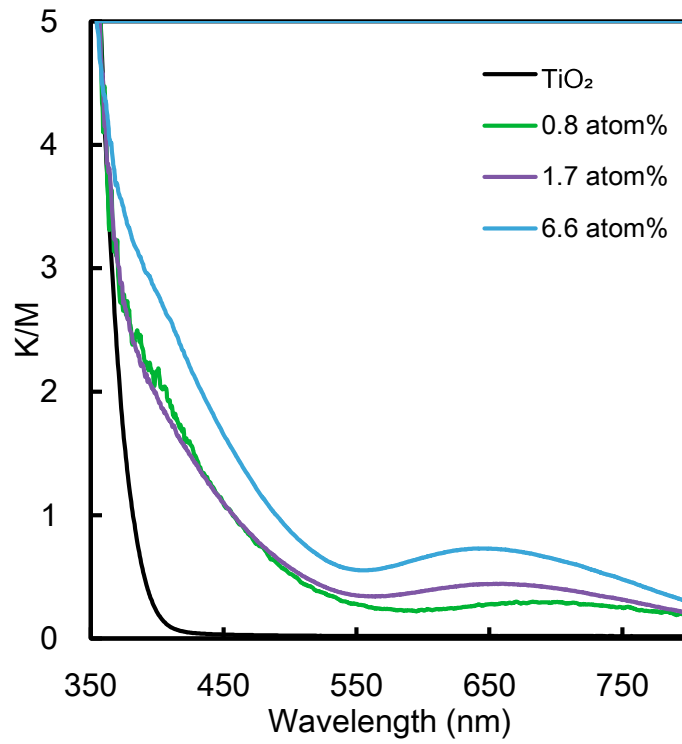


Figure 3-5 UV-vis diffuse reflectance spectra of TiO₂ and 0.8 – 6.6 atom% Cr-TiO₂ sintered at 200°C

Table 3-1 BET specific surface area and crystallite size of Cr-TiO₂.

Doping amount (atom%)	BET specific surface area (m ² g ⁻¹)					Crystallite size (nm) ^a				
	Sintering temperature (°C)									
	200	300	400	500	600	200 ^a	300 ^a	400 ^a	500	600
0.8	261	191	133	59.1	11.6	4.4	5.4	7.0	11.4 ^a	29.3 ^b
									21.9 ^b	
1.7	220	179	134	58.8	17.6	4.1	5.6	6.7	12.3 ^a	27.9 ^b
									21.0 ^b	
2.9	213	187	125	53.5	21.2	3.9	5.4	7.0	13.0 ^a	22.9 ^a
									18.7 ^b	26.6 ^b
6.6	242	186	125	64.3	22.0	4.5	5.2	7.0	12.2 ^a	22.6 ^a
									16.3 ^b	24.9 ^b

^aCrystallite size was evaluated from the anatase (101) XRD peak.

^bCrystallite size was evaluated from the rutile (110) XRD peak.

3. 3. 2. Valence states of the doped Cr ions near the surface and bulk of TiO₂.

Figure 3-6 shows XPS spectra of 6.6 atom% Cr-TiO₂ at 200 and 400°C. The peaks at 577.0 eV and 587.0 eV are attributed to the binding energies of Cr 2p_{3/2} and Cr 2p_{1/2}, respectively.²⁰⁾ No appreciable peak is present at 580 eV, which corresponds to the binding energy of Cr(VI).²⁰⁾ Both XPS spectra indicate that Cr exists as Cr(III) near the surface of TiO₂ sintered at 200 or 400°C. The XPS measurement mainly reflects the chemical environment on the surface, whereas XANES spectroscopy can provide information on the

bulk. Figure 3-7 shows the XANES spectra of 1.7, 6.6 atom% Cr-TiO₂ sintered at 200 or 400°C, and those of standard samples of Cr₂O₃ (Cr(III)) and K₂CrO₄ (Cr(VI)). A major characteristic of the XANES spectra of Cr(VI) is a sharp pre-edge peak around 5992 eV. Figure 3-7 shows that no pre-edge peak is observed for 1.7 or 6.6 atom% Cr-TiO₂ sintered at 200°C, and their spectra are similar to that of Cr₂O₃; this indicating that Cr exists as Cr(III); this is consistent with the XPS results. In contrast, for Cr-TiO₂ sintered at 400°C, a pre-edge peak is detected at 5992 eV, with a slight shift of the absorption edge to high energy. These observations indicate that some Cr(III) in the bulk is oxidized to Cr(VI) when 1.7 and 6.6 atom% Cr-TiO₂ are sintered at 400°C. The increase in the 4-CP conversion observed on Cr-TiO₂ with doping amounts greater than 1.7 atom% and sintering at 400°C is therefore attributable to the formation of Cr(VI). It is likely that because their ionic sizes are similar,¹⁸⁾ Cr(III) can be substituted for Ti(IV) in the TiO₂ lattice and can diffuse into the TiO₂ bulk during sintering, with Cr(VI) formation to maintain the charge balance. Kudo *et al.* reported that some Cr(VI) or oxygen defects were generated to maintain the charge balance when a mixture of TiO₂ and Cr₂O₃ are mixed and sintered at 1420 K for 10 hours. They also reported that the charge balance was maintained by co-doping Sb(V), and the formation of Cr(VI) and oxygen defects was suppressed.²¹⁾ As described in Chapter 2, the photocatalytic activity of Pt-TiO₂ increased with increasing ratio of Pt(II)/Pt(IV), which was evaluated by XPS. Spatial separation of the photogenerated carriers was promoted by trapping holes at Pt(II) and

electrons at Pt(IV), and this suppressed the recombination process. The ratio of Pt(II)/Pt(IV) on Pt-TiO₂ was varied by changing the concentration of TTIP that was added to the aqueous solution containing H₂PtCl₆ during synthesis. In the case of Cr-TiO₂, the oxidation of Cr(III) to Cr(VI) is promoted by sintering at higher temperatures. Scheme 3-1 shows the energy diagram of Cr-TiO₂ based on the redox potential²² of Cr(IV)/Cr(III) (2.1 V vs. SHE) and Cr(VI)/Cr(V) (0.6 V vs. SHE). High activation by formation of the mixed valence states of Cr ions can be explained as follows. At any doping amount and sintering temperature, because the photocatalytic activity of Cr-TiO₂ is lower than that of Pt-TiO₂, it is considered that holes are not generated in VB. In Cr-TiO₂, electrons are excited from Cr(III) to the CB of TiO₂ by absorbing visible light and the photogenerated Cr(IV) oxidatively degrades 4-CP and returns the original Cr(III) state. The doped Cr(VI) act as trapping sites for photogenerated electron. The recombination of photogenerated Cr(IV) and electrons is therefore suppressed by formation of mixed valence states of Cr ion. The XPS and XANES spectra show that Cr(III) is present both on the surface and in the bulk, but Cr(VI) is present only in the bulk. Such spatial separation of Cr(III) (photogenerated Cr(IV)) and Cr(VI) (trapping sites for photogenerated electrons) also enhances the photocatalytic activity by suppression of recombination.

Qiu *et al.* used XANES measurements to evaluate the Cu(I)/Cu(II) ratio in Cu(II)-grafted TiO₂.²³⁾ Similarly, the ratio of Cr(VI)/Cr(III) in Cr-TiO₂ was determined by

using Cr_2O_3 and K_2CrO_4 as standards.

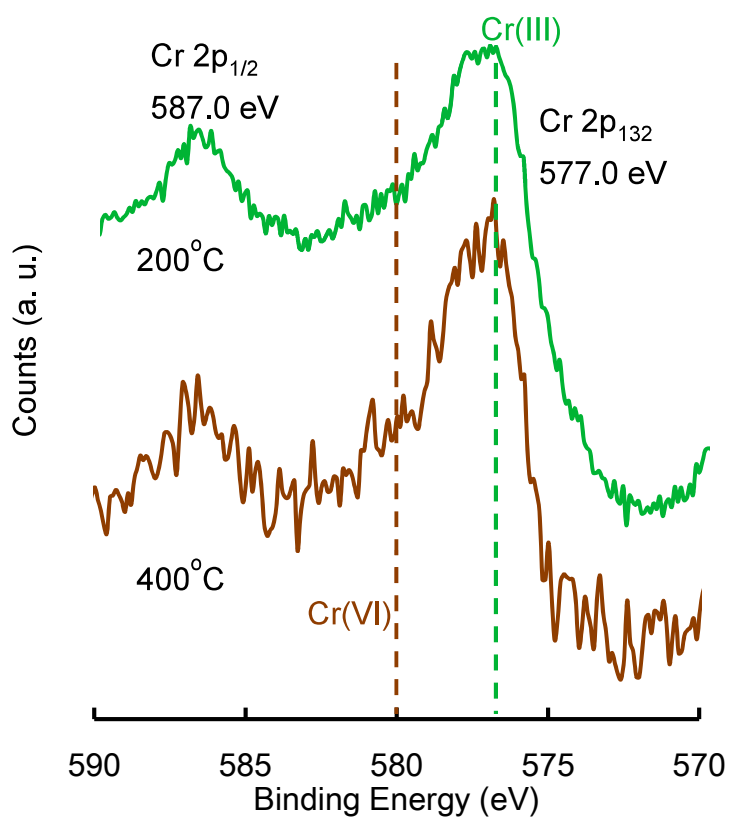


Figure 3-6 XPS spectra of 6.6 atom% Cr-TiO₂ sintered at 200 and 400°C.

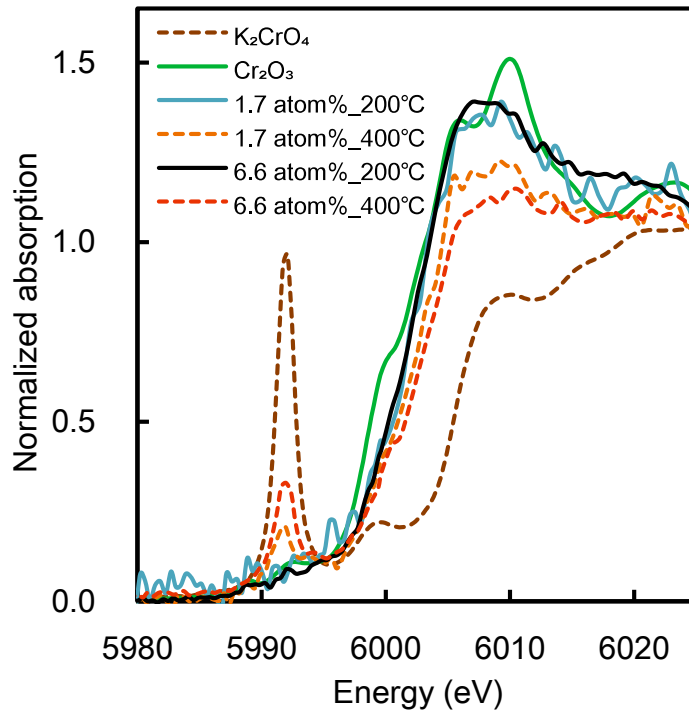
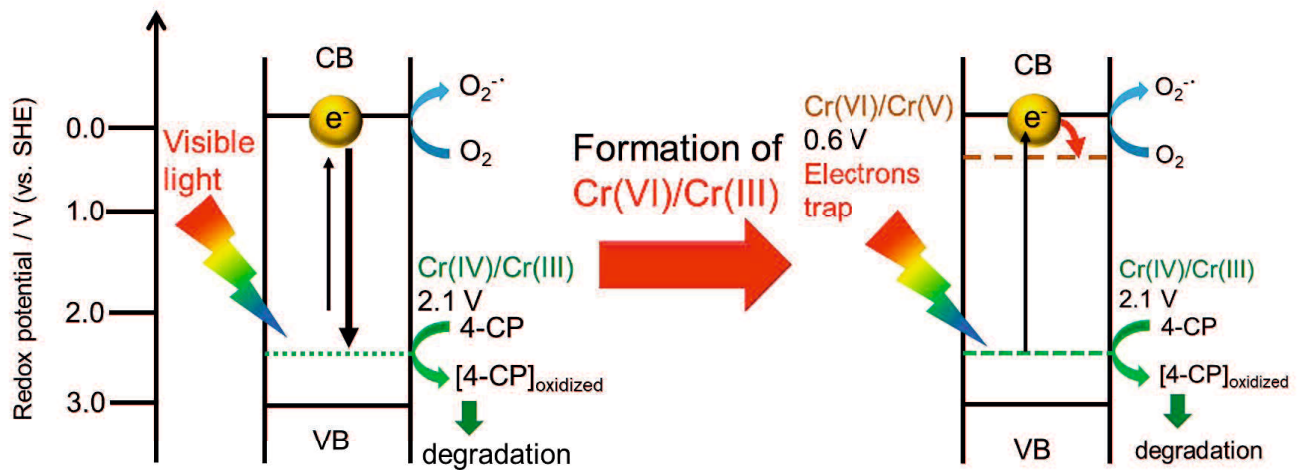


Figure 3-7 XANES spectra of Cr_2O_3 , K_2CrO_4 , and 1.7 and 6.6 atom% Cr- TiO_2 sintered at 200 and 400°C.



Scheme 3-1 Proposed mechanism for the electrons moving in the presence of Cr(III) and Cr(VI).

3. 3. 3. Relationship between Cr(VI)/Cr(III) ratio and photocatalytic activity on Cr-TiO₂.

The quantitative method of Cr(VI)/Cr(III) is as follows. The peak area of Cr(VI) at 5992 eV (A_{5992}) was estimated from the integrated value by setting the baseline in the range of 5989 - 5994 eV, and that for Cr(III) at 6010 eV (A_{6010}) was estimated from the integrated value by setting the baseline in the range of 6007 - 6013 eV. Figure 3-8 shows the XANES spectra of mixtures of Cr₂O₃ and K₂CrO₄, (Cr(VI) contents: 0 – 100%); the ratio of the peak areas (A_{5992}/A_{6010}) increases linearly, with increasing Cr(VI) content, as shown in the Figure 3-9. On the basis of this linearly, the Cr(VI)/Cr(III) ratio and 4-CP conversion after visible light irradiation for 150 min were maximum for Cr-TiO₂ sintered at 400°C (Figure 3-10(a)-(d)). Figure 3-11 shows the effect of the Cr(VI)/Cr(III) ratio on 4-CP conversion. The 4-CP conversion increased with increasing Cr(VI)/Cr(III) ratio in the bulk. This suggests that at high Cr(VI)/Cr(III) ratios, the photogenerated electrons are trapped at Cr(VI), recombination reaction is suppressed, and Cr(IV) oxidized 4-CP, which is adsorbed on the TiO₂ surface, as shown in Scheme 3-1. The enhancement of the photocatalytic activity observed for Cr-TiO₂ with doping amounts greater than 1.7 atom% and sintering at 300 – 500°C is therefore attributable to the suppression of the recombination of photogenerated carries by the co-presence of Cr(III) and Cr(VI).

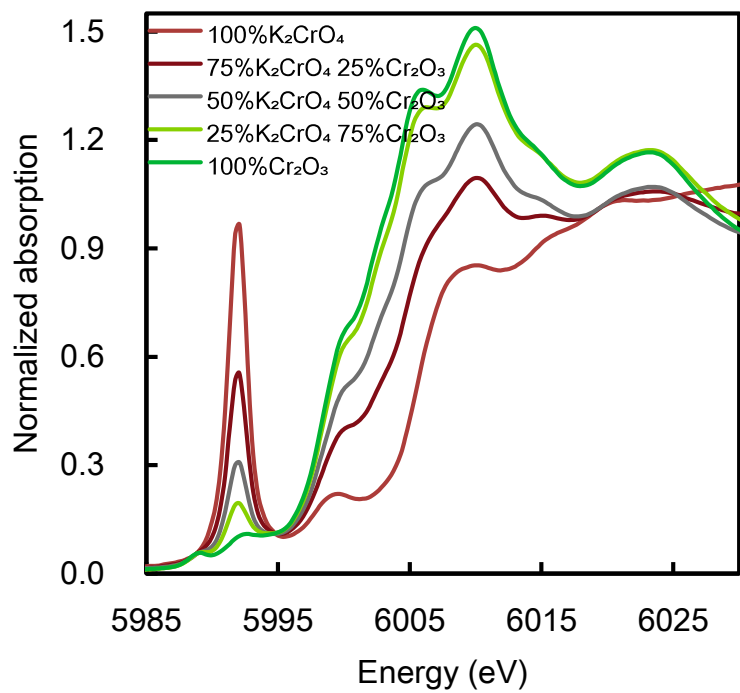


Figure 3-8 XANES spectra of the mixture of Cr_2O_3 and K_2CrO_4 .

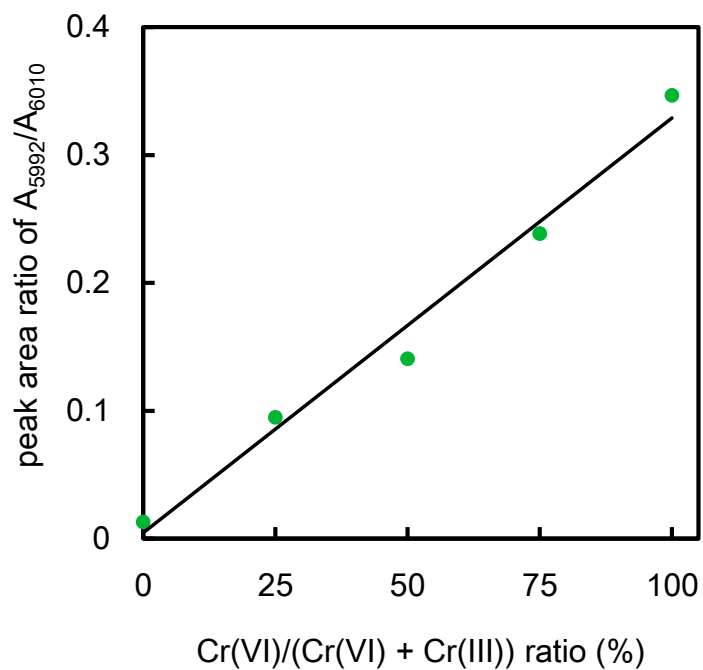


Figure 3-9 Linear relationship between Cr(VI) content and peak area ratio (A_{5992}/A_{6010}).

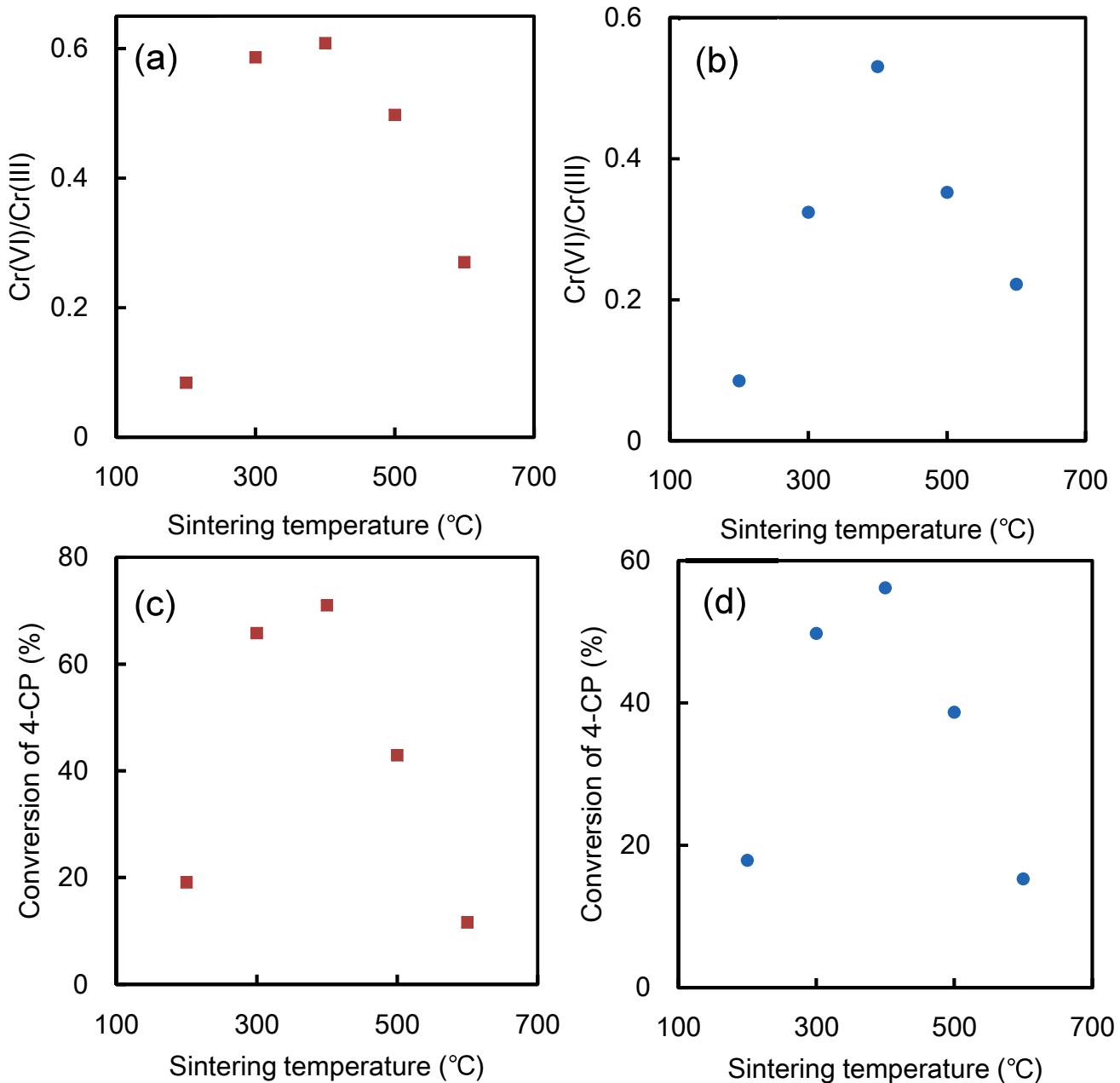


Figure 3-10 Plots of Cr(VI)/Cr(III) ratios and 4-CP conversions against sintering temperature after visible light irradiation for 150 min on 2.9 atom% ((a), (c)) and 6.6 atom% Cr-TiO₂ ((b), (d)).

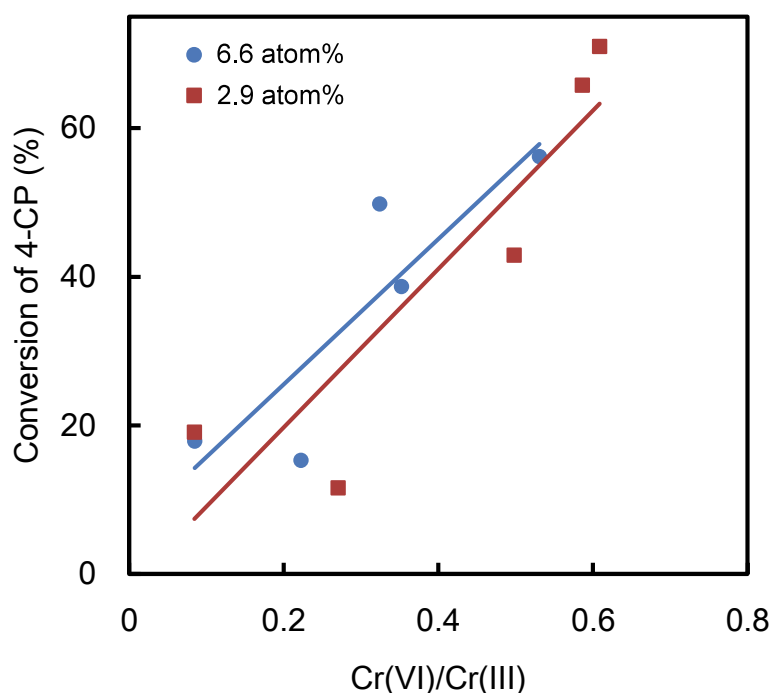


Figure 3-11 Relationship between Cr(VI)/Cr(III) ratio and 4-CP conversion after visible light irradiation for 150 min.

3. 3. 4. Effect of forming the mixed valence states on the lifetime of photogenerated carriers.

The suppression of recombination was confirmed by using TDR spectra measurements to estimate the lifetime of the photogenerated electrons. Figure 3-12 shows TDR spectra of 6.6 atom% Cr-TiO₂ sintered at 400°C after the excitation by a 400 nm laser flash. The broad absorption at around 900 - 1050 nm is assigned to electrons trapped in the

CB of TiO₂.²⁴⁻²⁸ Figure 3-13 shows the time profile of a normalized transient absorption at ca. 1000 nm for 6.6 atom% Cr-TiO₂ sintered at 200 - 600°C. These decay curves were fitted to two-exponential functions; the lifetimes are summarized in Table 3-2. The shorter lifetime (τ_1) is assigned to trapping of photogenerated electrons in the CB of TiO₂ at oxygen defects as the trap sites with shorter distance. The longer lifetime (τ_2) corresponds to trapping of photogenerated electrons at trap site (Cr(VI)) after the diffusion. The sintering temperature with longer τ_2 values are the following order: 400°C > 300°C > 500°C > 600°C > 200°C, which corresponds to the order of the photocatalytic activities, i.e. higher photocatalytic activities are obtained with Cr-TiO₂ with longer τ_2 values. This suggests that τ_2 is related to the trapping of photogenerated electrons at Cr(VI) sites. Indeed, as shown in Figure 3-14 (a) and (b), the τ_1 and τ_2 values increase with increasing Cr(VI)/Cr(III) ratio which were evaluated from the XANES spectra of 6.6 atom% Cr-TiO₂ sintered at 200 – 600°C. However, by coexisting with Cr(VI) (formation of mixed valence state), trap sites of photogenerated electrons are spatially separated, suggesting that recombination was suppressed, and high activation was achieved.

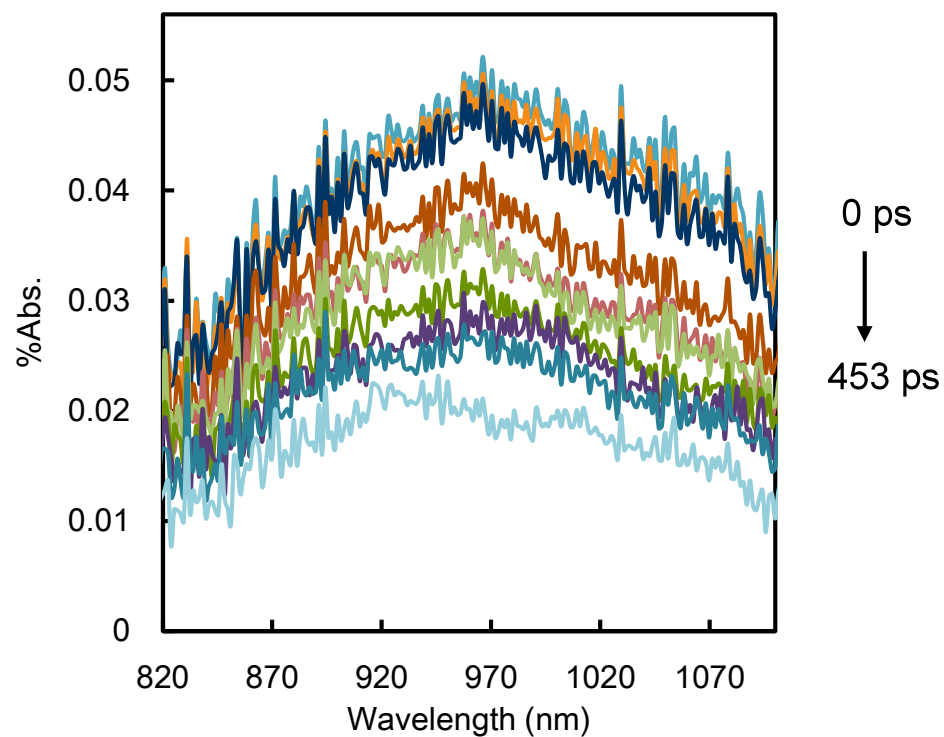


Figure 3-12 TDR spectra observed after 80 fs laser flash for 6.6 atom% Cr-TiO₂ sintered at 400°C.

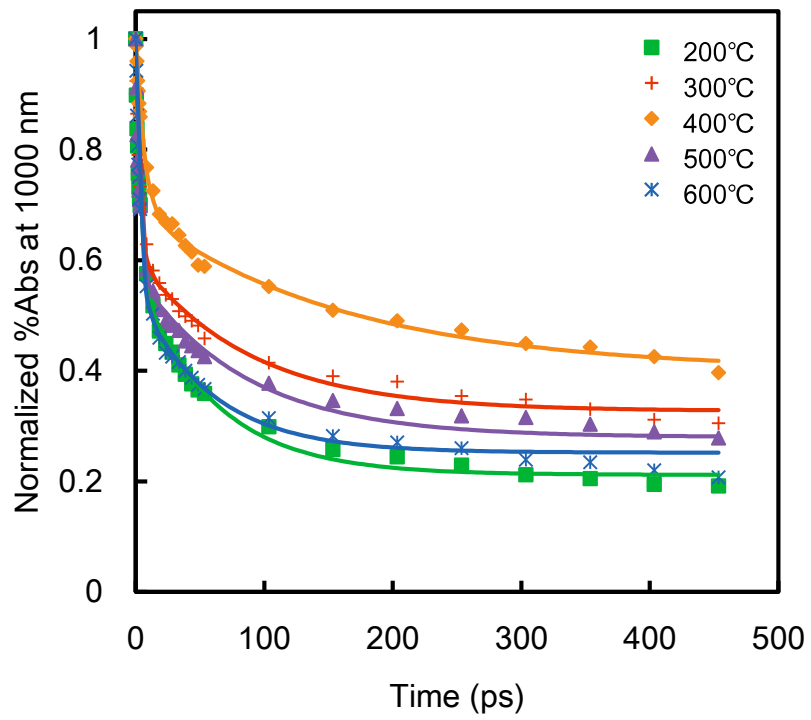


Figure 3-13 Time profiles of normalized transient absorption at 1000 nm for 6.6 atom% Cr-TiO₂ sintered at 200 - 600°C

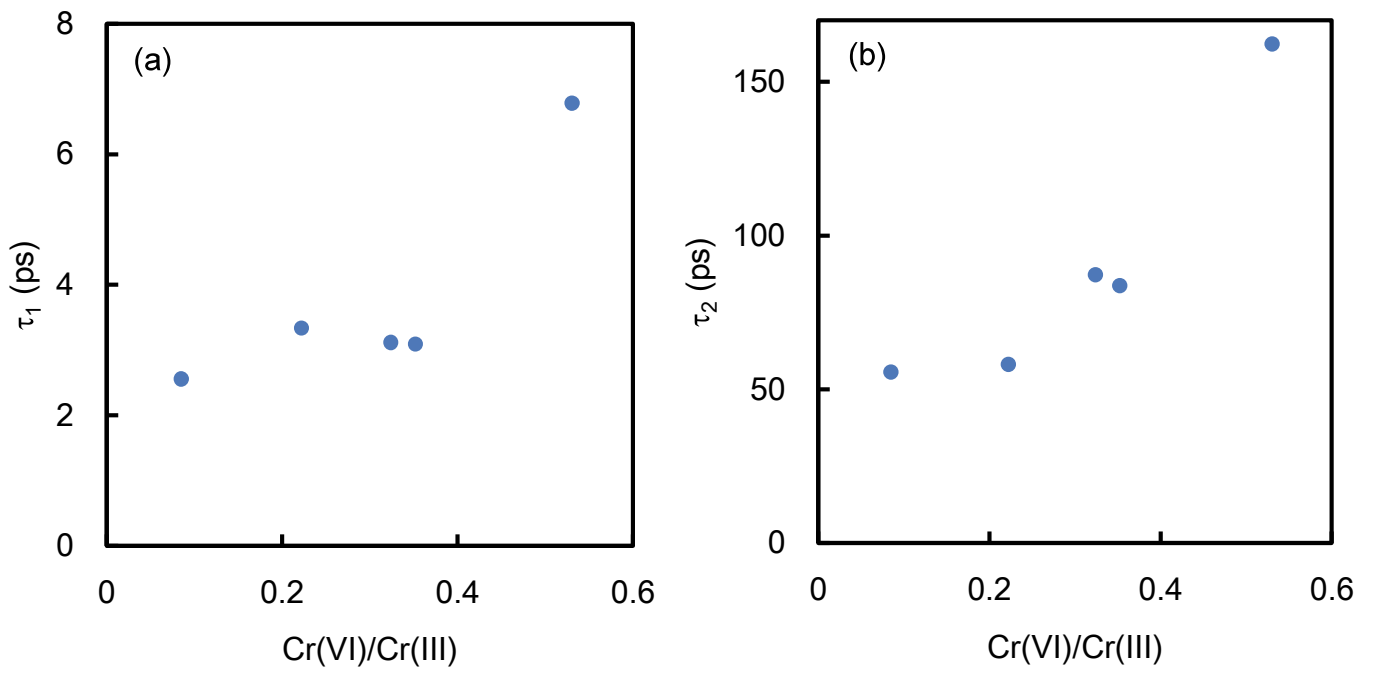


Figure 3-14 Relationship between (a): τ_1 (b): τ_2 for 6.6 atom% Cr-TiO₂ sintered at 200 - 600°C and Cr(VI)/Cr(III) ratio.

Table 3-2 Lifetimes (τ_1 and τ_2) of photogenerated electrons for 6.6 atom% Cr-TiO₂ (excitation wavelength: 400 nm). Ratios of τ_1 and τ_2 are in parenthesis.

Sintering temperature (°C)	τ_1 (ps)	τ_2 (ps)
200	2.6 (50.6%)	55.6 (49.4%)
300	3.1 (57.6%)	87.3 (42.4%)
400	6.8 (50.8%)	162.3 (49.2%)
500	3.1 (55.2%)	83.8 (44.8%)
600	3.3 (60.8%)	58.1 (39.2%)

3. 3. 5. A possible factor related to high activity of 0.8 atom% Cr-TiO₂.

Table 3-3 lists the τ_1 and τ_2 values calculated from the TDR spectra of 0.2 – 6.6 atom% Cr-TiO₂ sintered at 200°C. The τ_2 values increase with increasing amount of dopant. The maximum value, i.e., ca. 80 ps at 0.8 – 1.3 atom%, is consistent with the doping range for the highest photocatalytic activity, as shown in Figure 3-2. However, the τ_2 values cannot be attributed to electron trapping at Cr(VI) because no pre-edge peak due to Cr(VI) was detected in the XANES spectra for 0.8 atom% Cr-TiO₂ sintered at 200°C (Figure 3-15). It has been reported that oxygen vacancies in TiO₂ act as trapping sites for the photogenerated electrons. Oxygen vacancies are expected to form to balance the charge when metal ion

dopants are substituted for Ti(IV) in TiO₂ lattice.

An anatase TiO₂ supercell consisting of a 3 x 3 x 1 of optimized unit cell was used for structural optimization and XANES spectra calculations (Figure 3-16 (i)). Two types of Cr-TiO₂ consisting CrO₆ octahedron with Cr(III) and an oxygen vacancy, were modeled. Model_a showed that two neighboring Ti(IV) sites were replaced with Cr(III) and oxygen between them was removed, whereas in model_b, oxygen vacancy was located far from the two adjacent Cr(III) sites (Figure 3-16 (ii) and (iii)). The estimated energy for generating model_b is larger than that for model_a by 0.74 eV, therefore it is possible to form oxygen vacancies with a structure like that in model_a. Figure 3-17 shows the XANES spectra simulated from the models; they show that the observed spectra for 0.8 atom% Cr-TiO₂ are similar to the simulation for model_a rather than model_b. Oxygen defect generation at 0.75 – 1.18 eV below the CB level of TiO₂ has been reported.²⁹⁻³¹ The reason for the highest photocatalytic activity being achieved with ca. 0.8 atom% Cr-TiO₂ sintered at 200°C could be the presence of oxygen vacancies, like those in model_a, which act as electron trapping sites.

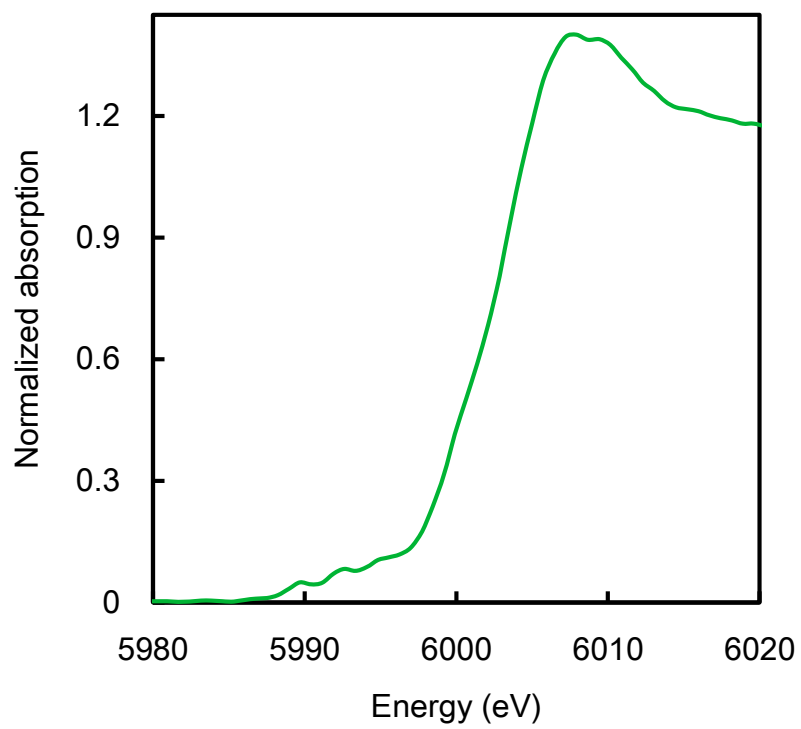


Figure 3-15 XANES spectra of 0.8 atom% Cr-TiO₂ sintered at 200°C.

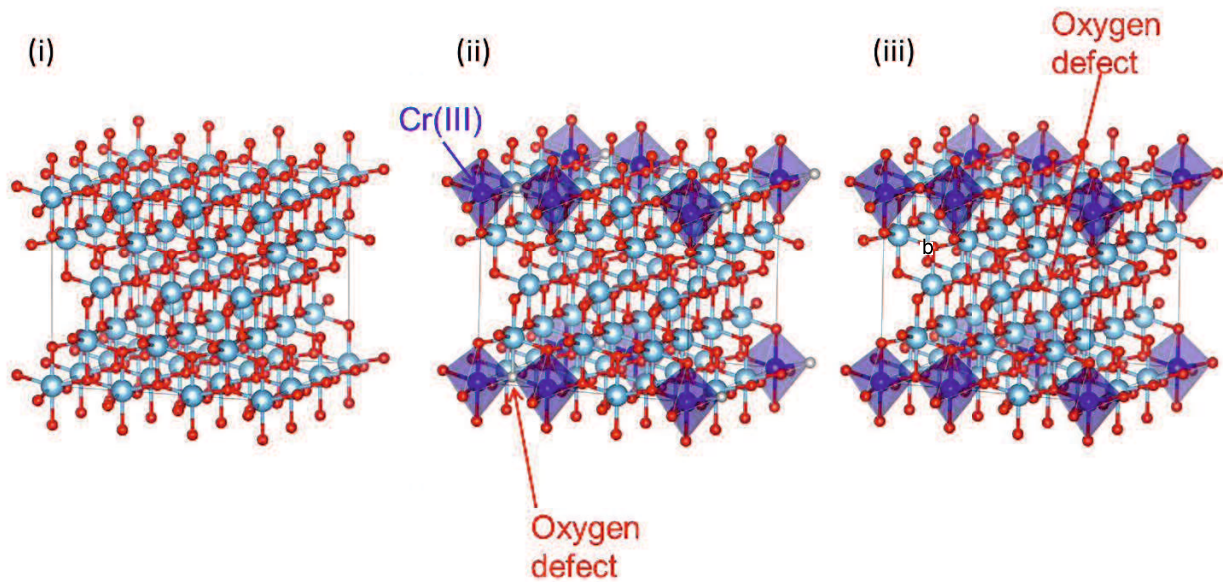


Figure 3-16 Local structure models of (i) anatase TiO₂ 3 x 3 x 1 supercell; (ii) model_a: two neighboring Ti(IV) were replaced with Cr(III) and oxygen between the atoms was withdrawn; and (iii) model_b: two neighboring Ti(IV) sites were replaced with Cr(III) and distant oxygen was withdrawn.

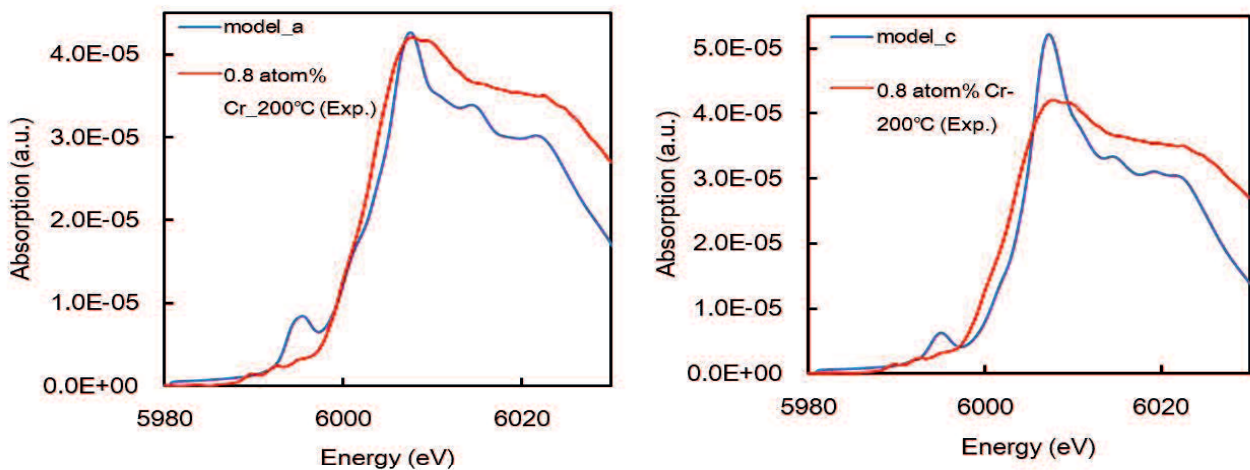


Figure 3-17 Comparisons of XANES spectra of model_a or model_b with that of 0.8 atom% Cr-TiO₂ sintered at 200°C.

Table 3-3 τ_1 and τ_2 for Cr-TiO₂ sintered at 200°C (excitation wavelength: 400 nm). Ratios τ_1 and τ_2 are in parenthesis.

Cr ion doping amount (atom%)	τ_1 (ps)	τ_2 (ps)
0.2	2.3 (46.7%)	72.2 (53.3%)
0.5	2.8 (50.0%)	78.6 (50.0%)
0.7	3.1 (53.3%)	78.3 (46.7%)
0.8	2.9 (52.2%)	80.0 (47.8%)
1.0	3.1 (55.1%)	81.1 (44.9%)
1.3	3.0 (54.2%)	80.4 (45.8%)
1.7	2.6 (53.9%)	65.7 (46.1%)
2.9	2.5 (51.3%)	57.1 (48.7%)
6.6	2.6 (50.6%)	55.6 (49.4%)

3. 4. Conclusion

Visible light responsive Cr-TiO₂ photocatalysts were prepared by conducting dialysis in the sol-gel method. TDR spectra of 6.6 atom% Cr-TiO₂ revealed that the τ_1 and τ_2 of photogenerated electrons were longer for Cr-TiO₂ with a higher photocatalytic activity because of suppression of the recombination of photogenerated carriers. The formation of Cr(VI) by sintering was a key factor in improving the photocatalytic activity of Cr-TiO₂ with doping amounts above 1.7 atom%. However, the highest photocatalytic activities were obtained with 0.68 - 1.3 atom%. Oxygen defects might be generated, instead of Cr(VI) formation, to maintain the charge balance by substituting for Ti(IV). Such oxygen vacancies can act as the electron traps to suppress recombination, and this enhanced the photocatalytic activities of 0.68 - 1.3 atom% Cr-TiO₂. In Chapter 2, some Pt(IV) was reduced to Pt(II) by changing the TTIP concentration in the sol - gel synthesis. In this Chapter, some Cr(III) was oxidized to Cr(VI) by sintering at high temperatures. The photocatalytic activity increased with increasing ratio of Pt(II) to Pt(IV). The co-presence of Pt(II) and Pt(IV) or Cr(III) and Cr(VI) enhanced the photocatalytic activity by suppressing recombination by increasing the spatial separation of the photogenerated carriers. Our results provide a new method for suppressing recombination by using metal ions. This will be beneficial for developing highly active visible light responsive photocatalyst.

References

- 1) M. Suzuki, N. Umesaki, T. Okajima, T. Tanaka, *J. Am. Ceram. Soc.*, 2016, **99**, 3151-3158.
- 2) M. Suzuki, N. Umesaki, T. Okajima, T. Tanaka, *J. Am. Ceram. Soc.*, 2018, **101**, 2653-2665.
- 3) E. Borgarello, J. Kiwi, M. Gratzel, E. Pelizzetti, M. Visca, *J. Am. Chem. Soc.*, 1982, **104**, 2996-3002.
- 4) M. Anpo, Y. Ichihashi, M. Takeuchi, H. Yamashita, *Stud. Surf. Sci. Catal.*, 1999, **121**, 305-310.
- 5) C. C. Pan, J. C. S. Wu, *Mater. Chem. Phys.*, 2006, **100**, 102-107.
- 6) K. B. Jaimy, S. Ghosh, S. Sankar, K. G. K. Warriar, *Mater. Res. Bull.*, 2011, **46**, 914-921.
- 7) X. Fan, X. Chen, S. Zhu, Z. Li, T. Yu, J. Ye, Z. Zou, *J. Mol. Catal. A-Chem.*, 2008, **284**, 155-160.
- 8) H. M. Yadav, T. V. Kolekar, A. S. Barge, N. D. Thorat, S. D. Delekar, B. M. Kim, B. J. Kim, J. S. Kim, *J. Mater. Sci.*, 2016, **27**, 526-534.
- 9) J. Zhu, Z. Deng, F. Chen, J. Zhang, H. Chen, M. Anpo, J. Huand, L Zhang. *Appl. Catal. B: Environ.*, 2006, **62**, 329-335.
- 10) M. Hamadani, A. S. Sarabi, A. M. Mehra, V. Jabbari, *Mat. Sci. Semicon. Proc.*, 2014, **62**, 161-166.
- 11) J. Choi, H. Park, M. R. Hoffmann, *J. Phys. Chem. C*, 2010, **114**, 783-792.
- 12) N. Nishiyama, Y. Fujiwara, K. Adachi, S. Yamazaki, *Appl. Catal. B: Environ.*, 2015, **176-177**, 347-353.
- 13) P. Rez, J. Bruley, P. Brohan, M. Payne, L. A. J. Garvie, *Ultramicroscopy*, 1995, **59**, 159-167.
- 14) S. J. Clark, M. D. Segall, C. J. Pickard, P. J. Hasnip, M. I. J. Robert, K. Refson, M. C. Payne, *Kristallogr. Cryst. Mater.*, 2005, **220**, 567-570.
- 15) J. P. Perdew, K. Burkner, M. Erzerhof, *Phys. Rev. Lett.*, 1996, **77**, 1463-1471.

- 16) A. M. Ruiz, G. Sakai, A. Cornet, K. Shimanoe, J. R. Morante, N. Yamazoe, *Sensor Actuat. B: Chem.*, 2003, **93**, 509-518.
- 17) Y-S. Jung, K-H. Kim, T-Y. Jang, Y. Tak, S-H. Baeck, *Curr. Appl. Phys.*, 2011, **11**, 358-361.
- 18) R. D. Shannon, *Acta Crystallogr., Sect. A: Cryst. Phys., Theor. Gen. Crystallogr.*, 1976, **32**, 751-767.
- 19) A. M. Luis, M. C. Neves, M. H. Mendonça, O. C. Monteiro, *Mater. Chem. Phys.*, 2011, **125**, 20-25.
- 20) D. Briggs, M. P. Seah (Eds.), *Auger and X-ray Photoelectron Spectroscopy*, Wiley, West Sussex, England, 1990.
- 21) H. Kato, A. Kudo, *J. Phys. Chem. B*, 2002, **106**, 5029-5034.
- 22) *Standard Potentials in Aqueous Solution*; (Eds) Marcel Dekker, Inc., New York, 1985.
- 23) X. Qiu, M. Miyauchi, K. Sunada, M. Minoshima, M. Liu, Y. Lu, D. Li, Y. Shimodaira, Y. Hosogi, Y. Kuroda, K. Hashimoto, *ACS NANO*, 2012, **6**, 1609-1618.
- 24) T. Yoshihara, R. Katoh, A. Furube, Y. Tamaki, M. Murai, K. Hara, S. Murata, H. Arakawa, M. Tachiya, *J. Phys. Chem. B*, 2004, **108**, 3817-3823.
- 25) T. Tachikawa, P. Zhang, Z. F. Bian, T. Majima, *J. Mater. Chem. A*, 2014, **2**, 3381-3388.
- 26) Z. F. Bian, T. Tachikawa, P. Zhang, M. Fujitsuka, T. Majima, *J. Am. Chem. Soc.*, 2014, **136**, 458-465.
- 27) K. Yamanaka, T. Ohwaki, T. Morikawa, *J. Phys. Chem. C*, 2013, **117**, 16448-16456.
- 28) M. Zhu, S. Kim, L. Mao, M. Fujitsuka, J. Zhang, X. Wang, T. Majima, *J. Am. Chem. Soc.*, 2017, **139**, 13234-13242.
- 29) D. C. Cronmeyer, *Phys. Rev.* 1959, **113**, 1222-1226.
- 30) C. D. Valentin, G. Pacchioni, A. Selloni, *J. Phys. Chem. C* 2009, **113**, 20543-20552.
- 31) M. Nishikawa, Y. Mitani, Y. Nosaka, *J. Phys. Chem. C*, 2014, **2**, 3381-3388.

Chapter 4 Factors affecting the photocatalytic activity of Cr-grafted TiO₂ under visible light irradiation

4.1 Introduction

In Chapter 3, the coexistence of Cr(III) and Cr(VI) enhances the photocatalytic activity of Cr-TiO₂. Recently, metal ion-grafted TiO₂ such as Cu-, Cr- and Fe-grafted TiO₂ has been developed as the visible light responsive photocatalyst.¹⁻⁹⁾ On Cr-grafted TiO₂ under visible light irradiation, electrons are excited from Cr(III) ions adsorbed on the TiO₂ surface to the CB by the interfacial charge transfer (IFCT) process.^{1,5)} The resulting Cr(IV) oxidatively degrades organic compounds adsorbed on the TiO₂ surface. On the other hand, in the case of Cu- or Fe-grafted TiO₂, electrons are excited from the VB of TiO₂ to Cu(II) or Fe(III) ions adsorbed on the surface by the IFCT process and then the organic compounds are directly oxidized by the photogenerated holes.²⁻⁴⁾

Regarding factors to enhance the photocatalytic activity of these metal-ion-grafted TiO₂, Irie *et al.* reported that the improvement of the crystallinity of TiO₂ on which the Cu(II) and Fe(III) ions were grafted increased the photocatalytic activity for the degradation of 2-propanol in the gas phase.³⁾ However, there are few reports on metal-ion-grafted TiO₂ in aqueous solution. In recent years, we have already reported that the number density of Cu ions near the TiO₂ surface affect significantly the photocatalytic activity of Cu-grafted TiO₂.¹⁰⁾ In the Cr-grafted TiO₂ and Cr-TiO₂, the valence state and the location of Cr ions are

different. Moreover, the BET specific surface area and the crystal form of TiO₂ as a matrix are also different.

In this Chapter, the photocatalytic activity and physical properties of Cr-grafted TiO₂ and Cr-TiO₂ were compared. I investigated the effect of the number density of Cr ions near the TiO₂ surface and the sintering temperature on the photocatalytic activity of Cr-grafted TiO₂.

4. 2. Experimental

4. 2. 1. Materials.

As mentioned in the Chapter 2 and 3, all reagents were purchased from Wako Pure Chemicals Industries Ltd (Osaka, Japan) and used without further purification unless otherwise noted. TiO₂ (MT-150A, TAYCA CORPORATION (Osaka, Japan)) was used for the synthesis of Cr-grafted TiO₂.

4. 2. 2. Preparation of Cr-grafted TiO₂ powder.

Cr-grafted TiO₂ powders was prepared according to the literature.^{1, 5)} 10 ml of water was added to a mixture of CrCl₃ · 6H₂O and TiO₂ in which the Cr content was 0.1-1.6 atom% against Ti. This mixture was stirred for 1 h in a water bath at 90°C, then filtered with a membrane filter (Merck Millipore Ltd., USA, VSWP02500 0.025 μm) and washed with

water. The concentration of Cr(III) ion in the filtrate was determined by ICP-AES to estimate the Cr content adsorbed on TiO₂ powder. The obtained powder was dried at 110°C for 24 h and ground into fine powder by using agate mortar and pestle.

4. 2. 3. Characterization and evaluation of the photocatalytic activity of Cr-grafted TiO₂ powder.

XRD, BET, diffuse reflectance UV-vis absorption spectra, XPS measurements and XANES measurements were carried out as described in Chapter 2 and 3. The photocatalytic performance on Cr-grafted TiO₂ was examined as described in the Chapter 3.

4. 3. Results and discussion

4. 3. 1. Comparison of Cr-grafted TiO₂ and Cr-TiO₂.

Figure 4-1 shows the time course of the 4-CP conversion on 0.78 atom% Cr-grafted TiO₂ and 0.82 atom% Cr-TiO₂ sintered at 200°C, which exhibits the highest photocatalytic activity as mentioned in Chapter 3. At the irradiation for 150 min, the 4-CP conversion of the Cr-TiO₂ is about 4.7 times higher than that of Cr-grafted TiO₂. Figure 4-2 shows the comparison of the 4-CP conversion of 0.82 atom% Cr-TiO₂ unsintered and sintered at 100°C and 0.78 atom% Cr-grafted TiO₂ after visible light irradiation for 150 min, indicating that these three are relatively similar compared with much higher 4-CP conversion on 0.82 atom%

Cr-TiO₂ sintered at 200°C. The BET specific surface areas of Cr-TiO₂ unsintered and sintered at 100 and 200°C were almost the same as 252 - 308 m² g⁻¹. In addition, the crystalline form was the anatase phase and their crystalline sizes of the (101) face were almost constant to be 3.8 - 4.4 nm. On the other hand, the BET specific surface area of TiO₂ of MT-150A used for the synthesis in Cr-grafted TiO₂ was 103 m² g⁻¹ and the crystal form was rutile with the crystallite size of 14.3 nm estimated from the (110) face, indicating remarkable difference from those physical properties of Cr-TiO₂. These findings suggest that the difference in the 4-CP conversion might be attributable to the existence manner of Cr ion. Irie *et al.* have reported using the XANES spectra that Cr exists as Cr(III) in the Cr-grafted TiO₂.⁵⁾ Furthermore, they calculated the Cr - O bond length of the Cr-grafted TiO₂ by curve fitting analysis based on the FEFF standard of FT-EXAFS spectra and demonstrated that the obtained value was similar to the bond length of Cr - O of Cr₂O₃.⁵⁾ Based on these results, they reported that the Cr(III) in the Cr-grafted TiO₂ seemed to form an amorphous-like Cr₂O₃ clusters and attach to the TiO₂ surface. Previously, I have reported that the photocatalytic activity is strongly influenced by the number density of Cu ion on the TiO₂ surface in the Cu-grafted TiO₂.¹⁰⁾ Therefore, the experiments were performed to clarify how the photocatalytic activity of the Cr-grafted TiO₂ was affected by changing the number density of Cr ions on the TiO₂ surface.

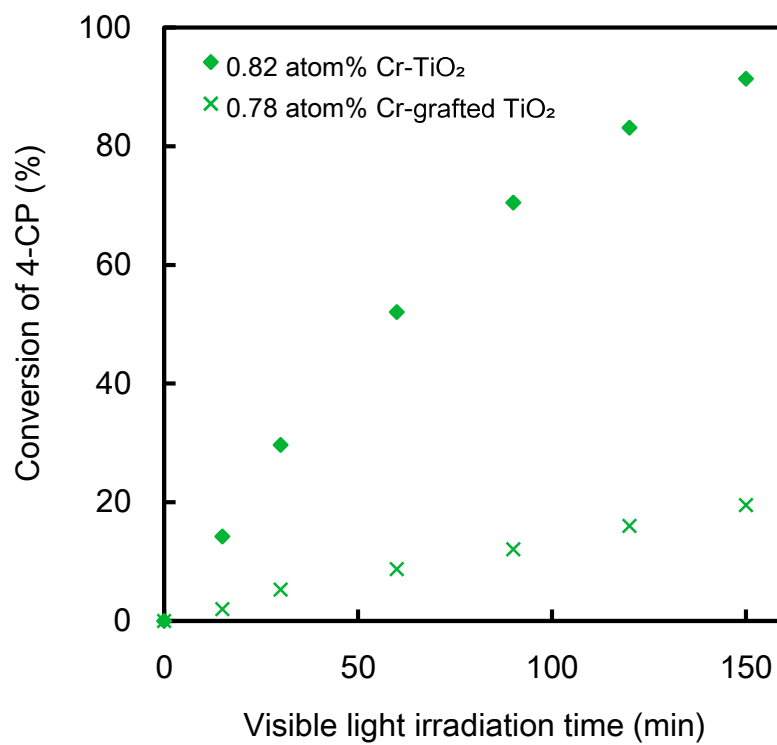


Figure 4-1 Time course of the 4-CP conversion on 0.78 atom% Cr-grafted TiO₂ and 0.82 atom% Cr-TiO₂ under visible light irradiation.

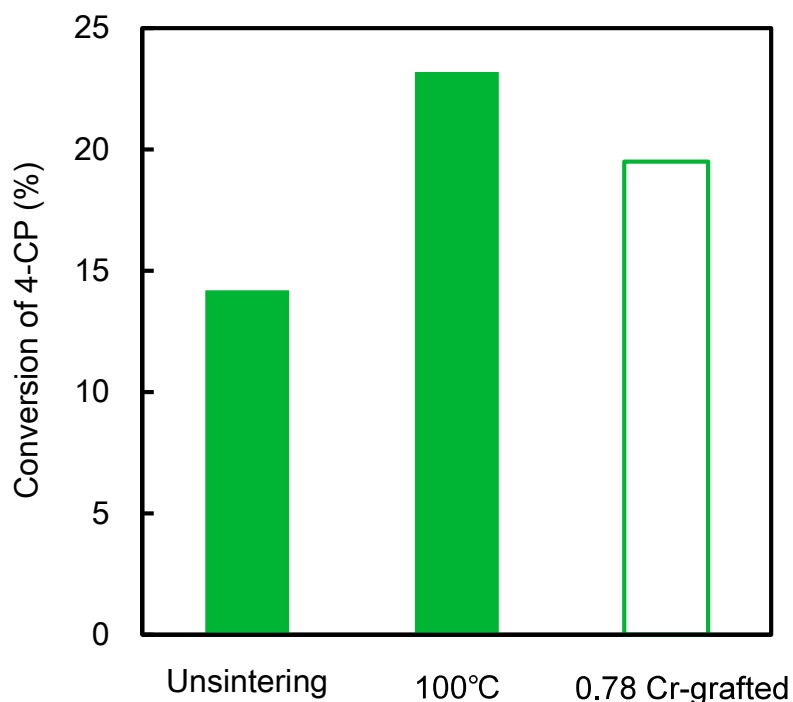


Figure 4-2 Comparison of the photocatalytic activity at visible light irradiation for 150 min on 0.82 atom% Cr-TiO₂ unsintered and sintered at 100°C and 0.78 atom% Cr-grafted TiO₂.

4. 3. 2. Effect of number density of Cr ion of the Cr-grafted TiO₂ on the 4-CP conversion.

Figure 4-3 shows the 4-CP conversion on 0.78 atom% Cr-grafted TiO₂ at visible light irradiation for 150 min, which was synthesized after sintering TiO₂ at 200 – 600°C. Table 4-1 lists the BET specific surface area and the crystalline size of TiO₂ of 0.78 atom% Cr-grafted TiO₂. As the sintering temperature increases, the BET specific surface area decreases and the crystalline size increases. As shown in Figure 4-3, the 4-CP conversion

hardly depends on the sintering temperature. Since the amount of Cr ions on TiO₂ was constant to be 0.78 atom%, the number density of Cr ions near the TiO₂ surface increased as the BET specific surface area decreased. The number density of Cr ions was calculated by the following equation.

$$\text{Number density of Cr ion} = \frac{\text{Amount of Cr ion (mol)}}{\text{SSA of Photocatalyst (m}^2\text{g}^{-1}) \times \text{weight of Photocatalyst (0.2 g)}}$$

In Figure 4-4, the 4-CP conversion at visible light irradiation for 150 min is plotted against the number density of Cr ions, indicating that the 4-CP conversion was not affected. Irie *et al.* have reported that Cu-grafted TiO₂ synthesized after sintering TiO₂ at 950°C showed higher quantum efficiency compared with the unsintered TiO₂ for the degradation of gaseous 2-propanol due to the improved crystallinity of TiO₂.³⁾ Previously, I investigated the relationship between the photocatalytic activity and the number density of Cu ions near the surface of Cu-grafted TiO₂ and found the linearity between them.¹⁰⁾ For comparison, the obtained data with Cu-grafted TiO₂ are also plotted in Figure 4-4. Such a difference of the dependence of the 4-CP conversion on the number density of metal ions between Cr-grafted TiO₂ and Cu-grafted TiO₂ seems to be due to the difference in their visible light responsive mechanisms as shown in Scheme 4-1 and Scheme 4-2, respectively. When Cr-grafted TiO₂ is

irradiated with visible light, Cr(IV) is generated by the electron transfer from Cr(III) adsorbed on the TiO₂ surface to the CB (IFCT process). Such an electron transfer occurs under visible light since the standard redox potential of Cr(IV)/Cr(III) is 2.1 V (vs. NHE) and then, the generated Cr(IV) oxidizes the organic compounds adsorbed on TiO₂ surface to form Cr(III).^{1,}

⁵⁾ The electrons excited in the CB of TiO₂ reduce oxygen. According to this mechanism, the visible light is absorbed by Cr(III) ion grafted on TiO₂, leading to the formation of Cr(IV) which oxidizes 4-CP. Therefore, it is expected that the degradation of 4-CP proceeds more efficiently as the number density of Cr(III) near the TiO₂ surface increases. However, the oxygen adsorbed on TiO₂ becomes less with an increase in the Cr(III) density. As a result, the electrons recombine with Cr(IV). On the other hand, in the case of Cu-grafted TiO₂, electrons are excited from the VB of TiO₂ to Cu(II) ions grafted on the surface by the IFCT process under visible light irradiation (Scheme 4-2).^{2, 4)} The photogenerated holes in the VB are strong oxidants to degrade 4-CP. Irie *et al.* speculated with Cu-grafted TiO₂ that multiple electron reduction of oxygen occurs via Cu(I) adsorbed on the TiO₂ surface to evolve hydrogen oxide (two-electron reduction) or water (four-electron reduction).⁴⁾ That is, the 4-CP is efficiently degraded by the photogenerated holes when the TiO₂ surface in the Cu-grafted TiO₂ are exposed to visible light. The increase in the number density of Cu ions reduces the TiO₂ surface which is exposed to visible light. As a result, the formation of the photogenerated holes is suppressed, decreasing the photocatalytic activity.

In Chapter 3, Cr ions in Cr-TiO₂ were diffused thermally into TiO₂ bulk by sintering and substituted with Ti. As a result, in order to maintain the charge balance, oxygen defects or Cr(VI) were generated (formation of trap sites of photogenerated carriers) and Cr-TiO₂ was highly activated. Even in Cr-grafted TiO₂, it is expected that high activation is achieved by sintering to promote thermal diffusion of Cr ions into TiO₂ bulk and to form trap sites for the photogenerated carriers. The effect of the sintering at 200 – 600°C of the Cr-grafted TiO₂ on the photocatalytic activity is investigated in the next section.

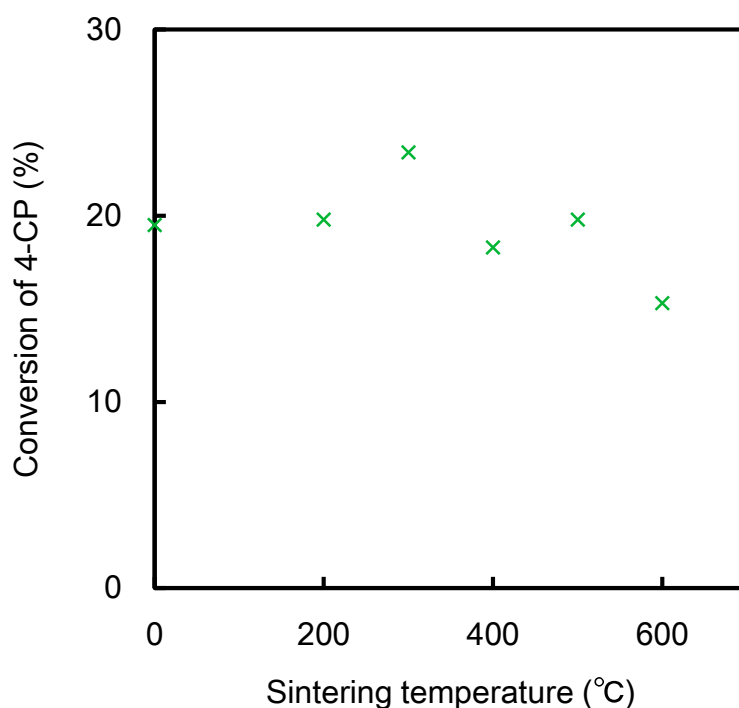


Figure 4-3 Effect of the sintering temperature of TiO₂ before grafting on the conversion of 4-CP after the visible light irradiation for 150 min.

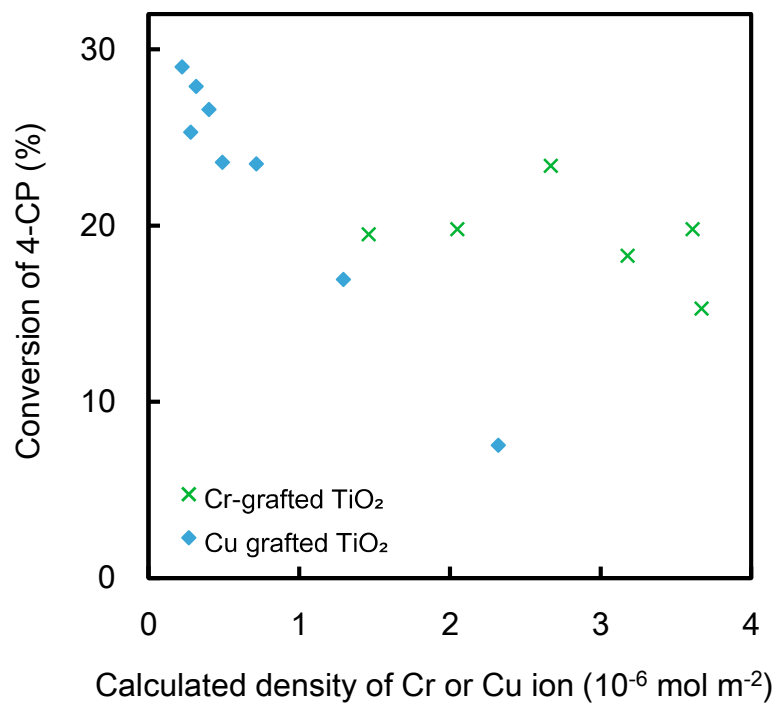
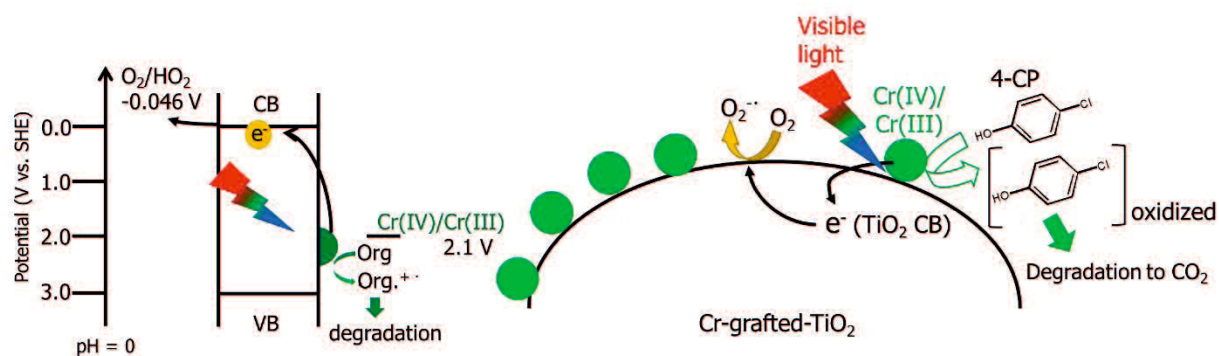


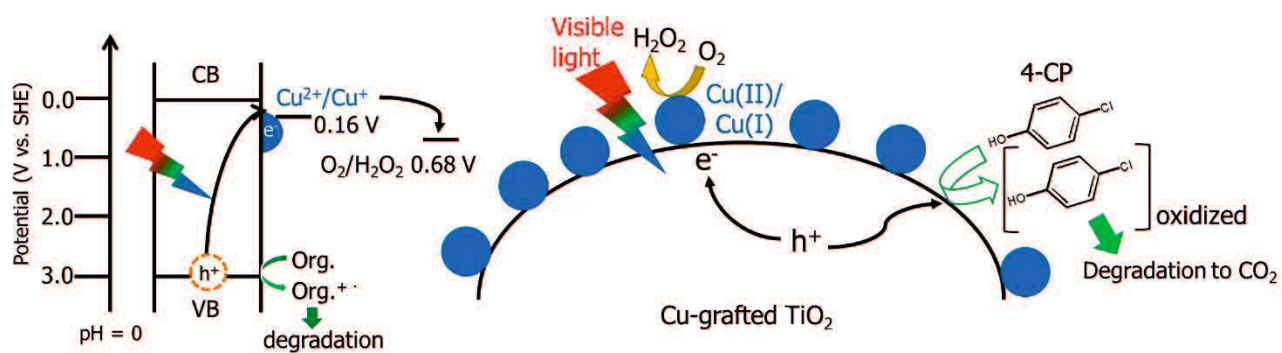
Figure 4-4 Effect of the number density of Cr or Cu ion on the TiO₂ surface on the conversion of 4-CP after the visible light irradiation for 150 min.

Table 4-1 Effect of the sintering temperature of TiO₂ before grafting of Cr ion on the BET surface area and crystalline size.

Sintering temperature (°C)	BET specific surface area (m ² g ⁻¹)	Crystalline size (nm)
Unsintering	103.0	14.5
200	73.3	15.8
300	56.2	17.4
400	47.2	19.9
500	41.5	22.4
600	32.7	26.9



Scheme 4-1 Mechanism of visible light responsive Cr-grafted TiO₂.



Scheme 4-2 Mechanism of visible light responsive Cu-grafted TiO₂.

4. 3. 3. Effect of the sintering of Cr-grafted TiO₂ on the 4-CP conversion.

Figure 4-5 shows the dependence of the 4-CP conversion on the sintering temperature of 0.78 atom% Cr-grafted TiO₂. Table 4-2 lists the BET specific surface area and the crystalline size after sintering 0.78 atom% Cr-grafted TiO₂. The 4-CP conversions are almost the same on Cr-grafted TiO₂ unsintered or sintered at 200°C and remarkably increase by sintering at higher temperatures than 300°C. The highest photocatalytic activity is obtained with 0.78 atom% Cr-grafted TiO₂ sintered at 400°C, which is comparable to 0.82 atom% Cr-TiO₂ sintered at 200°C. As shown in Figure 4-6, the XPS spectra of Cr-grafted TiO₂ unsintered and sintered at 200 and 300°C indicate a broad peak around 577.0 eV which almost agrees with the energy value of 2p_{3/2} of Cr₂O₃ (576.8 eV), suggesting that most of Cr ion exist as Cr(III) near the TiO₂ surface. The XANES spectra in Figure 4-7 indicate that the pre-edge peak is not detected on 0.78 atom% Cr-grafted TiO₂ unsintered and sintered at 200°C whereas it is observed at 5992 eV with a slight shift of the absorption edge to higher energy when being sintered at 400°C. Therefore, the highest photocatalytic activity observed at 400°C is attributable to the formation of Cr(VI). The coexistence of Cr(III) and Cr(VI) suppressed the recombination of photogenerated carriers as described for Cr-TiO₂ in Chapter 3. However, no pre-edge peak was detected in the XANES spectra for 0.78 atom% Cr-grafted TiO₂ sintered at 300 and 500°C. As shown in the diffuse reflection spectra in Figure 4-8, absorption at around 450 nm becomes higher by sintering at 300 – 500°C. Furthermore,

absorption at 600 – 800 nm due to the d-d transition¹¹⁾ shows red shift and disappears with an increase in the sintering temperature. Such the similar spectral change was obtained with 0.82 atom% Cr-TiO₂ sintered at 200°C whose XANES spectra depicted no pre-edge peaks attributable to Cr(VI). The high photocatalytic activity observed with Cr-grafted TiO₂ sintered at 300 and 500°C might be the formation of oxygen defects.

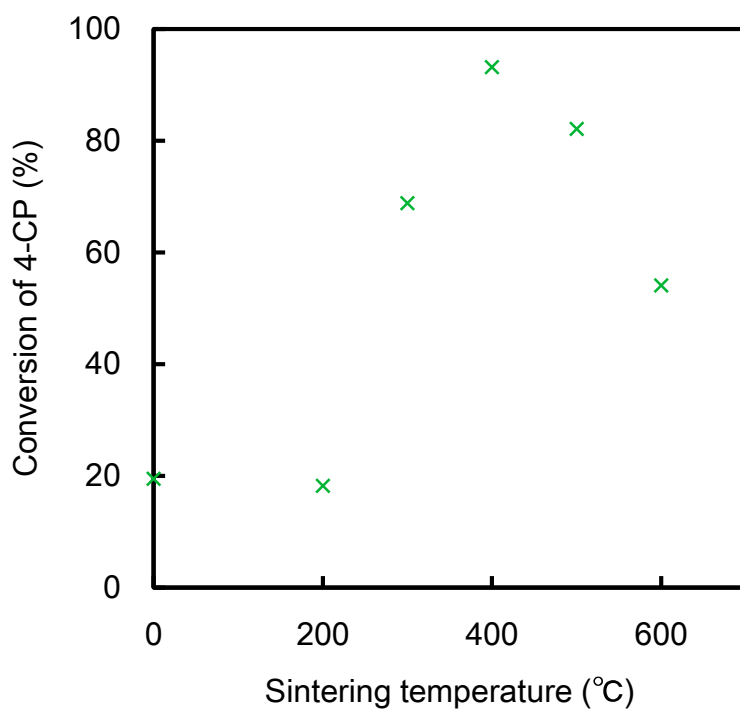


Figure 4-5 Effect of the sintering of the Cr-grafted TiO₂ on the 4-CP conversion at the visible light irradiation for 150 min.

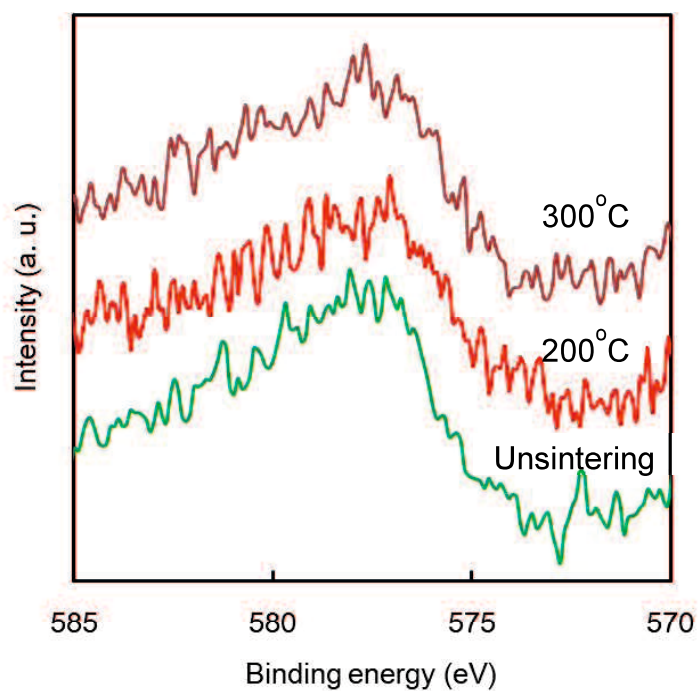


Figure 4-6 XPS spectra of 0.78 atom% Cr-grafted TiO₂ unsintered and sintered at 200 and 300°C.

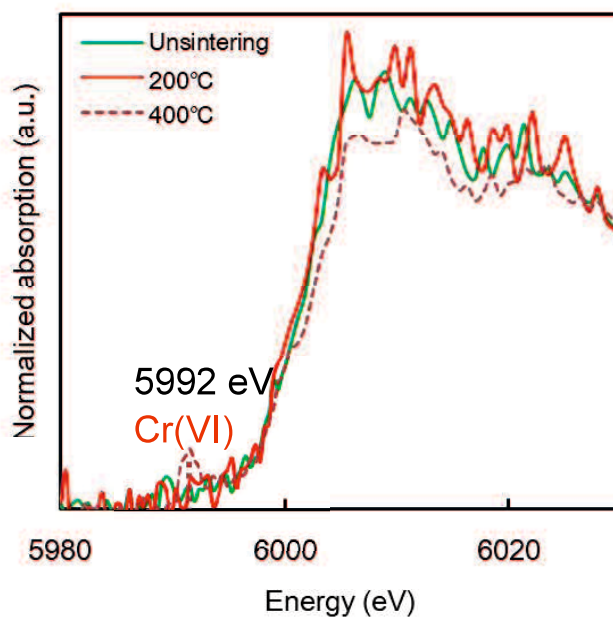


Figure 4-7 XANES spectra of 0.78 atom% Cr-grafted TiO₂ unsintered and sintered at 200 and 300°C.

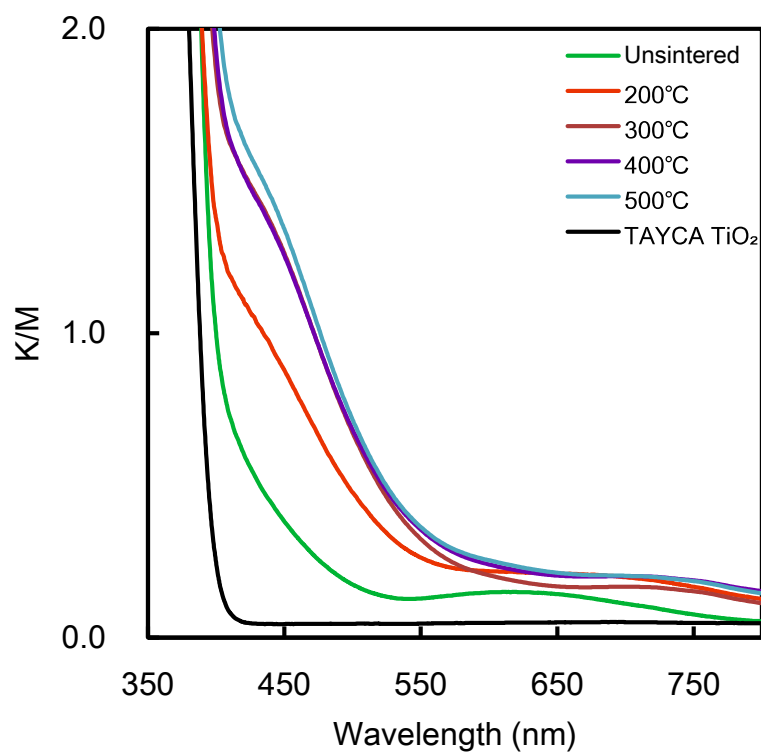


Figure 4-8 Diffuse reflectance UV-vis spectra of TiO₂ and Cr-grafted TiO₂.

Table 4-2 Effect of the sintering temperature on the BET surface area and crystalline size of Cr-grafted TiO₂.

Sintering temperature (°C)	BET specific surface area (m ² g ⁻¹)	Crystalline size (nm)
Unsintering	103.0	14.5
200	88.5	14.5
300	63.7	16.7
400	55.4	18.5
500	45.2	22.0
600	34.3	27.6

4. 4. Conclusion

The 4-CP conversion of Cr-grafted TiO₂ was lower than that of Cr-doped TiO₂. However, the 4-CP conversion was significantly improved when Cr-grafted TiO₂ was sintered at the temperature higher than 300°C. Notably, Cr-grafted TiO₂ sintered at 400°C showed the high 4-CP conversion comparable to the 0.82 atom% Cr-TiO₂ sintered at 200°C. Since the formation of Cr(VI) was observed, it suggests that the co-existence of Cr(III) and Cr(VI) enhanced the photocatalytic activity of Cr-grafted TiO₂ like Cr-TiO₂.

References

- 1) H. Irie, S. Miura, R. Nakamura, K. Hashimoto, *Chem. Lett.*, 2008, **37**, 252-253.
- 2) H. Irie, S. Miura, R. Nakamura, K. Hashimoto, *Chem. Phys. Lett.*, 2008, **457**, 202-205.
- 3) H. Yu, H. Irie, Y. Shimodaira, Y. Hosogi, Y. Kuroda, M. Miyauchi, K. Hashimoto, *J. Phys. Chem. C*, 2010, **114**, 16481-16487.
- 4) H. Irie, K. Kamiya, T. Shibanuma, S. Miura, D. A. Tryk, T. Yokoyama, K. Hashimoto, *J. Phys. Chem. C*, 2009, **113**, 10761-10766.
- 5) H. Irie, T. Shibanuma, K. Kamiya, S. Miura, T. Yokoyama, K. Hashimoto, *Appl. Catal. B: Environ.*, 2010, **96**, 142-147.
- 6) M. Liu, R. Inde, M. Nishikawa, X. Qiu, D. Atarashi, E. Sakai, Y. Nosaka, K. Hashimoto, M. Miyauchi, *ACS Nano*, 2014, **8**, 7229-7238.
- 7) M. Liu, X. Qiu, K. Hashimoto, M. Miyauchi, *J. Am. Chem. Soc.*, 2013, **135**, 10064-10072.
- 8) M. Liu, X. Qiu, M. Miyauchi, K. Hashimoto, *Chem. Mater.*, 2011, **23**, 5282-5286.
- 9) H. Yu, H. Irie, K. Hashimoto, *J. Am. Chem. Soc.*, 2010, **132**, 6898-6899.
- 10) N. Nishiyama, K. Kozasa, S. Yamazaki, *Appl. Catal. A: Gen.*, 2016, **527**, 109-115.
- 11) J. Zhu, Z. Deng, F. Chen, J. Zhang, H. Chen, M. Anpo, J. Huand, L Zhang. *Appl. Catal. B: Environ.*, 2006, **62**, 329-335.

Chapter 5 Conclusion

Visible light responsive TiO_2 doped with Pt or Cr ion (Pt- TiO_2 , Cr- TiO_2) was prepared by conducting dialysis in the sol-gel method.

In the literature reported so far, there are many inconsistent results regarding the optimal doping amount and sintering temperature for the synthesis of M- TiO_2 . This thesis has demonstrated for the first time that the photocatalytic activity increases linearly with the ratio of Pt(II)/Pt(IV) in Pt- TiO_2 or Cr(III)/Cr(VI) in Cr- TiO_2 . The TDR spectra measurements revealed that the lifetime of the photogenerated carriers increased with increasing the ratio of Pt(II)/Pt(IV) or Cr(III)/Cr(VI). Similarly, the linear relationship was obtained with Pt- TiO_2 prepared by the conventional sol - gel method. That is, even in M- TiO_2 synthesized by different methods, there is a possibility that a unified view can be obtained simply by investigating the valence state and location of the doped metal ion. Moreover, our Pt- TiO_2 had much higher photocatalytic activity than commercially available TiO_2 under solar simulator light irradiation. Our results indicate that controlling the mixed valence states of metal dopants in TiO_2 is a new strategy to develop highly active photocatalysts under solar light.

By using the findings obtained in this thesis, inorganic semiconductor materials that cannot absorb visible light because of a wide band gap energy value (SnO_2 , ZnO , ZrO_2 , etc.), might be activated as photocatalysts by doping with metal ions and by controlling their mixed

valence states.

The visible light responsiveness of Cr-TiO₂ was explained by utilizing the redox potentials of Cr ions. It was speculated that the photogenerated Cr(IV) degraded 4-CP oxidatively on the surface of Cr-TiO₂ because the photocatalytic activity of Cr-TiO₂ was not as high as Pt-TiO₂ on which 4-CP was oxidized by the photogenerated holes. This fact indicates the oxidizing power of Cr-TiO₂ is lower than the photogenerated holes in TiO₂. Organic compounds can be mineralized to CO₂ on TiO₂ due to the strong oxidizing power of the photogenerated hole. However, CO₂ is very stable, and it is very difficult to convert CO₂ to valuable organic compounds. Therefore, the lower oxidizing power of Cr-TiO₂ might be promising as a mild oxidant under visible light irradiation. The results of this thesis show the possibility of controlling the oxidation reaction by utilizing the redox potentials of metal ion dopants while suppressing the recombination by controlling their mixed valence states.

Because of the possibility of application to various inorganic semiconductors and development of photoinduced mild oxidizing agents for organic synthesis, this thesis gives not only academic novelty but also a great ripple effect on the industry.

Acknowledgements

I am deeply grateful to Prof. Suzuko Yamazaki for her excellent and invaluable guidance throughout my thesis. Without her constant guidance, encouragement and above all her cooperation, my thesis would not have taken this shape. I would like to express my deep gratitude to her for my research freely and for having kindly watched over me.

I would like to thank the referees Prof. Kensuke Honda, Prof. Katsuya Ishiguro, Prof. Toshihiro Murafuji and Prof. Jun Kawamata.

I would like to express my gratitude to all my teachers in Yamaguchi University, especially Assoc. Prof. Kenta Adachi and Assoc. Prof. Ryo Tsunashima. Their keen interest in all my studies has inspired me in many ways.

I am grateful to Dr. Hiroyuki Setoyama for help on the measurements of XANES spectra by using beamline 11 of Kyusyu Synchrotron Light Research Center (BL 11) and fruitful discussion. I am grateful to Dr. Toshihiro Okajima for measurements and simulations of XANES spectra of Cr-TiO₂ and constructive comments.

I am grateful to Prof. Kei Inumaru at Hiroshima University for the measurements of XPS spectra of 6.6 atom% Cr-TiO₂ sintered at 200°C.

The measurements of XRD and ICP-AES were performed at the Center for Instrumental Analysis, Yamaguchi University. I am grateful to technical staff, Mr. Yoji Morifuku.

I also thank Assoc. Prof. Tasuma Suzuki and Mr. Tsuyoshi Tonosaki at Yamaguchi University for measurements of XPS spectra.

I would like to express my sincere gratitude to Prof. Tetsuro Majima and Assoc. Prof. Mamoru Fujitsuka at Osaka University for help on the measurements of femtosecond TDR spectra and in-depth and extensive discussion.

Special thanks to Functional Material Chemistry laboratory and my friends for making my school life happy.

I have helped countless people in my life so far, not just those listed here. I will never forget that and will continue to live with gratitude.

Finally, I am deeply indebted to my parents for their unconditional love and financial supports throughout my life. I sincerely express my gratitude to my sister, grandfather and grandmother. This thesis consists of their great supports and unlimited love.

Naoto Nishiyama

August, 2018

Publication list

[1] Naoto Nishiyama, Keisuke Kozasa, Toshihiro Okajima, Mamoru Fujitsuka, Tetsuro Majima and Suzuko Yamazaki, “Factors affecting photocatalytic activity of visible light responsive titanium dioxide doped with chromium ions” , *Catalysis Science & Technology*, *In Press (2018)*, Doi:10.1039/C8CY01411F.

[2] Naoto Nishiyama and Suzuko Yamazaki, “Effect of mixed valence states of platinum ion dopant on photocatalytic activity of titanium dioxide under visible light irradiation” , *ACS OMEGA*, **2017**, 2, 9033-9039.

[3] Naoto Nishiyama, Keisuke Kozasa and Suzuko Yamazaki, “Photocatalytic degradation of 4-chlorophenol on titanium dioxide modified with Cu(II) or Cr(III) ion under visible light irradiation” , *Applied Catalysis A: General*, **2016**, 527, 109-115,